The Role of Oxidative Stress in Streptozotocin-induced Early and Late Stage Diabetes Mellitus in the Rat (*Rattus norvegicus*, Berkenhout 1769)

Dissertation

zur Erlangung des Doktorgrades
- Dr. rer. nat -
des Fachbereichs Biologie
der Universität Hamburg

vorgelegt von

Maria Christina Wendt

aus Hamburg

Hamburg 2005

Genehmigt vom
Fachbereich Biologie der
Universität Hamburg
auf Antrag von Herrn Professor Dr. med. T. MÜNZEL
Weitere Gutachter der Dissertation:
Herr Professor Dr. L. RENWRANTZ

Tag der Disputation: 10. Dezember 2004

Hamburg, den 26. November 2004

Professor Dr. Arno Frühwald
Dekan

EMORY UNIVERSITY SCHOOL OF MEDICINE
DEPARTMENT OF MEDICINE
DIVISION OF CARDIOLOGY
Suite 319, Woodruff Memorial Research Building
1639 Pierce Drive Atlanta, Georgia 30322

October 26, 2004

To whom it may concern:

I have read Maria Wendt's thesis and I confirm that the English is correct in grammar and content. In fact, the writing is better than that of many native English speakers.

Sincerely,

Kathy K. Griendling

Kathy K. Griendling, Ph.D.
Professor of Medicine

Acknowledgments

I would like to extend my sincere thanks to the following people:

Prof Dr Thomas Münzel, for giving me the opportunity to do my PhD in his laboratory, for his guidance and unfailing support throughout and for always making time when there was none. Prof Münzel, I am especially indebted to you for your continuous financial support, even when times were tough. I greatly appreciate the opportunity you gave me to present my results, here and overseas, for always supporting collaborative work and thereby allowing me to gain further experience in different laboratories, in my opinion an essential necessity in the field of research. I thank you for having allowed me the space to be creative and to follow my own ideas and yet at the same time keeping me on track. The time in your laboratory has contributed substantially to recognizing my future vocation, and I thank you for that.

Prof Alexander Mülsch, for appearing at the right place at the right time. I have great respect for your critical and sincere approach to science and would like to thank you for your time as well as for the constructive and valuable discussions we have had.

Claudia Kuper, who, together with Hartwig made the need for a radio in the lab redundant – 8 hours of sole entertainment! What's more, your contribution to my northern slang is unmistakable! Thanks, Claudia for letting them 'wriggle' so relentlessly.

Hartwig Wieboldt, the Inspector, whose balanced nature and extraordinary organisational skills were indispensable for the smooth running of the laboratory (and the people in it). Thank you for frequently helping me to put things back into perspective and above all, of course, I owe to you my future career! I will do my best so that you get your share of the deal.

Andreas Daiber, for the many so essential scientific discussions and for bringing the vast chemical reactions of $^{\bullet}NO$ and $O_2^{\bullet-}$ a little closer to my heart.

Matthias Oelze, who would drop everything to help, unconditionally, anytime, anywhere and with anything - a rare quality. I don't know where life's path will lead us, but Hamburg is not that big so I am sure we will smell each other out before long.

Michael August, for always lending an ear when things didn't work the way they should and of course for the many hours spent on solving the so frustrating computer hiccups.

Andrei Kleschyov, for the late evening brainstorming sessions. Life will be 'so strange' without you and your 'ironDETC'.

Meike Coldewey, Denise Lau, Eberhard Schulz, Karsten Sydow, Uli Hink, Hanke Mollnau, Stefan Baldus, Natalie Obermeyer and Anna Mazur and all other colleagues, past and present, who shared with me the many turbulent as well as joyous times that research brings with it. I thank you all for a terrific working atmosphere, for all the fun and laughter and for seeing this through with me in every way.

Kati Szöcs, for her strong moral support, for always being there to discuss anything at all and for trying so hard to occasionally get my mind off things. Its great to have you here, although NOTHING will live up to the times we have had in Atlanta!

All my **many dear friends**, here and across the miles, who stuck this out with me. A huge thank you for all the letters, emails and calls and thanks too for all your patience. Things will be different from now on, I promise……

And finally my **mother**, whose enduring love, remarkable wisdom and amazing strength as well undying faith, day in and day out, near and afar, are the grounds on which this work was accomplished.

And the one who made all this possible: Thank you **J.C**.!

Table of Contents

1 INTRODUCTION 1

1.1 Diabetes mellitus 1

1.1.1 Type 1 diabetes 2

1.1.2 Type 2 diabetes 2

1.1.3 Clinical manifestation of diabetes 3

1.2 Endothelial (dys)function 3

1.2.1 The endothelium 3

1.2.2 Normal endothelial function and vasorelaxation 4

1.2.3 Endothelial dysfunction 9

1.3 Oxidative stress and endothelial dysfunction 9

1.3.1 Reactive oxygen species (ROS) 9

1.3.2 Enzymatic ROS sources 11

1.3.3 ROS, endothelial dysfunction and diabetes mellitus 15

1.4 Aim of the study 19

2 MATERIALS AND METHODS 20

2.1 Materials 20

2.1.1 Chemicals 20

2.1.2 Kits and Assay Solutions 20

2.1.3 Antibodies 21

2.1.4 Consumables 21

2.1.5 Instruments 21

2.1.6 Software 22

2.2 Methods 22

2.2.1 Animals 22

2.2.2 Tissue preparation 23

2.2.3 Isometric tension studies 24

2.2.4 Determination of angiotensin converting enzyme (ACE) activity in serum 25

2.2.5 Protein measurements according to the method of Bradford 25
2.2.6 sGC activity of aortic homogenates 25
2.2.7 cGMP/cAMP enzymeimmunoassay (EIA) of aortic tissue 26
2.2.8 Cryosectioning of aortic rings 27
2.2.9 Oxidative fluorescent microtopography 27
2.2.10 Immunofluorescent histochemistry 28
2.2.11 SDS-polyacrylamide gel electrophoresis (PAGE) and Western blot analysis 28
2.2.12 Chemiluminescent detection of ROS with lucigenin, coelenterazine and L-012 32
2.2.13 Measurement of NADPH-dependent oxidase(s) activity in membrane fractions of heart and aorta 32
2.2.14 Measurement of vascular NO by electronparamagnetic resonance (EPR) spin trapping 33
2.2.15 DAN assay for the detection of nitrite (NO_2^-) and nitrate (NO_3^-) in serum 34
2.2.16 Statistical analysis 34

3 RESULTS 35

3.1 Blood glucose levels and body weights 35

3.2 Isometric tension studies 35
3.2.1 Vasoreactivity in response to ACh, NTG and SNP 36
3.2.2 Vasoreactivity in response to KCl and phenylephrine 40

3.3 ACE activity in serum 43

3.4 sGC activity in aorta 44

3.5 cGMP levels in aorta 45

3.6 cAMP levels in aorta 46

3.7 ROS levels in aortic rings detected by CL using lucigenin, coelenterazine and L-012 47

3.8 Oxidative fluorescent microtopography 50

3.9 NADPH-dependent oxidase(s) activity of membrane fractions from heart and aorta 52

3.10 Immunohistochemical detection of eNOS 54

3.11 Vascular NO levels detected by EPR spin trapping..... 55

3.12 Serum levels of NO_2^- and NO_3^- 56

3.13 Western blot analysis..... 57

3.13.1 Expression of the NAD(P)H oxidase subunits nox1, nox4 and $p67^{phox}$ 57

3.13.2 Expression of eNOS 59

3.13.3 Expression of SOD 60

3.13.4 Expression of sGC and cGK-I 62

3.13.5 Expression of P-VASPser239 63

3.13.6 Expression of HO-1 65

4 DISCUSSION 66

4.1 Influence of early and late stage diabetes on vascular reactivity to relaxing stimuli..... 68

4.2 Influence of early and late stage diabetes on contractile properties of rat aorta..... 72

4.3 The role of NO in diabetic vascular dysfunction 73

4.4 The role of the NO/sGC/cGK-I signaling pathway 76

4.5 Vascular ROS production..... 78

4.6 The role of the NAD(P)H oxidase in vascular tissue 81

5 SUMMARY AND CONCLUSION 85

6 ABBREVIATIONS..... 87

7 REFERENCES 89

8 PUBLICATIONS, ABSTRACTS AND PRESENTATIONS 101

8.1 Publications..... 101

8.2 Abstracts..... 103

8.3 Presentations..... 105

1 Introduction

For the body to carry out essential functions like growth, repair, physical activity and maintenance of body temperature, food must be consumed and utilized. This occurs via thousands of different chemical reactions that are all linked to form chains and this network of reactions is encompassed in the term 'metabolism'. One very central metabolic process is the splitting of glucose with the production of ATP (energy), in the absence of oxygen, known as glycolysis. Glucose enters the cell by facilitated diffusion via a family of glucose transporters (GLUT). In skeletal, cardiac and adipose tissue, GLUT4 is the transporter responsible for glucose uptake and a hormone called insulin stimulates this transporter. Insulin is a peptide secreted by the ß-cells of the islet of Langerhans in the pancreas. It is synthesized in the rough endoplasmic reticulum as proinsulin, a folded peptide consisting of an A and a B chain connected by disulfide bonds. The folding of the peptide is facilitated by a connecting peptide (C-peptide), which is detached before proinsulin is secreted via granules as insulin into the bloodstream. The physiological effects of insulin are far reaching and although it is best known for its hypoglycemic effect (by increasing glucose uptake into cells), it can also facilitate cellular K^+ uptake and stimulate both protein synthesis and lipogenesis. Therefore, insulin deficiency can have serious physiological consequences resulting in extracellular glucose excess (hyperglycemia) and intracellular glucose depletion, a situation that has been referred to as 'starvation in the midst of plenty'. The extensive consequence of insulin deficiency is demonstrated in humans where this is associated with a common and serious pathological condition referred to as 'diabetes mellitus'.

1.1 Diabetes mellitus

The World Health Organization estimates that more than 177 million people worldwide suffer from diabetes mellitus, a figure that is likely to double within the next 20 years. The economic and human cost of this disease is devastating. Eighteen million Americans currently have diabetes and the estimated lifetime risk for Americans born in 2000 is 1 in 3. The total cost of diabetes in the United States in 2002 was $132 billion.

Diabetes is the most common cause of blindness among adults, the most common cause of non-traumatic amputations and end-stage renal disease and the sixth most common cause of death. In Germany, every 19 minutes a person with diabetes suffers a heart attack. Yet only limited

knowledge exists about the pathogenesis, the cardiovascular consequences, and the prevention of this disease.

There are two main forms of diabetes:

1.1.1 Type 1 diabetes

Type 1 diabetes, also referred to as insulin-dependent diabetes mellitus (IDDM), accounts for 5-10 % of all cases of diabetes and is due primarily to autoimmune-mediated destruction of ß-cells of the islets of Langerhans of the pancreas. This results in insufficient insulin production to regulate blood glucose levels, resulting in hyperglycemia. It is not known by what mechanisms the autoimmune response is triggered, but it was shown that environmental factors have a particularly powerful influence on the appearance of type I diabetes. Very low rates of type 1 diabetes were found in Asian populations, whereas Finland shows the world's highest incidence [1]. However, other Baltic States like Estonia whose population is ethnically very similar to that of Finland, suffer only a third the incidence. Interestingly, it was recently suggested that macrolides produced by *Streptomyces* species may function as a trigger in genetically susceptible people. These species are ubiquitously present in soil and may be taken up through the diet by infested vegetables [2]. Of note, *Streptomyces* species are the source of streptozotocin, an agent used to produce experimental diabetes in rodents.

It is still not known how to prevent or reverse diabetes type 1 in a sufficiently innocuous manner to be therapeutically useful. Patients suffering from type 1 diabetes are entirely dependent on exogenous insulin. The frequency of this disease is relatively low compared to type 2 diabetes, and although the onset of the disease can occur at any age, this form of diabetes usually strikes children and young adults.

1.1.2 Type 2 diabetes

Type 2 diabetes, also referred to as non-insulin-dependent diabetes mellitus (NIDDM) accounts for over 90 % of diabetic cases worldwide. It usually begins with insulin resistance, a disorder in which the cells do not use insulin properly. As the need for insulin rises, the pancreas gradually becomes overwhelmed and loses its ability to produce insulin. Related disorders include impaired glucose tolerance and impaired fasting glucose. The term metabolic syndrome or syndrome X is used when these disorders go hand in hand with risk factors such as obesity, insulin resistance/hyperinsulinemia, hypertension and dyslipedemia. People with type 2

diabetes are not dependent on exogenous insulin, and although they may require it for control of blood glucose, following a careful diet and exercise program and taking oral medication may be sufficient to control blood glucose levels. Type 2 diabetes is associated with obesity, physical inactivity, family history of diabetes and race/ethnicity. Although this disease occurs more frequently in the elderly there is, as a result of our changing lifestyles, an alarming increase in type 2 diabetes in children. It is most pronounced in non-European populations (Native American, Pacific Islands, Australian Aboriginals), while Asia shows the highest potential for increases in people with type 2 diabetes.

1.1.3 Clinical manifestation of diabetes

An essential clinical symptom of diabetes is a capillary blood glucose level of >110 mg/dl after overnight fasting. Type 1 diabetes is also associated with polyuria, polydipsia and weight loss, while symptoms of type 2 diabetes are often more unspecific and include headaches, increased tiredness and increased infections, and often diabetic complications (see below) may be the first warning signs.

Vascular disease is the main etiology for death and for a great percent of morbidity in patients with diabetes. Diabetes affects both small vessels (microangiopathy) and large vessels (macroangiopathy). Diabetic microangiopathy includes retinopathy, which is the leading cause of blindness, neuropathy which leads to erectile dysfunction and a sensory loss and damage to limbs with subsequent amputation, and nephropathy resulting in renal failure. Macroangiopathy is manifested by atherosclerosis, which, by a complex mechanism, results in the narrowing of the vessel lumen and presents the leading cause of cardiovascular disease and stroke. Cardiovascular disease accounts for about 50 % of all deaths among people with diabetes, and risk factors include high blood pressure, high serum cholesterol, obesity and smoking.

Other complications of diabetes are peridontal diseases, ketoacidosis and hyperosmolar coma.

1.2 Endothelial (dys)function

1.2.1 The endothelium

Endothelial cells line the internal lumen of vessel walls and serve as an interface between the circulating blood and the underlying vascular smooth muscle cells (SMC). The endothelial cells, however, are no longer considered a simple mechanical barrier between blood and tissue.

Chemical mediators secreted by endothelial cells are important in regulating both vascular tone (nitric oxide ($^{\bullet}$NO), endothelin-1, thromboxane A_2, endothelium-derived hyperpolarizing factor (EDHF)) and blood fluidity (tissue plasminogen activator, prostacyclin (PGI_2)) and play a key role in vascular cell growth (platelet derived growth factor, angiotensin II) and inflammation (adhesion molecules). The correct interplay between these endothelium-derived vasoactive substances is fundamental for maintaining vascular homeostasis. However, the balance can be disturbed due to the strategic, yet vulnerable position of the endothelium at the blood/vessel wall interface, making it a target organ for damaging effects of cardiovascular risk factors such as chronic smoking, hypertension, hyperlipidemia and diabetes, eventually leading to atherosclerosis.

1.2.2 Normal endothelial function and vasorelaxation

1.2.2.1 The NO/cGMP pathway

Probably the most significant and widely studied vasoactive substance regulating vascular tone is the endothelium-derived relaxing factor (EDRF) discovered by Furchgott and Zawadzki in 1980 [3] and identified by Palmer et al [4] to be $^{\bullet}$NO. $^{\bullet}$NO has potent anti-atherosclerotic properties and works in concert with PGI_2 to inhibit platelet aggregation [5]. It also inhibits the attachment of neutrophils to endothelial cells and the expression of adhesion molecules. In high concentrations, $^{\bullet}$NO can inhibit the proliferation of smooth muscle cells [6].

A simplified scheme of the $^{\bullet}$NO signaling pathway involved in vasodilation is shown in Fig. 1.1. Endogenous $^{\bullet}$NO is produced from the conversion of L-arginine to L-citrulline by nitric oxide synthase (NOS) in the presence of molecular oxygen and NADPH. NOS contains both flavin adenine dinucleotide (FAD) and flavin mononucleotide (FMN) and requires the cofactor tetrahydrobiopterin (BH_4) for $^{\bullet}$NO formation. Three isoforms of NOS have been identified. NOS-I (nNOS, isolated from brain) and NOS-III (eNOS, isolated from endothelial cells) are termed constitutive NOS, produce nanomolar levels of $^{\bullet}$NO and are regulated by Ca^{2+}-calmodulin. In response to certain stimuli (shear stress, achetylcholine), eNOS produces $^{\bullet}$NO, which is known to be the most potent endogenous vasodilator in the body. NOS-II (iNOS, isolated from macrophages) is Ca^{2+}-calmodulin independent and is termed the inducible NOS, activated only under pathophysiological situations in which macrophages exert cytotoxic effects in response to cytokines.

•NO produced in the endothelium diffuses to the underlying vascular smooth muscle cells where it activates the soluble guanylate cyclase (GC). The GC enzyme, which converts GTP to 3',5'-cyclicGMP (cGMP) and pyrophosphate, consists of two families, namely the membrane bound or particulate GCs (pGC) and the soluble GCs (sGC). Various subtypes of pGC have been identified of which pGC-A is found in the vasculature as well as in heart, kidney and spleen. pGC-A is activated by two cardiac hormones released into the bloodstream, namely atrial natriuretic peptide (ANP) and B-type natriuretic peptide (BNP), which modulate blood pressure [7]. sGC is a heme protein and an obligate heterodimer consisting of α and ß subunits and is activated by small gaseous molecules like •NO and carbon monoxide (CO). The binding of •NO to the iron (FeII) of the heme group within the enzyme results in its activation, while full activation of the enzyme requires thiols like cysteine or glutathione. CO, which is a reaction product of the breakdown of heme by hemoxygenase (HO), has also been shown to stimulate sGC, however it is about 40-100 times less potent and efficacious than •NO [8].

Activation of sGC results in the hydrolysis of GTP to form the second messenger cGMP. The effects of cGMP are mainly mediated through cGMP-dependent protein kinases (cGK) but also by modifying the function of cGMP-gated cation channels and certain phosphodiesterases (PDE). The cGK can, through different mechanisms, lower the intracellular calcium concentration leading to the dephosphorylation of the myosin light chain and thus to the relaxation of the vessel wall. Type I cGK (cGK-I) is thought to modulate •NO-induced relaxation, as acetylcholine (ACh)-induced endothelium-dependent vasorelaxation was completely abolished in cGK-I knockout mice [9]. A validated substrate for cGK-I is the vasodilator-stimulated phosphoprotein (VASP), a protein localized at actin filaments, focal adhesions and dynamic membrane regions which is expressed in platelets, endothelial cells and smooth muscle cells [10]. VASP can be phosphorylated at 3 distinct sites (serine239, serine157 and threonine278) by both cGK-I and cAMP-dependent kinases (cAK) with overlapping specificity and efficiency. However, cGK-I preferentially phosphorylates serine239 (VASP phosphorylation on ser239), while cAK prefers serine157. The VASP phosphorylation on ser239 was shown to be a reliable marker of the activity of the NO/cGMP/cGK pathway in both animal models of endothelial dysfunction [11, 12] and in humans [13].

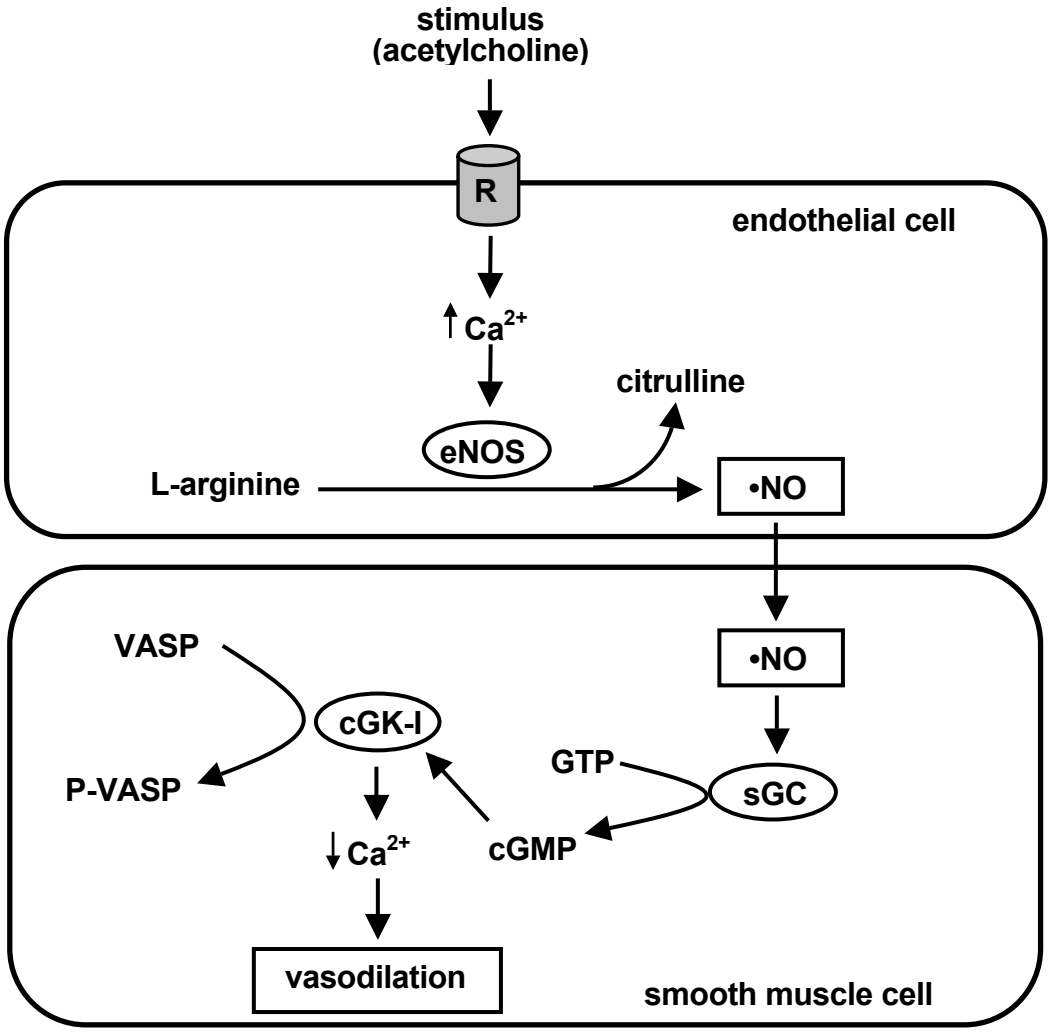

Fig. 1.1. Scheme showing the regulation of vascular tone via the NO/cGMP pathway. eNOS: endothelial nitric oxide synthase, cGK-I: cGMP-dependent protein kinase-I, •NO: nitric oxide, R: receptor, sGC: soluble guanylyl cyclase, VASP: vasodilator stimulated phosphoprotein. For details see text section 1.2.2.1.

1.2.2.2 The arachidonic acid/cAMP pathway

Eicosanoids are a group of signaling substances that include prostaglandins (PG), thromboxanes and leukotrienes and the regulation of their production is crucial in maintaining vascular tone. Their production is initiated by the release of arachidonic acid from membrane bound phospholipids by phospholipase A_2 (see Fig 1.2. for scheme). Arachidonic acid produces eicosanoids by three different groups of enzyme. Firstly, it is converted to PGH_2 by PGH_2-

synthase. This enzyme is rate limiting and has both cyclooxygenase (cox) activity (incorporating two molecules of oxygen into arachidonic acid to form PGG_2) and peroxidase activity (catalyzing a 2 electron reduction of PGG_2 to form PGH_2). PGH_2-synthase is therefore also referred to as cox and two known isoforms exist (cox-1 and cox-2). While cox-2 is considered the inducible form, cox-1 is constitutively expressed but may also be induced, for example by shear stress [14].

While PGH_2 in itself can bind to smooth muscle cells and cause vasoconstriction, it may be further metabolized via 3 major pathways: In endothelial cells and smooth muscle cells, PGI_2-synthase converts PGH_2 to PGI_2 which is a strong vasodilator and inhibitor of platelet aggregation while in platelets, PGH_2 is converted by thromboxane synthase to form thromboxane A_2, which promotes vasoconstriction and platelet aggregation. PGH_2 may also be converted by various endoperoxidases to form other prostaglandins (PGE_2, PGF_2, PGD_2).

An important mediator of PGI_2-induced vasodilation is the second messenger cAMP, which is formed from ATP by the G-protein-coupled activation of adenylate cyclase. cAMP activates protein kinase A and regulates the flow of calcium through ion channels. This results in the lowering of the intracellular calcium concentration leading to the dephosphorylation of the myosin light chain and thus to the relaxation of the vessel wall.

Arachidonic acid may also be converted by lipoxygenases to 5-hydroperoxyeicosatetraenoic acid (5-HPETE), which is the precursor of leukotrienes, which in turn are mediators of allergic responses and inflammation. Finally, arachidonic acid may be converted to several epoxyeicosatrienoic acids (EETs) and hydroxyeicosatetraenoic acids (HETEs) by cytochrome P450 (CYP) monooxygenase. This is a group of more than 300 enzymes expressed primarily in the liver, however some isoforms have been localized in vascular smooth muscle cells and endothelium. Recently, the EETs formed by the CYP-2C family were postulated to be the putative endothelium-derived hyperpolarizing factor (EDHF). This factor is thought to mediate the NO/PGI_2-independent component of endothelium-dependent vasorelaxation observed in coronary, mesenteric and renal arteries. In fact, CYP 2C was described as an EDHF synthase in coronary arteries [15].

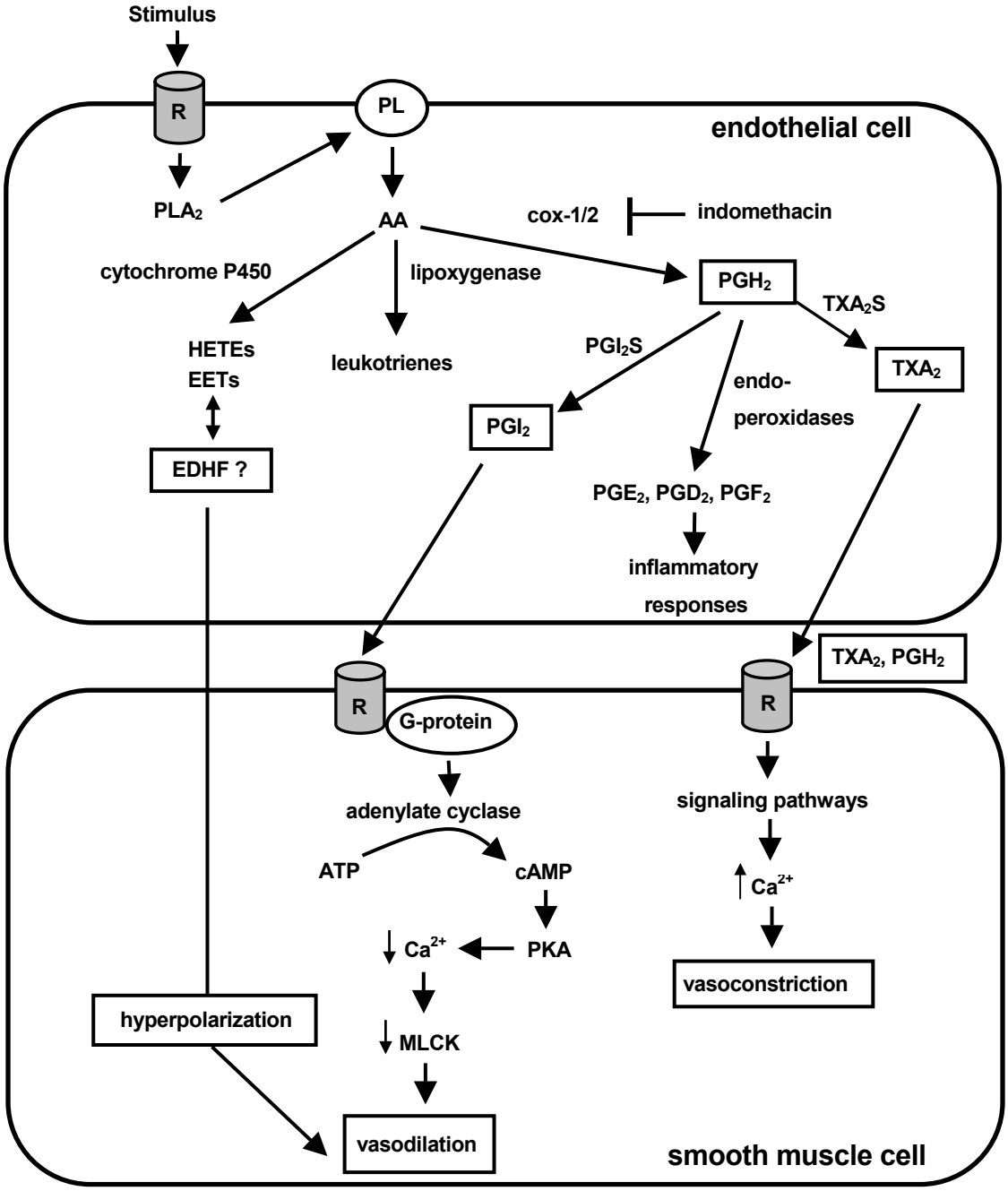

Fig. 1.2. Scheme showing the regulation of vascular tone by the arachidonic acid pathway. EDHF: endothelium-derived hyperpolarizing factor, MLCK: myosin light chain kinase, PGI_2S: prostacyclin synthase, PKA: protein kinase A, PL: phospholipids, PLA_2: phospholipase A_2, R: receptor, TXA_2S: thromboxane A_2 synthase. For detailed description see text, section 1.2.2.2.

1.2.3 Endothelial dysfunction

As discussed above, the most widely recognized function of endothelial cells pertains to the regulation of vascular tone and is therefore characterized by an imbalance of endothelium-derived relaxing and contracting factors. Traditionally, the term 'endothelial dysfunction' is used to describe the impairment of endothelium-dependent relaxation in response to endothelium-dependent vasodilators such as ACh. Endothelial dysfunction is an early hallmark of pathological disorders and risk factors associated with atherosclerosis, including hypertension, diabetes, hyperlipidemia, chronic smoking and familiar disposition. Recent studies show that endothelial dysfunction assessed in coronary and peripheral arteries predict long term progression of atherosclerosis and prognosis in patients with coronary artery disease, peripheral vascular disease and hypertension [16]. The mechanisms underlying endothelial dysfunction are multifactorial and include alterations in the arachidonic acid pathway, the NO/cGMP/cGK signaling pathway, changes in the activity/expression of eNOS and decreased vascular $^{\bullet}$NO bioavailability due to increased production of reactive oxygen species (ROS) (see below). Due to its important anti-atherosclerotic properties, in any condition where an absolute or relative $^{\bullet}$NO deficit is encountered, the process of atherosclerosis is initiated or accelerated.

1.3 Oxidative stress and endothelial dysfunction

1.3.1 Reactive oxygen species (ROS)

The term "oxidative stress" refers to a condition in which cells are subjected to excessive levels of reactive oxygen species, called ROS, either due to increased formation of these species or due to an imbalance between reactive oxygen species and antioxidant defense systems. ROS are highly reactive molecules that are characterized either by the presence of unpaired electrons (i.e. they are radicals) such as the superoxide anion ($O_2^{\bullet -}$), the hydroxyl radical ($^{\bullet}$OH) and singlet oxygen ($O_2{}^1\Delta g$), or by its high reactivity towards oxidizable targets due to their electron acceptor properties, such as hydrogen peroxide (H_2O_2), hypochlorite (OCl^-), ozone (O_3), and peroxinitrite ($ONOO^-$) (see Fig.1.3. for scheme).

$O_2^{\bullet -}$ is formed by one electron reduction of oxygen by a variety of oxidases that take reducing equivalents from NADPH or NADH (or from xanthine/hypoxanthine in the case of xanthine oxidase). Because it is an anion, it has a limited permeability through cell membranes. Furthermore, it is even more unstable than $^{\bullet}$NO and disproportionates very rapidly and

spontaneously into molecular oxygen and H_2O_2. Its intracellular target range is therefore limited to close proximity of its source. Under physiological conditions, its lifespan and range of action is further limited by superoxide dismutase (SOD). This enzyme exists as 3 isoforms, occuring either extracellularly (ecSOD), in the cytoplasm (Cu/ZnSOD) or in the mitochondria (MnSOD) and accelerates the spontaneous decay of $O_2^{\bullet-}$ to form H_2O_2 and O_2. However, under pathological conditions, $O_2^{\bullet-}$ may react with $^{\bullet}NO$ (with a reaction rate that is about 3 times faster than the dismutation reaction with Cu/Zn SOD) to form the potent oxidant **$ONOO^-$**. $ONOO^-$ initiates both DNA single strand breakage and lipid peroxidation and it may nitrate and/or oxidize amino acid residues in proteins such as tyrosine or cysteine, which affects many signal transduction pathways.

H_2O_2 is not a free radical; however, it is an oxidant that can serve as a second messenger. It has a longer half-life than $O_2^{\bullet-}$ and can diffuse longer distances and is thus able to influence signaling events at more distant sites. It is thought to propagate its signal by oxidizing active site cysteine residues. If not degraded by catalase or glutathione peroxidases it can, in the presence of metals such as copper (Cu^+) or iron (Fe^{2+}), lead to the production of the hydroxyl radical **$^{\bullet}OH$** (Fenton reaction). This is the most reactive oxygen free radical and unspecifically oxidizes all target molecules within its reach. Therefore, $^{\bullet}OH$ is not regarded as a signaling molecule.

Some ROS are ideal signaling molecules since they are rapidly generated, highly diffusible, easily degradable and ubiquitously present in all cell types. They are important for the normal functioning of the cell; however, excessively high levels of ROS cause damage to cellular proteins, membrane lipids, and nucleic acids. This may lead to controlled (apoptosis) or uncontrolled (cytolysis) cell death.

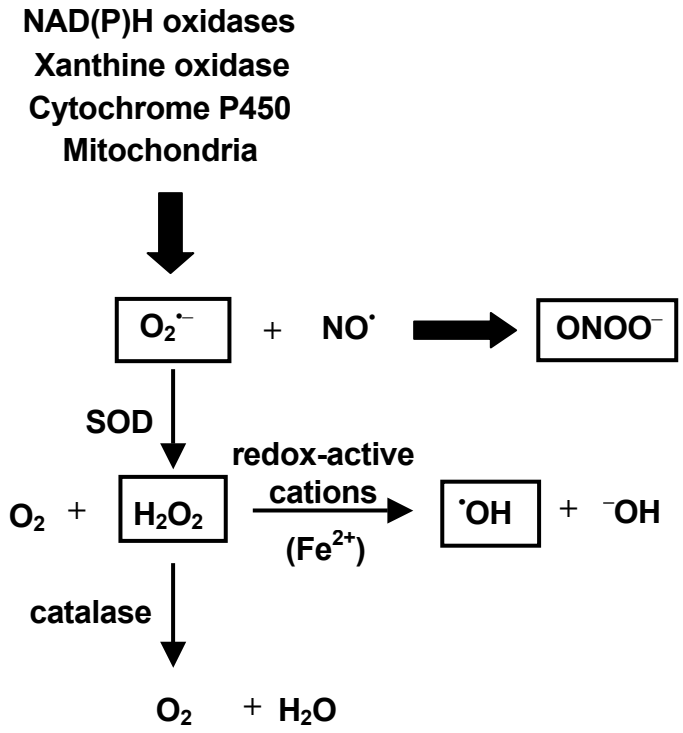

Fig. 1.3. Scheme showing the formation of reactive oxygen species (ROS) that may play a role in causing oxidative stress, leading to endothelial dysfunction.

1.3.2 Enzymatic ROS sources

Oxidoreductases are enzymes that catalyze redox reactions and they form the major source of $O_2^{\bullet-}$. Enzymes that play an important role in ROS production in the vasculature include the following:

Xanthine oxidase (XO), which is a biochemically modified form of xanthine dehydrogenase, catalyzes the oxidation of hypoxanthine and xanthine to uric acid with the concomitant formation of $O_2^{\bullet-}$ and H_2O_2. The dehydrogenase form uses NAD^+ rather than oxygen as electron acceptor and therefore does not produce ROS. XO activity is the greatest in liver and intestine but is also found in endothelial cells.

Cytochrome P450 (CYP) monooxygenases are membrane bound, heme-containing oxidases found primarily in the liver. Apart from the group of CYP that metabolizes arachidonic acid (see section 1.2.2.2), these enzymes oxidize, peroxidize and/or reduce cholesterol, vitamins, steroids and xenobiotics in an oxygen and NADPH-dependent manner. However, during their reaction cycle, CYP enzymes can generate $O_2^{\bullet-}$, H_2O_2 and $^{\bullet}OH$ (by transferring electrons to the active bound oxygen instead of the central heme iron). Because these enzymes have been shown to exist in endothelial and smooth muscle cells, their ROS production may play a significant role in increasing oxidative stress within the vascular wall. Indeed, Fleming et al. [17] could show that the isozyme CYP 2C9 was a functionally significant source of ROS in coronary arteries.

The **mitochondrial respiratory chain** (in particular complex III and IV) can be another source of ROS. This can occur through electrons, which leak from the electron transport chain and reduce oxygen to form $O_2^{\bullet-}$. Although the percentage of electrons, which leak from the normal pathway is quite low (1-2%), mitochondria can, because of their high overall activity, produce considerable amounts of ROS. However, due to the high concentrations of MnSOD within the mitochondria, the $O_2^{\bullet-}$ levels are kept low and only H_2O_2 permeates the membrane to enter the cytosol.

The **NAD(P)H oxidases** are a group of plasma membrane-associated enzymes that have best been studied in neutrophils. They catalyze the production of $O_2^{\bullet-}$ by the one-electron reduction of oxygen, using NADPH as the electron donor:

$$\mathbf{2O_2 + NADPH \rightarrow 2O_2^{\bullet-} + NADP^+ + H^+}$$

The enzyme consists of five components (see Fig.1.4.): $p22^{phox}$ and $gp91^{phox}$ (phox for PHagocyte OXidase) are membrane associated and form the heterodimeric flavohemeprotein known as cytochrome b558. Together, these subunits form the catalytic component of the oxidase. $p47^{phox}$, $p67^{phox}$ and $p40^{phox}$ are found in the cytosol. Upon activation of the enzyme, $p47^{phox}$ becomes phosphorylated and together with $p67^{pox}$ and $p40^{phox}$ translocates to the membrane where it associates with cytochrome b558 to form the active enzyme complex. Activation of the enzyme also requires the small molecular weight guanine nucleotide-binding protein rac-1/2 that binds GTP and migrates to the membrane along with the core cytosolic complex. The exact function of each subunit has been the subject of much research. $p47^{phox}$ is

mainly responsible for transporting the cytosolic complex to the membrane, but needs to be extensively phosphorylated by protein kinase C to do this. $p67^{phox}$ is thought to stabilize rac that in turn seems to be essential for membrane translocation. $p40^{phox}$ was recently shown to be phosphorylated by protein kinase C, this however, resulted in an inhibition of the oxidase activity [18]. Neutrophil NADPH oxidase activation results in the release of large amounts of $O_2^{\bullet-}$ in the so-called 'oxidative burst', which plays an important part in host defence against microbial infection. However, the last years have established the existence of a family of non-phagocytotic oxidases that share many characteristics with that of the NADPH oxidase found in neutrophils. These oxidases have been identified in many cell types including endothelial cells [19], smooth muscle cells [20] and adventitial fibroblasts [21]. To date, a non-phagocyte NAD(P)H-oxidase is thought to be the major source of ROS production in the vascular wall. Although it is structurally similar to that found in the neutrophils, vascular smooth muscle cells of large arteries lack the catalytic moiety $gp91^{phox}$. Recently, two novel homologues of $gp91^{phox}$ (also referred to as nox2) have been identified in these cells, namely nox1 and nox4 (nox for non-phagocytic oxidase) [22, 23]. Both nox1 and nox4 mRNA was also detected in endothelial cells and fibroblasts, but only nox1 mRNAs were detectable in inflammatory cells [24]. Overexpression of nox1 in fibroblasts and nox4 expression in the kidney increased superoxide production [22, 25], while in adipose cells H_2O_2 production was increased [26], indicating that these NAD(P)H-oxidase subunits are functionally important.

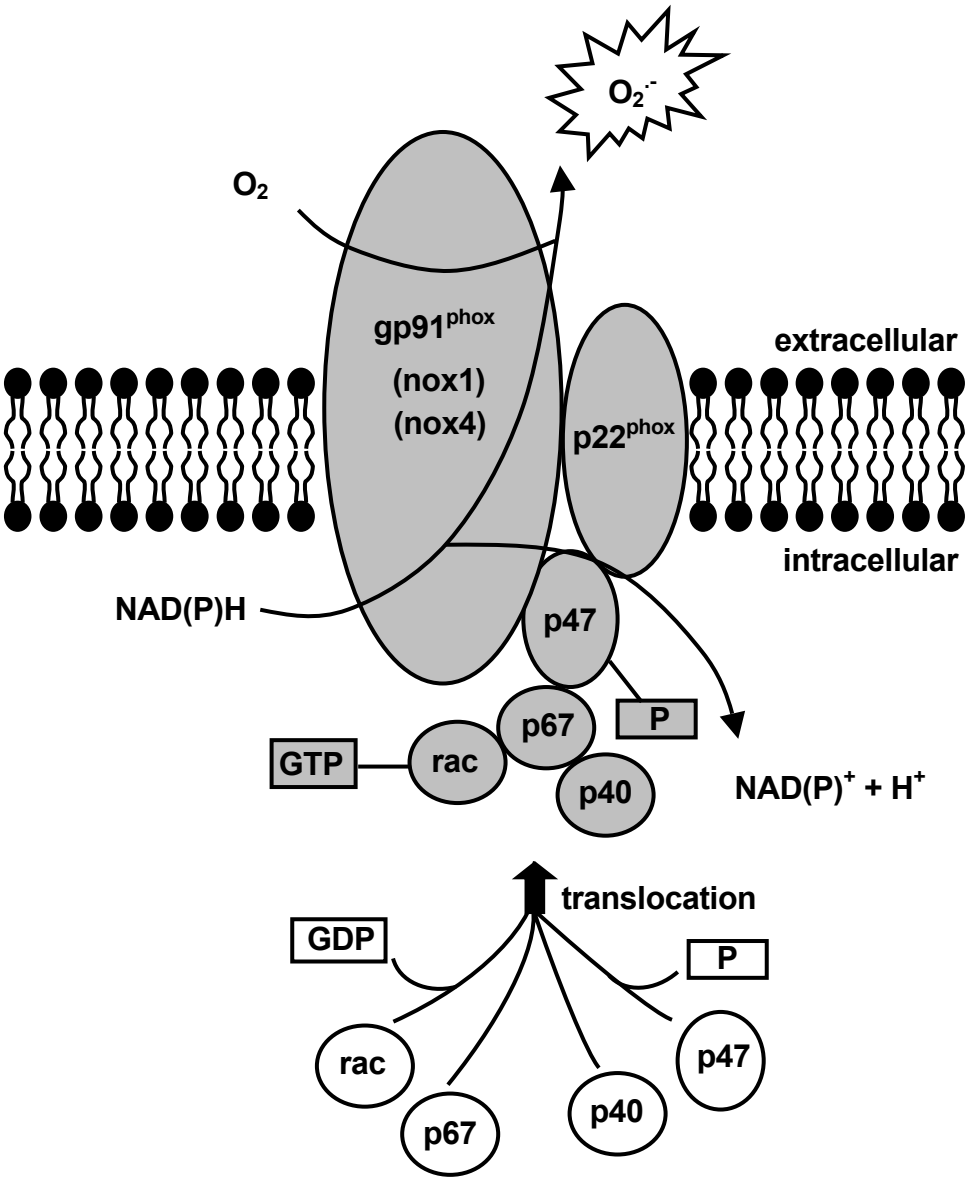

Fig. 1.4. Structure of the neutrophil NAD(P)H-oxidase. The cytosolic subunits translocate to the membrane to form the active enzyme complex (shaded area), which then reduces molecular oxygen (O_2) to form $O_2^{\bullet-}$. The catalytic subunit $gp91^{phox}$ is lacking in smooth muscle cells but instead these cells express the homologues nox1 and nox4. P= phosphorylation. For details see text, section 1.3.2.

1.3.3 ROS, endothelial dysfunction and diabetes mellitus

Abnormal endothelial function in the setting of diabetes has been documented in animal models as well as in humans (for review see [27]). Although the underlying mechanisms are still unclear, ROS seem to play a crucial role in the pathogenesis of this disease, shown by studies in humans where administration of vitamin C was able to correct endothelial dysfunction [28, 29]. The mechanisms by which diabetes can lead to hyperglycemia-induced oxidative stress are multifactorial [27] (see Fig. 1.5. for scheme) and include the following:

1.3.3.1 Advanced glycosylation end products (AGE)

ROS in diabetes may be the result of the non-enzymatic interaction of glucose with the amino side chains on proteins or lipoproteins (in particular lysine) leading, through a series of oxidative and non-oxidative reactions, to the irreversible formation of Schiff-bases called advanced glycosylation end products (AGE), or Maillard products. Some of the individual AGE are formed in reactions of proteins with glucose only under oxidative conditions and these are termed glycoxidation products. AGE can accumulate in tissue over time and can either on their own or via their receptors (RAGE), found on endothelial cells, smooth muscle cells and macrophages, inactivate enzymes by altering their structure and function, thus promoting ROS formation. In particular, the glycosylation of low-density lipoproteins (LDL) can decrease its receptor-mediated clearance and increase the susceptibility of LDL to oxidative modification. This increases its uptake by macrophages resulting in foam cells, an early step in the development of atherosclerosis. AGE have also been shown to quench endothelial derived $^{\bullet}$NO [30-32]. However, the role of AGE in endothelial dysfunction is controversial and several authors found no beneficial effect of the AGE inhibitor aminoguanidine on endothelium-dependent vasodilation [33, 34], showing that AGE are unlikely to interfere with vascular smooth muscle cell reactivity.

1.3.3.2 Polyol pathway

In tissue that does not require insulin for cellular glucose uptake such as blood vessels, hyperglycemia activates the polyol pathway in which aldose reductase reduces the aldehyde form of glucose to form sorbitol. Because this reaction requires NADPH, an increase in the polyol pathway flux may result in the depletion of cellular NADPH, which is a cofactor for many enzyme including NOS and the antioxidant glutathione reductase. Sorbitol is then

oxidized to fructose by the enzyme sorbitol dehydrogenase, while NAD^+ is reduced to NADH. It was proposed that the most likely mechanism by which this pathway induces oxidative stress is due to decreased regeneration of reduced glutathione, as a result of the depletion of the NADPH stores. However, blocking the sorbitol pathway with aldose reductase inhibitors improved peripheral nerve conduction but had little effect on diabetic retinopathy, indicating that this may not be an important pathway in diabetic microvasculopathy [35].

1.3.3.3 Activation of protein kinase C

Another glucose induced alteration in cellular metabolism that may play a role in endothelial dysfunction is the activation of protein kinase C (PKC) [36]. Activation of PKC has now been demonstrated in all vascular tissue involved in diabetic complications [37]. In vascular tissue, hyperglycemia causes the de novo synthesis of diacylglyerol (DAG), the physiological activator of PKC, mainly through the glycolytic pathway. Incubation of endothelial cells and smooth muscle cells with high glucose concentrations was shown to increase intracellular DAG levels, leading to PKC activation [38]. Tesfamarin et al. demonstrated that incubation of aortic rings with high glucose caused endothelial dysfunction, which was reversed by simultaneous incubation of the tissue with the PKC inhibitor H2222 [39]. In addition, the PKC inhibitor LY333531 prevented the hyperglycemia induced reduction in endothelium-dependent vasodilation in humans [40]. The activation of PKC can regulate many cellular function including vascular permeability, contractility, cellular proliferation and signal transduction mechanisms. A common denominator for these abnormalities may be the formation of ROS. Although the ability of PKC to induce ROS is well established [41, 42], the mechanisms by which PKC induces vascular dysfunction remain unclear. There is a growing body of evidence showing that PKC mediates the phosphorylation of eNOS, thereby reducing the activity of the enzyme [43]. Furthermore, the activity of the superoxide producing enzyme NAD(P)H-oxidase (see section 1.3.3.4) was shown to increase in a PKC-dependent manner in response to glucose [41], while in vessels from diabetic patients the NAD(P)H-oxidase derived $O_2^{\bullet-}$ production was abrogated by the PKC-inhibitor chelerythrine [44].

Finally, in vitro studies have shown that in addition to PKC-mediated activation of $O_2^{\bullet-}$ producing-enzymes, $O_2^{\bullet-}$ per se is an activator of PKC, leading to increased oxidative stress in a positive feedback manner [45].

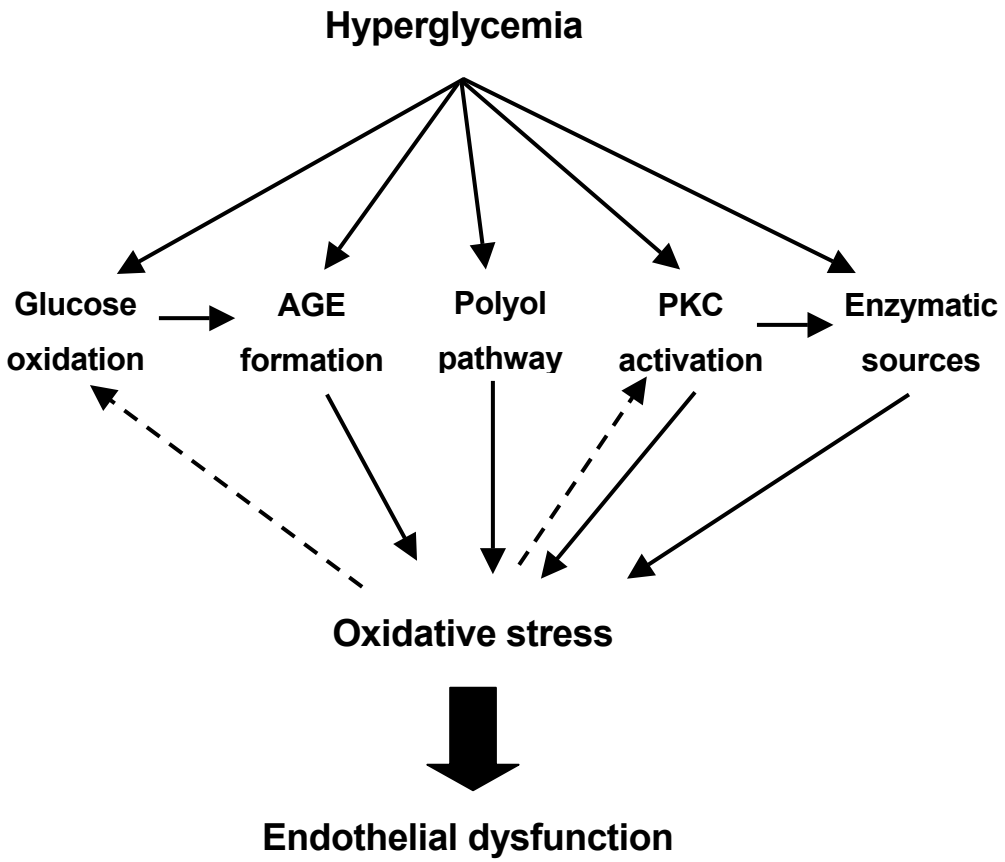

Fig. 1.5. Scheme showing the hyperglycemia-induced pathways that may be involved in the pathophysiology of endothelial dysfunction. The dashed lines indicate positive feedback mechanisms.

1.3.3.4 Enzymatic superoxide production

Other sources of excess ROS generation in the setting of hyperglycemia may be ascribed to the increased activity of several $O_2^{\bullet-}$ producing enzymes:

The enzyme **NOS** can become uncoupled under certain pathophysiological conditions. This happens when the cofactor BH_4 is oxidized to BH_2 so that electrons flowing from the reductase domain to the oxygenase domain are diverted to molecular oxygen rather than to L-arginine, with the resulting formation of $O_2^{\bullet-}$. Furthermore, $ONOO^-$ may, at low concentrations, disrupt the zinc-thiolate complex within the catalytic site of NOS, thereby uncoupling the enzyme [46].

The uncoupled NOS thus turns into an $O_2^{\bullet-}$ producing enzyme, with a concomitant decrease in $^{\bullet}NO$ production. Evidence for the existence of a dysfunctional, uncoupled NOS in diabetes is given by studies in animal models [47] and human diabetes [44, 48].

Desco et al. [49] showed that in a rat model of type 1 diabetes, there was an increased release of **xanthine oxidase** (XO) from the liver into the plasma. The binding of XO to the glucosaminoglycans on endothelial cells can result in increased local $O_2^{\bullet-}$ formation, as observed in aortic rings of these animals. This was restored by administration of heparin, which releases XO from the vessel wall. In addition, endothelial dysfunction in hypertensive diabetic patients was improved by acute inhibition of XO by oxypurinol [50]. Moreover, increased levels of XO were found in the plasma of diabetic mice, concomitant with increased $O_2^{\bullet-}$ levels, which were restored with oxypurinol [51].

A link between **mitochondria** and oxidative stress in the setting of diabetes was found by Brownlee et al [52] who showed that hyperglycemia-induced ROS production in bovine aortic endothelial cells was abrogated by inhibitors of the mitochondrial respiratory chain or by overexpression of either uncoupling protein-1 (UCP-1: an uncoupler of oxidative phosphorylation) or the mitochondria specific MnSOD. Furthermore, this group showed that normalizing mitochondrial ROS production blocked three pathways of hyperglycemic damage: it prevented the glucose induced activation of PKC, formation of AGE and sorbitol accumulation [52].

The **NAD(P)H-oxidase** is known to be the major source of ROS in the vascular wall and any dysfunction could play an important role in maintaining vascular tone. Kim et al. could show an increase in rac-1 membrane translocation associated with an increased NAD(P)H-oxidase activity in aortic smooth muscle cells cultured in high glucose medium [53]. This group also found an upregulation of $p22^{phox}$ mRNA in the aorta of OLETF rats, a model of type 2 diabetes [54]. Furthermore, in the saphenous veins and mammary arteries of diabetic patients, the expression of the NAD(P)H-oxidase subunits $p22^{phox}$, $p67^{pox}$ and $p47^{phox}$ was increased, again associated with an increase in the activity of the enzyme [44].

1.4 Aim of the study

Despite the overwhelming evidence of endothelial dysfunction in diabetes, there are reports in animal models of both enhanced [55-57] and unaltered [58, 59] endothelium-dependent relaxation. Moreover, there are discrepancies with regard to the time of onset of endothelial dysfunction in rat models of diabetes: 1 week in intestinal arterioles [60], 2 weeks in hindquarters but not femoral arteries [61], 4-6 weeks in mesenteric arteries [62] or 4 weeks in aorta [63]. These differences may be explained by the fact that the mechanism of endothelium-dependent vasodilation may be distinct, depending on the vascular preparation of the study. This is illustrated by the presence of impaired vasodilation in vivo in the mesenteric circulation or in the isolated perfused mesentery of diabetic rats and by its absence in the isolated aorta of the same animal [64].

In addition, studies show that the alterations in endothelial function seen in the setting of diabetes seem to be transient. In aortas from spontaneously diabetic rats, the relaxation response to ACh was enhanced at 12 weeks but decreased at 36 weeks of age [65]. In contrast, Pieper [66] found an enhanced ACh relaxation of rat aorta 24h after induction of diabetes, no change at 1-2 weeks and an impaired relaxation at 8 weeks. Interestingly, patients in early uncomplicated stages of diabetes type 1 show increased blood flow in tissues prone to vascular complications such as the kidney [67] and retina [68] as well as in skin [69]. Thus, Wascher et al. [70] suggested the possibility that endothelial dysfunction in type 1 diabetes is a transient phenomenon, however the mechanism underlying this chronology remains unclear. It is difficult to reconcile the divergent data concerning the endothelium-dependent vasoreactivity in diabetes, mainly because of the different experimental conditions used with regard to type of animal model, type of vascular bed studied, type and doses of diabetogenic agent administered, duration of the disease and type of vasodilator used.

Thus, the purpose of this study was to shed more light on the vascular consequences of early (2 weeks) and late (8 weeks) stage diabetes, in particular with respect to oxidative stress, endothelial (dys)function and the NO/sGC/cGK-I signaling pathway, using a well established model of type 1 diabetes, the streptozotocin (STZ)-induced diabetic rat [71].

2 Materials and Methods

2.1 Materials

2.1.1 Chemicals

[^{32}P]cGMP	NEN
2-Mercaptoethanol	Promega
Acrylamide/bis (40% solution)	BioRad
Ammonium persulfate	BioRad
Cantharidin	Biomol
Coelenterazine	Calbiochem
DAN (2,3-diaminonaphthaline)	Sigma
Dihydroethidium	Molecular Probes
Heparin (Liquemin® N 2500)	Roche
L-012	WAKO
Lucigenin	Sigma
Mounting medium (Vectashield)	Vector Labs
Nitroglycerin (Nitrolingual®)	Pohl-Boskamp
O.C.T.™ compound	SAKURA
Phosphate buffered saline	Gibco
Pre-stained Protein Ladder (BenchMark™)	Invitrogen
Protease Inhibitor for General Use	Sigma
Protein Ladder (BenchMark™)	Invitrogen
Streptozotocin	Sigma

All other chemicals were of highest purity grade purchased from either Sigma, Merck or Alexis.

2.1.2 Kits and Assay Solutions

BioRad Protein Assay Standard II	BioRad
BioRad Protein Assay	BioRad
cAMP enzymeimmunoassay (EIA)	Amersham
cGMP enzymeimmunoassay (EIA)	Amersham
ECL™ Western Blotting Detecting Reagents	Amersham

2.1.3 Antibodies

Alexa Fluor 594 labeled goat anti-mouse antibody	Molecular Probes
Anti-mouse IgG, horseradish peroxidase labeled	Vector
Anti-rabbit IgG, horseradish peroxidase labeled	Vector
Anti-sheep IgG, horseradish peroxidase labelled	Upstate

For a list of primary antibodies see Table 2.1.

2.1.4 Consumables

Autoradiography films (Biomax MR)	Kodak
Cryotube™ vials (2 ml)	Nunc
Haemo-Glukotest 20-800R test strips	Roche
Microcon® YM-30 filter device	Millipore
Microscope slides (SuperFrost®Plus)	Menzel-Gläser
Nitrocellulose membrane (Protran®)	Schleicher&Schuell
Serum clotting tubes (7.5ml) (S-monovette®)	Sarstedt

2.1.5 Instruments

Amplifier (Mac-Lab/8^{e})	ADSystems
Blotting apparatus (Mini-Trans-Blot transfer cell)	BioRad
Camera (Retiga 1300)	QImaging
Centrifuge (R5810)	Eppendorf
Cryostat (Frigocut 2800)	Reichert-Jung
Electrophoresis apparatus (Mini-PROTEAN 3)	BioRad
EPR Spectrometer (MiniScope 200)	Magnettech
Film processor (Curix 60)	Agfa
Lumat LB 9507	Berthold
Microscope (Leica DML)	Leica
Modular Automatic Analyzer	Roche
Power supply (PowerPac 3000)	BioRad
Reflolux® S glucose monitoring system	Roche
Scanner (Epson GT-9600)	Biometra
Scintillation counter Packard 1900	Packard

Spectrophotometer for 96-well plates (MRX TC Revelation)	Dynex Technology
Spectrophotometer for cuvettes (DU-640)	Beckmann
Thermomixer comfort	Eppendorf
Ultracentrifuge (Discovery M120)	Sorvall

2.1.6 Software

Chart 4.0	ADSystems
IPLab 3.6	Scananalytics
ScanPack 3.0	Biometra
SimgaStat 1.0	Jandel Scientific

2.2 Methods

2.2.1 Animals

The present study was performed in accordance with the guidelines for animal experimentation at the University Hospital Eppendorf, Hamburg, Germany.

Male Wistar rats (Charles River, Sulzfeld, Germany), 8 weeks of age and weighing 250-300 g were anesthetized with diethyl ether. The rats were placed on their sides and the tails were briefly inserted into warm water to dilate the vein. A single dose of STZ (70 mg/kg body weight) in 0.1 M citrate buffer was injected into the tail vein in a total volume of 0.5 ml. The animals were allowed to recover and received a standard chow and water ad libitum. 24 h after STZ injection and at the time of sacrifice, blood glucose levels were monitored with a Reflolux® S meter using Haemo-Glukotest 20-800R test strips (Roche, Mannheim, Germany). Animals were divided into two groups: one group of animals was sacrificed 2 weeks after STZ injection and the other group 8 weeks after STZ injection. These groups are hereafter referred to as the '2 week treatment group' and the '8 week treatment group', respectively.

Citrate buffer: *0.1M Citric acid (A)*

0.1M Trisodium citrate (B)

add solution A to solution B until pH is 4.5

2.2.2 Tissue preparation

Animals were sacrificed between 7 and 9 a.m. by an overdose of diethyl ether. Body weights were recorded. Each animal was cut open longitudinally from the abdomen to the thorax, cutting through the ribcage on either side. Blood was rapidly drawn into a 10 ml syringe by cardiac puncture and transferred into serum clotting tubes. Blood glucose levels were determined. To prevent blood clotting, heparin (1000 I.U in 1 ml saline) was injected into the heart after blood withdrawal. After resection of the lung and heart, the aorta was excised in one piece, dissecting from the bifurcation of the common iliac arteries to the end of the aortic arch. Care was taken not to exert tension on the aorta, which was immediately placed into a tube containing ice cold Krebs-HEPES buffer. The heart was removed into a tube containing the same buffer.

The tissue and blood was swiftly transported to the laboratory where the aortas were trimmed of adhering fat and connective tissue while being kept moist with ice cold Krebs-HEPES solution. The aortas were divided into the thoracic and abdominal sections by cutting near the coeliac axis. In order to ensure an undamaged and intact endothelial layer, care was taken not to exert unnecessary pressure or tension on the tissue. The aortas were carefully flushed free of residual blood, cut into rings of various sizes and were either stored on ice until further analysis or shock-frozen in liquid nitrogen and stored at -80 ^{o}C. For some experiments it was necessary to remove the endothelium and this was achieved by repeatedly turning the aortic rings over curved forceps.

Tubes containing blood samples were centrifuged at 2000*g* for 10 min at 4 ^{o}C. Aliquots of serum were transferred into cryotubes, shock-frozen in liquid nitrogen and stored at -80 ^{o}C for further analysis.

Krebs-HEPES buffer:

99 mM NaCl
4.69 mM KCl
2.5 mM $CaCl_2$
1.2 $MgSO_4$
25 mM $NaHCO_3$
1.03 mM K_2HPO_4
20 mM HEPES
11.1 mM Glucose
pH 7.35

2.2.3 Isometric tension studies

From the trimmed aorta (see section 2.2.2) rings of equal size (0.5cm) were cut with a scalpel. Each ring was mounted on a pair of stainless steel hooks. The hooks were used to mount the ring in the organ chamber by fixing the lower hook to a support while the upper hook was connected by a wire thread to a force transducer which continuously recorded the contractile tension of the ring. The mounted ring was surrounded by an all-glass chamber filled with Krebs buffer. To prevent the formation of prostaglandins, 10 μM indomethacin was added to the buffer. The buffer was constantly aerated with a gas mixture consisting of 95 % O_2, 5 % CO_2. The overflow side-arm on each chamber set the volume of buffer in the chamber at 25 ml. The chamber was also connected to a reservoir and pump for washing purposes. The buffer was maintained at 37 ^{o}C by a circulating water bath that pumped water through the outer jackets of the glass chambers. Any change in isometric tension of the rings was transmitted via the transducer to an amplifier (Mac-Lab/8e) and was digitally converted to a signal that could be registered on a computer. Signals were analysed using the Chart 4.0 software (ADSystems, Chalgrove, UK).

The initial mounting tension of each ring was set at 0.4 g. Over the next 30-60 min, the tension was progressively increased to an optimal resting tension of 3 g. Next, the maximum tension of the rings was determined with a KCl dose-response curve obtained by the cumulative addition of KCl to give final concentrations of (mM) 5, 10, 20, 40 and 80. The resulting maximum tension was set as 100 % and KCl was washed out. It was then necessary to produce a steady level of contraction of the rings before adding the relaxing agent. This was done by the addition of 1 mM phenylephrine, a dose that caused 30-50 % constriction with respect to the maximal contraction achieved with KCl.

After preconstricting with phenylephrine, the endothelium-dependent relaxation of the rings was determined by the cumulative addition of ACh to the chambers in steps of 0.5 log units to give final concentrations of 10^{-9} to $10^{-5.5}$ M. To test the endothelium-independent relaxation, either nitroglycerin (NTG) or sodium nitroprusside (SNP) was cumulatively added to the chambers in steps of 0.5 log units from 10^{-9} to $10^{-4.5}$ M and 10^{-5} M, respectively. Finally, the vasodilation obtained with each dose of relaxing agent was expressed as percent of the maximum response to phenylephrine.

To determine the response of aortic rings to vasoconstrictors we used dose-response curves for KCl (see above) and phenylephrine (from 10^{-9} to 10^{-5} M). Vasoconstrictor responses were expressed as the change in g tension recorded.

Krebs buffer: *118.3 mM NaCl*
4.69 mM KCL
1.87 mM $CaCl_2$
1.2 mM $MgSO_4$
1.03 mM K_2HPO_4
25.0 mM $NaHCO_3$
11. 1 mM Glucose
pH 7.4

2.2.4 Determination of angiotensin converting enzyme (ACE) activity in serum

ACE activity was determined by the Department of Clinical Chemistry at the University Hospital Eppendorf. The assay is based on the hydrolysis of the substrate FAPGG (N-[3-(2-furyl)acryloyl]-L-phenylalanyl-glycylglycine) by ACE present in the serum sample, resulting in a decrease in the absorbance at 340 nm which is detected spectrophotometrically by a Modular Analyzer (Roche, Mannheim, Germany).

2.2.5 Protein measurements according to the method of Bradford

Protein measurements were performed with the BioRad Protein Asssay (BioRad, Munich, Germany) based on the Bradford method [72]. Protein samples of unknown concentration (5 µl) were added to 795 µl of dH_2O in a clean test tube. A standard curve was prepared from a bovine albumin stock (0.1 mg/ml) (BioRad Protein Standard) to give final concentrations of (µg/ml) 0, 0.5, 1, 2, 4, 6, 8, and 10. To each standard, 5 µl of solvent, used in the preparation of the unknown samples was added. Finally, 200 µl of Dye Reagent Concentrate was added to each tube to give a final volume of 1 ml. All samples were mixed, allowed to stand for 10 min and the optical density at 595 nm was measured in a spectrophotometer DU-640 (Beckmann, Krefeld, Germany). Unknown protein concentrations were calculated from the standard curve.

2.2.6 sGC activity of aortic homogenates

Shock-frozen aortic segments were homogenised in liquid nitrogen using a mortar and pestle, resuspended in lysis buffer (250 mg homogenate in 1 ml buffer, 10 mM TrisHCl, pH 7.8, 0.25 M sucrose, 5 mM $MgCl_2$, 200 µM EGTA, 1 mM dithiothreitol (DTT), 2 mM benzamidine

and 10 µg/ml leupeptin) and cleared by centrifugation at 13,000*g* for 30 min. GC activity was assessed on the basis of the formation of [^{32}P]cGMP. 10 µg protein extract was incubated at 37 °C for 10 min in buffer containing 15 mM TrisHCl, pH 7.4, 3 mM $MgCl_2$, 1.5 mg/ml creatine phosphate, 0.1 mg/ml creatine phosphokinase, 0.9 mg/ml glutathione, 0.5 mM isobutylmethylxanthine (IBMX), 1 µM SOD, 0.5 mM DTPA, 0.03 mM L-NNA, 0.1 mM GTP and 0.1 mM cGMP. In some cases, 100 µM SNP was added for maximal stimulation of NO-sensitive sGC. Reactions were started by the addition of [α-^{32}P]GTP (0.1 µCi). The reaction was stopped by adding 0.4 ml zinc acetate (120 mM) and 0.5 ml sodium carbonate (125 mM) and the sample was centrifuged at 10,000*g* for 10 min. Supernatant (800 µl) was loaded onto aluminium oxide chromatography columns (ICN, Eschwege, Germany) and prewashed with 100 M perchloric acid. The columns were flushed twice with 5 ml of water and [^{32}P]cGMP was eluted with 5 ml 0.5 M TrisHCl, pH 8. The radioactivity was determined in a scintillation-counter. Specific sGC activity was expressed as nmol cGMP formed per min per mg protein.

2.2.7 cGMP/cAMP enzymeimmunoassay (EIA) of aortic tissue

The cGMP and cAMP content of aorta was determined using the respective Biotrak EIA kit (Amersham Pharmacia, Freiburg, Germany). Aortic segments (0.5 cm) were preincubated in Krebs-Hepes buffer (see section 2.2.2) at 37 °C for 20 min in the presence of 0.5 mM IBMX, a phosphodiesterase inhibitor. To stimulate the production of cyclic nucleotides, ACh (40 nM) or SNP (100 nM) was added for 5 min followed by immediate shock-freezing of the tissue in liquid nitrogen. Frozen tissue was pulverized in liquid nitrogen using a mortar and pestle and resuspended in assay buffer (supplied in the kit) containing 0.1 mM IBMX. The samples were left on ice for 30 min with occasional mixing, followed by centrifugation at 10.000*g* for 10 min. The supernatant was removed and the protein content determined by the method of Bradford (see section 2.2.5). Each same sample was used for the determination of both cGMP and cAMP.

Each EIA was performed according to the instructions supplied by the manufacturer. Briefly, 2 µg protein (for cGMP determination) and 5 µg protein (for cAMP determination) was diluted in 1 ml of Assay Buffer and samples were acetylated with a solution consisting of 1 volume acetic anhydride and 2 volumes triethylamine. 100 µl of antiserum (rabbit anti-cGMP or cAMP) was added to a 96 well plate pre-coated with donkey anti-rabbit IgG. 50 µl of either sample or standard (known amount of cGMP or cAMP) was added to each well and the plate was incubated at 4 °C for 2 hours. After the addition of 100 µl of cGMP- (cAMP) peroxidase

conjugate to all wells, the plate was incubated for a further 1 hour at 4 °C. All wells were washed thoroughly, the TMB enzyme substrate was added and the plate was incubated for 30 min at room temperature. The reaction was stopped by the addition of 100 µl sulphuric acid (1 M) and the optical density was read at 450 nm in a spectrophotometer (MRX TC Revelation, Dynex Technology, Germany). The amount of cGMP or cAMP was calculated from a standard curve generated from known amounts of cyclic nucleotide.

2.2.8 Cryosectioning of aortic rings

Aortic rings (0.5 cm) were placed upright into a small cup formed out of aluminium foil containing O.C.T.™ compound. The cup containing the ring was carefully immersed into a pentane-containing beaker submerged in liquid nitrogen which resulted in the rapid freezing of the tissue. Frozen, O.C.T.™-embedded tissue was stored at -80 °C until further use. Cryosections were cut with a cryostat (Frigocut 2800, Reichert-Jung, Bensheim, Germany) at -25 °C at a thickness of 6 µm and were transferred onto SuperFrost®Plus microscope slides (Menzel-Gläser, Germany). These slides were either used directly or were stored for up to 2 weeks at -80 °C.

2.2.9 Oxidative fluorescent microtopography

Enzymatically intact cryosections (see section 2.2.8) were incubated with the superoxide-sensitive fluorescent dye dihydroethidium (DHE) (1 µM) and incubated for 30 min at 37 °C in a humidity chamber. The reaction was stopped by placing the slides at 4 °C for 30 min. Slides were coverslipped and kept in the dark until the fluorescence (absorbance: 518 nm, emission: 605 nm) was detected using a Leica DML microscope equipped with a Retiga 1300 camera (QImaging, Burnaby, Canada) and images were recorded using the IPLab 3.6 software (Scananalytics ,Virginia, USA) .

DHE stock:	*1 mM in DMSO*
DHE working solution:	*1 µM in phosphate buffered saline (PBS)*

2.2.10 Immunofluorescent histochemistry

Cryosections (see section 2.2.8) were fixed in ice cold acetone at -20 °C for 10 min. Sections were allowed to air-dry and were then rehydrated in PBS for 10 min. To block non-specific binding, slides were incubated for 2 hours at room temperature with PBS containing 0.1 % Triton/10 % goat serum (Sigma, Taufkirchen, Germany). This was followed by an incubation with an anti-eNOS antibody (Transduction, Lexington, KY, USA) diluted in PBS/5 % goat serum to a final concentration of 5 µg/ml, overnight at 4 °C in a humidity chamber. Sections were washed extensively and probed with the fluorescently labeled goat anti-mouse antibody Alexa Fluor 594 (Molecular Probes, Karlsruhe, Germany) for 1 hour at room temperature. After a final washing step, slides were mounted in Vectashield (Vector Laboratories, Peterborough, UK). Fluorescence (absorbance: 585 nm, emission: 610 nm) was detected through a 20x oil objective with a Leica DML microscope equipped with a Retiga 1300 camera (QImaging, Burnaby, Canada) and images were recorded using the IPLab 3.6 software (Scananalytics, Virginia, USA).

PBS: *137 mM NaCl*
2.7 mM KCl
8.3 mM Na_2HPO_4
1.47 mM KH_2PO_4
pH 7.4

2.2.11 SDS-polyacrylamide gel electrophoresis (PAGE) and Western blot analysis

Aortic rings (1 cm) were preincubated at 37 °C for 10 min in Krebs-HEPES (see section 2.2.2) buffer containing the protease inhibitors 10 µg/ml aprotinin, 7 µg/ml pepstatin and 5 µg/ml leupeptin. Tissue was then shock-frozen in liquid nitrogen and homogenized with a mortar and pestle. The powder was resuspended in homogenization buffer containing 1 % Triton-X100 (v/v), 10 µg/ml aprotinin, 5 µg/ml leupeptin, 7 µg/ml pepstatin, 1 µM cantharidin and 0.5 mM PMSF and samples were allowed to stand on ice for 1 hour at room temperature with occasional mixing. Samples were cleared by centrifugation at 10.000*g* for 10 min at 4 °C. The supernatant was removed and its protein content determined by the method of Bradford (see section 2.2.5). Laemmli Sample Buffer (3x) was added to the supernatant (1:2), the sample was denatured for 5 min at 95 °C and stored at -20 °C until further use.

SDS-PAGE was performed using the Mini-PROTEAN 3 electrophoresis cell (BioRad). Cast gels consisted of 10 % or 12 % running and 4 % stacking parts. An equal amount of protein (usually 10-20 µg) was loaded onto each lane. A BenchMark™ Protein Ladder (ranging from 10-220 kDa) (Invitrogen, Karlsruhe, Germany) as well as a BenchMark™ Pre-Stained Protein Ladder (ranging from 10-200 kDa) (Invitrogen, Karlsruhe, Germany) was run on each gel. Gels were run in running buffer at 80-150V until the proteins of interest had separated sufficiently, usually 1.5 h. The gel was removed from the electrophoresis assembly and proteins were transferred from the gel to a Protran® nitrocellulose membrane (Schleicher&Schuell, Dassel, Germany) using the Mini-Trans-Blot transfer cell (BioRad). Blotting was performed at 4 ^{o}C in Blotting buffer at a constant current of 200 mA for 1-2 hours, depending on the size of the proteins of interest.

After the protein transfer was complete, the membrane was cut horizontally into segments, each segment containing one protein of interest. Non-specific binding sites of all segments were blocked overnight at 4 ^{o}C (see Table 2.1. for blocking reagents used). The next morning, each membrane segment was incubated with the antibody against the protein of interest (primary antibody)(see Table 2.1.) for 2 hours at room temperature, with gentle shaking. An antibody against α-actinin was used to verify equal protein loading. Membranes were washed 3 times for 15 min followed by incubation with a horseradish peroxidase-labeled secondary antibody (see Table 2.1.) for 1 hour at room temperature. Again, membranes were washed extensively and then covered for 1 min with ECL™ Western Blotting Detecting Reagent (Amersham Biosciences, Freiburg, Germany) with a final volume of 0.125 ml/cm^2 membrane. After allowing excess fluid to drain off, membranes were covered with sandwich wrap and immediately exposed to autoradiography films (Biomax MR, Kodak, New York, USA) which were developed in a Curix 60 film processor (Agfa, Morstel, Belgium). Bands were scanned with an Epson GT-9600 scanner (Biometra, Munich, Germany) and densitometrically quantified using the ScanPack 3.0 software (Biometra, Munich, Germany).

The nox4 antibody was kindly provided by John F. Keaney Jr (Boston University, MA, USA). It was produced by immunizing rabbits with a synthetic peptide corresponding to residues 140-153 of human nox4 and the antibody was affinity purified. Immunoblotting yielded a band of ~70 kDa that was not present when the antibody was pretreated with competing peptide (ELNAARYRDEDPRK).

Table 2.1. Antibodies and washing buffers used for Western blotting analysis. Membranes were blocked overnight in blocking buffer and blocking reagent as shown. The number shown in brackets corresponds to the concentration of blocking reagent used for the dilution of primary and secondary antibodies. HO-1: hemoxygenase-1; HRP: horseradish peroxidase; HG: hemoglobin; *: kind gift from John F. Keaney Jr, Boston, USA.

Primary antibody/Antigen	Company	Concentration	Secondary antibody/ HRP labeled	Concentration	Washing/ Blocking buffer	Blocking reagent
α-actinin	Sigma	1:5000	rabbit	1:10 000	TBST	1% HG
eNOS	Transduction	1:1000	mouse	1:10 000	TBST	5% (3%) BSA
HO-1	Stressgen	0.2 µg/ml	mouse	1:10 000	TBST	5% (3%) BSA
nox1	Santa Cruz	1 :100	goat	1:10 000	TBST	5% (3%) BSA
nox4	*	1 :1000	rabbit	1:10 000	TBST	5% (3%) BSA
$p67^{phox}$	Transduction	1:500	mouse	1:10 000	TBST	5% (3%) BSA
P-VASP (16C2)	Calbiochem	1.5 µg/ml	mouse	1:10 000	PBSTT	1% HG
sGC	Calbiochem	1:2000	rabbit	1:10 000	TBST	5% (3%) BSA
SOD	Upstate	1 µg/ml	sheep	1:2000	PBSTT	5% (3%) milk

Homogenization buffer: *20 mM Tris-HCL*
250 mM Sucrose
3 mM EGTA
20 mM EDTA
pH 7.5

3x Laemmli Sample Buffer:	*125 µl 1M Tris-HCl (pH 6.8)*
	500 µl SDS (20 %)(w/v)
	300 µl Glycerol
	10 µl Bromophenol Blue (0.25 %) (w/v)
	50 µl 14.3 M 2-Mercaptoethanol
	make up to 1 ml with dH_2O
4 % Stacking gel:	*1.2 ml 0.5 M Tris-HCl (pH 6.8)*
	0.5 ml Acrylamide/bis solution (40 %)
	50 µl SDS (10 %) (w/v)
	50 µl Ammonium persulfate (10 %) (w/v)
	5 µl TEMED
	make up to 5 ml with dH_2O
*10% **(12%)** Running gel:*	*2.5 **(2.5)** ml 1.5 M Tris-HCl (pH 8.8)*
	*2.5 **(3)** ml Acrylamide/bis Solution (40%)*
	*100 **(100)** µl SDS (10 %) (w/v)*
	*100 **(100)** µl Ammonium persulfate (10 %) (w/v)*
	*10 **(10)** µl TEMED*
	make up to 10 ml with dH_2O
Running buffer:	*25 mM Tris-HCl*
	192 mM Glycine
	0.1 % SDS (w/v)
Blotting buffer:	*25 mM Tris-HCl*
	192 mM Glycine
	make up to 800 ml with dH_2O
add:	*200 ml Methanol*

PBSTT:	*150 mM NaCl*
	16 mM Na_2HPO_4
	4 mM NaH_2PO_4
add:	*0.3 % Triton- X100 (v/v)*
	0.05 % Tween-20 (v/v)
TBST:	*20 mM Tris-HCl*
	137 mM NaCl
	pH 7.6
add:	*0.1 % Tween-20 (v/v)*

2.2.12 Chemiluminescent (CL) detection of ROS with lucigenin, coelenterazine and L-012

Aortic segments (0.3 cm) were incubated in Krebs-HEPES buffer (see section 2.2.2) for 30 min either in the presence or absence of 1 mM L-NNA. In some cases segments were preincubated at 37 ^{o}C for 25 min after which ACh (1 µM) was added for 5 min. Segments were carefully removed from the incubation vial and transferred into a tube containing 250 µl of either L-012 (100 µM), coelenterazine (5 µM) or lucigenin (5 µM) in Krebs-HEPES buffer. The CL was immediately determined in a Lumat LB 9507 (Berthold, Bad Wildbad, Germany). Counts were recorded every 30 secs over a time period of 15 min (for L-012 and coelenterazine) and every 1 min over a time period of 10 min for lucigenin. After measurements were completed, the aortic segments were removed from the tube and allowed to air-dry. The dry weight of the segments was determined and results expressed as either relative light units (RLU)/min/mg dry weight or as % of control.

2.2.13 Measurement of NADPH-dependent oxidase(s) activity in membrane fractions of heart and aorta

Tissue was homogenized (glass/glass) in homogenization buffer containing 50 mM Tris-HCl, pH 7.4, 10 mM dithiothreitol (DTT) and a Protease Inhibitor Cocktail for General Use and centrifuged at 2000*g* for 5 min at room temperature. The supernatant was removed and centrifuged at 20,000*g* for 20 min at 4 ^{o}C. Again the supernatant was removed and

centrifuged at 100,000*g* for 60 min at 4 °C. When preparing membrane fractions from aorta, the centrifugation step at 2000*g* was omitted whereby the 100,000*g* step yielded the particulate fraction. The pellet was resuspended in homogenization buffer and further diluted in PBS to give a final protein concentration of 0.5 mg/ml for aortic suspensions and 0.7 mg/ml for heart suspensions and a final DTT concentration of 200 µM. The lucigenin (5 µM)-derived CL of the membrane suspensions was detected in a Lumat LB 9507 (Berthold, Bad Wildbad, Germany) in the presence of 200 µM NADPH. In some cases, rotenone (10 µM), diphenyleneiodonium (DPI) (10 µM), hypoxanthine (1 mM), or NADH (200 µM) was added to the samples. Omitting DTT from the sample had no effect on the lucigenin-derived CL.

2.2.14 Measurement of vascular $^{\bullet}$NO by electronparamagnetic resonance (EPR) spin trapping

Segments of abdominal rat aorta (10 mm) were incubated at 37 °C for 1 h min in 24-well plates in 1 ml Krebs-HEPES buffer (see section 2.2.2). The buffer was exchanged 4x with fresh pre-warmed buffer. The last exchange was done with 750 µl buffer instead of 1ml and either ACh (1 µM) or calcium ionophore A23187 (10 µM) was added in a total volume of 10 µl. This was followed by immediate addition of 250 µl of a colloidal iron diethyldithiocarbamate ($Fe^{II}(DETC)_2$) stock solution (see below). The samples were incubated for 1 h at 37 °C, removed from the solution and transferred with forceps into a 1 ml syringe filled with Krebs-HEPES buffer. The transfer was facilitated by removing the tip of the syringe with a scalpel. The syringe was carefully immersed into liquid nitrogen where it was stored until further use.

On the day of the EPR studies, syringes containing tissue samples were removed from the liquid nitrogen and the frozen sample/buffer pellet was carefully ejected into a Dewar flask (Wilmad, Buena, NJ, USA) filled with liquid nitrogen which was immediately inserted into a table top x-band spectrometer Miniscope S200 (Magnettech, Berlin, Germany). Recordings were made at 77 K and the instrument was set at 10 mW microwave power, 1 mT amplitude modulation, 100 kHz modulation frequency, 60 seconds sweep time and 10 scans. After analysis, samples were allowed to thaw and the area of the tissue was determined.

For quantification of the $^{\bullet}$NO-$Fe(DETC)_2$ formed in the samples, freshly prepared solution containing known amounts of mononitrosyl-iron-N-methyl-D-glucamine dithiocarbamate were used. Results are expressed as pmol $^{\bullet}$NO formed per min per cm^2.

Preparation of the Fe^{II}-$(DETC)_2$ stock solution: Two separate tubes each containing 10 ml of Krebs-HEPES buffer, placed on ice were deoxygenated for 30 min under a flow of nitrogen gas. 3.6 mg Na-DETC was added to one tube and 2.24 mg $FeSO_4.7H_2O$ to the other. Immediately after both substances were dissolved (about 30 secs) the two solutions were poured together and carefully aspirated (without air bubbles) into an Eppendorf combitip. The formed 400 µM Fe^{II}-$(DETC)_2$ colloid stock solution was used immediately.

2.2.15 DAN assay for the detection of nitrite (NO_2^-) and nitrate (NO_3^-) in serum

Frozen serum samples were thawed on ice and centrifuged through a Microcon® YM-30 filter device (Millipore) to remove traces of hemoglobin. To determine serum NO_2^- levels, a standard curve was prepared from KNO_2 in PBS, in the range of 0-10 µM. Serum samples were diluted 1:1 with PBS and 200 µl of standard/sample was mixed with 20 µl of DAN (2,3-diaminonaphthaline) reagent and incubated on a shaker for 30 min at room temperature. To determine both NO_2^- and NO_3^- levels, samples were diluted 1:8 in PBS. Nitrate reductase (0.2 U), FAD (5 µM) and NADPH (45 µM) were added to 200 µl of diluted sample and incubated at 37 ^oC for 30 min. Both samples and standards were incubated with 20 µl of DAN reagent on a shaker for 30 min at room temperature. All reactions were stopped by the addition of 20 µl 3 N NaOH. The fluorescence was detected on a fluorescence plate reader (Twinkle LB 970, Berthold, Bad Wildbad, Germany) using an excitation and emission wavelength of 360 nm and 430 nm, respectively.

DAN stock: *32 mM in DMSO*
DAN reagent: *dilute DAN stock 1:100 in 1 N HCl*

2.2.16 Statistical analysis

Results are expressed as mean±SEM. Data were analyzed using a one-way ANOVA or an unpaired Student's t-test, as appropriate. The EC_{50} values for the isometric tension experiments were obtained by logit-transformation. A Scheffe's post-hoc test was used to examine differences between groups when significance was indicated. P values < 0.05 were considered significant.

3 Results

3.1 Blood glucose levels and body weights

In order to verify a diabetic state in STZ-treated rats, blood glucose levels and body weights were assessed. All rats having received STZ had blood glucose levels >400 mg/dl 24h after injection and >500 mg/dl at the time of sacrifice. This was significantly higher than the blood glucose levels of control animals at the time of sacrifice (170±3.8 mg/dl). Furthermore, the body weights of the diabetic animals were significantly lower compared to the control group (Table 3.1). Because the blood glucose levels of the diabetic animals at the time of sacrifice were outside the detection limit of the instrument, whole blood was in some cases immediately diluted with saline and measured. After correcting for the dilution, these values were consistently found to be between 600 and 700 mg/dl. The diabetic animals were also characterized by polyuria.

Table 3.1. Animal body weights and blood glucose levels. Data are expressed as the mean ± SEM, *p<0.05 compared to controls within same treatment group.

	2 weeks		8 weeks	
	body weight (g)	blood glucose (mg/dl)	body weight (g)	blood glucose (mg/dl)
Control (n=25)	386.2 ± 5.5	177.9 ± 4.4	498.6 ± 7.6	170.0 ± 3.8
Diabetes (n=25)	259.0 ± 7.3 *	>500 *	255.6 ± 7.8 *	>500 *

3.2 Isometric tension studies

This bioassay is used to determine the vasodilatory responses of aortic tissue to physiological and pharmacological substances. To test vessel responses, we used ACh as an endothelium-dependent vasodilator and NTG and SNP as an endothelium-independent vasodilator. Furthermore, we tested the response of aortic rings to the vasoconstrictors phenylephrine (Phe) and KCl.

3.2.1 Vasoreactivity in response to ACh, NTG and SNP

In control aortic rings of the 2 week treatment group, ACh elicited half maximal vasorelaxation (EC_{50}) at (-logM) 7.28±0.05 and maximal relaxation (85.27±3.07 %) at (-logM) 5.5 (Fig. 3.1.). In the diabetic animals, the ACh-induced EC_{50} ((-logM) 7.26±0.05) was not different to that of controls, however the efficacy was significantly increased in the diabetic animals compared to controls (controls: 85.27±3.07 %, diabetes: 92.39±1.31 %; $p<0.05$). In control animals of the 8 week treatment group, ACh induced half maximal vasorelaxation at (-logM) 7.54±0.04. However, in the diabetic animals of this group, the EC_{50} was markedly shifted to the right (-logM) 7.14±0.05, $p<0.05$ compared to controls, and the efficacy (87.14±1.77 %) also decreased significantly compared to that of controls (93.27±0.94 %, $p<0.05$) (Fig. 3.1.).

When the endothelium was removed from the aortic rings, no relaxation was observed in the any of the groups, showing that the vasodilatory effect of ACh is entirely endothelium-dependent (Fig. 3.2.).

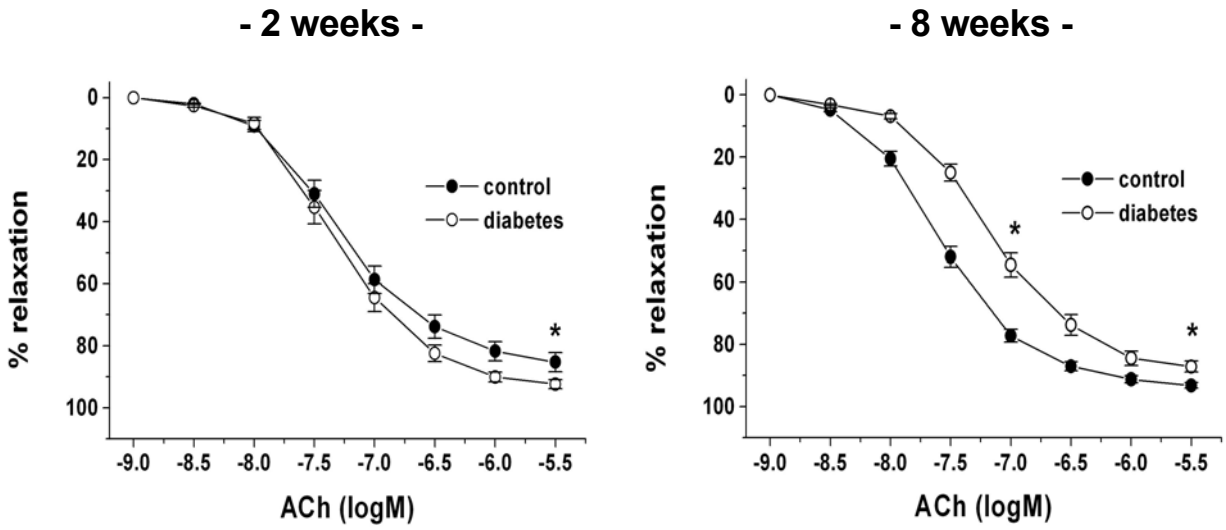

Fig. 3.1. Effect of the endothelium-dependent vasodilator acetylcholine (ACh) on the relaxtion of aortic rings of 2 and 8 week control and diabetic animals. Data are expressed as the mean ± SEM of 14 animals (2 week treatment group) and 30 animals (8 week treatment group), * $p<0.05$ compared to controls.

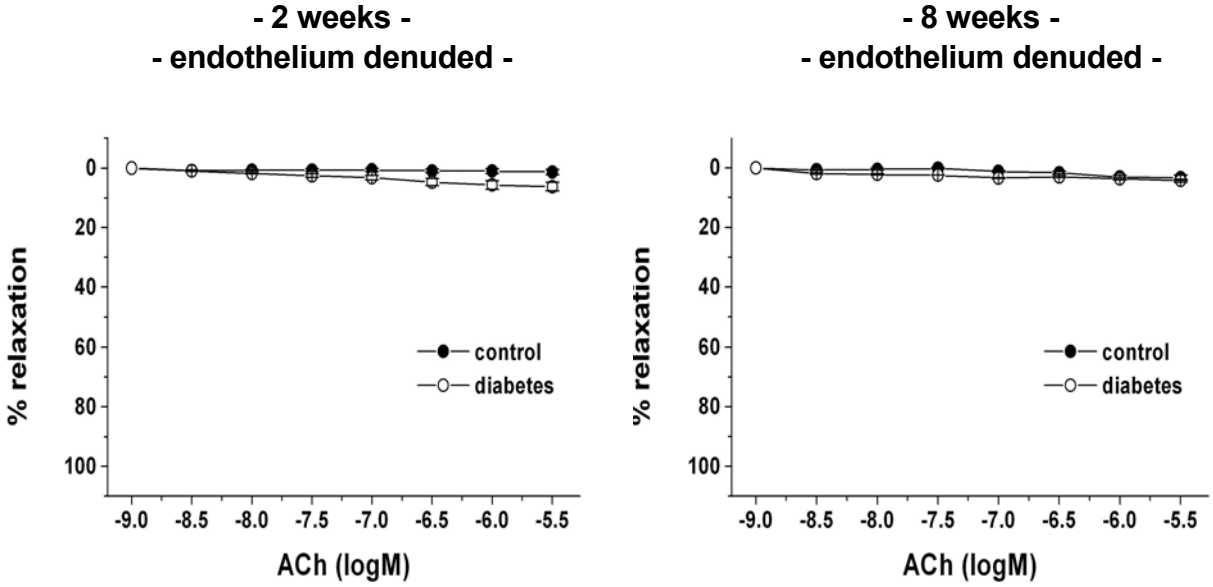

Fig. 3.2. Effect of the endothelium-dependent vasodilator acetylcholine (ACh) on the relaxtion of endothelium-denuded aortic rings of 2 and 8 week control and diabetic animals. Data are expressed as the mean ± SEM of 6 animals per group.

In response to NTG, the control animals of the 2 week treatment group relaxed half maximally at (-logM) 7.49±0.07 with an efficacy of 99.02±0.20 % (Fig. 3.3.). However, in the diabetic animals of this group, half maximal relaxation was significantly enhanced (-logM) 7.74±0.03 compared to controls while the efficacy in these animals (99.62±0.15 %) was not different to that of controls. In the control animals of the 8 week treatment group, NTG elicited half maximal relaxation at (-logM) 7.73±0.03; however, in the diabetic animals of this group, there was a significant shift to the right of the NTG-induced relaxation curve (EC_{50}: (-logM) 7.480.03), pointing towards a possible defect in the ability of SMC to relax (Fig. 3.3). Similar to the 2 week treatment group, we observed no change in the efficacy of NTG in the 8 week treatment group (control: 99.80±0.13 %, diabetes: 99.29±0.24 %).

When the endothelium was removed from the aortic rings, the control animals of the 2 week treatment group relaxed half maximally at (-logM) 7.51±0.06 and this did not differ significantly from the EC_{50} of the diabetic animals ((-logM) 7.58±0.06) (Fig. 3.4.). No differences where observed in the efficacy between control and diabetic animals (controls: 99.75±0.24 %, diabetes: 98.99±0.23 %). In the control animals of the 8 week treatment group, endothelium-denudation resulted in NTG-induced half maximal relaxation at (-logM) 7.64±0.05 and this did not differ significantly from that of the diabetic animals (-logM) 7.57±0.06) (Fig. 3.4.). However, at NTG concentrations of $10^{-6.5}$ to $10^{-5.0}$ M, we observed a significant rightward shift of the NTG-induced relaxation curve in the diabetic animals compared to controls.

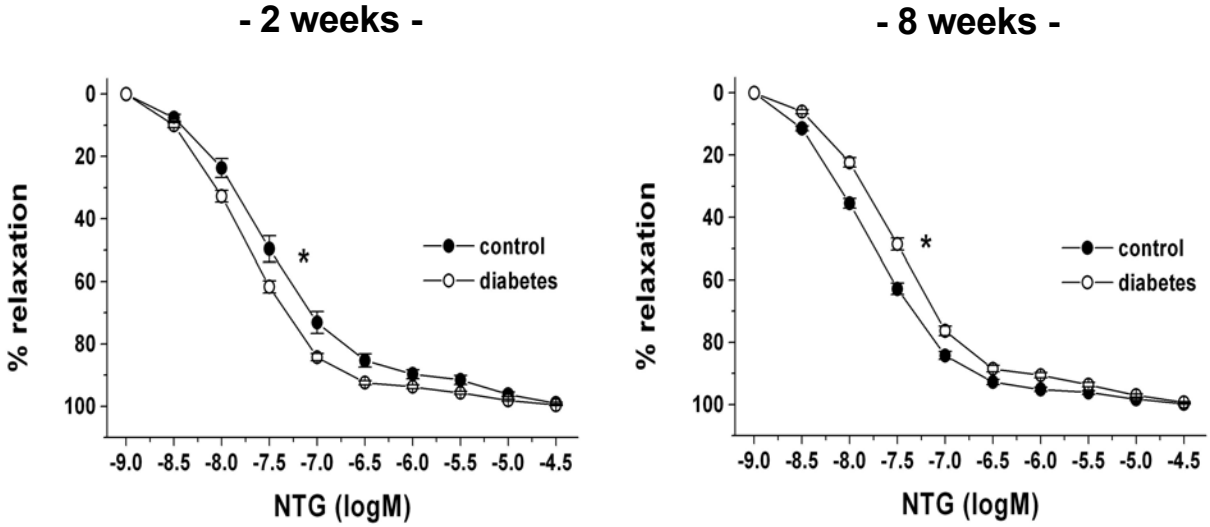

Fig. 3.3. Effect of the endothelium-independent vasodilator nitroglycerin (NTG) on the relaxtion of aortic rings of 2 and 8 week control and diabetic animals. Data are expressed as the mean ± SEM of 14-16 animals per group, EC_{50} * $p<0.05$ compared to controls.

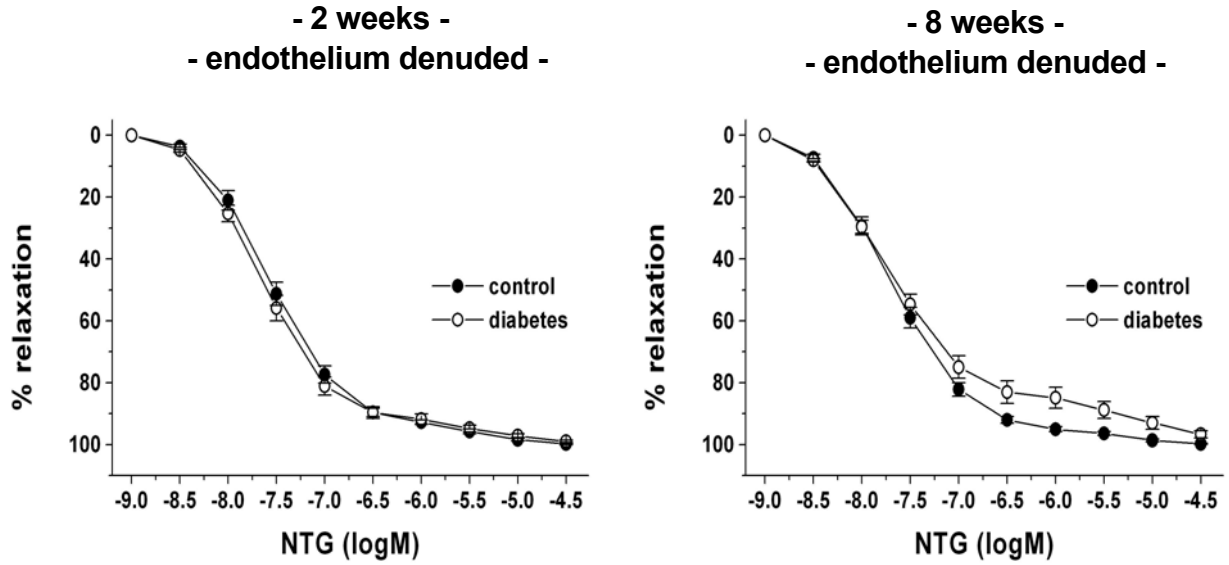

Fig. 3.4. Effect of the endothelium-independent vasodilator nitroglycerin (NTG) on the relaxtion of endothelium-denuded aortic rings of 2 and 8 week control and diabetic animals. Data are expressed as the mean ± SEM of 6 animals (2 week treatment group) and 20 animals (8 week treatment goup).

In the 2 week treatment group, the $^{\bullet}$NO donor SNP elicited half maximal relaxation to a similar extent in both the control ((-logM) 8.15±0.01) and diabetic ((-logM) 8.11±0.01) animals (Fig. 3.5.) and there was no difference in the efficacy (control: 100 %, diabetes 100 %). However, in the control animals of the 8 week treatment group, SNP induced half maximal relaxation at (-logM) 8.52±0.057 and this was slightly but significantly shifted to the right in the diabetic animals ((-logM) 8.34±0.036) (Fig. 3.5.). Again, there was no difference in the efficacy of SNP in this group (control: 100 %, diabetes 100 %) (Fig. 3.5.).

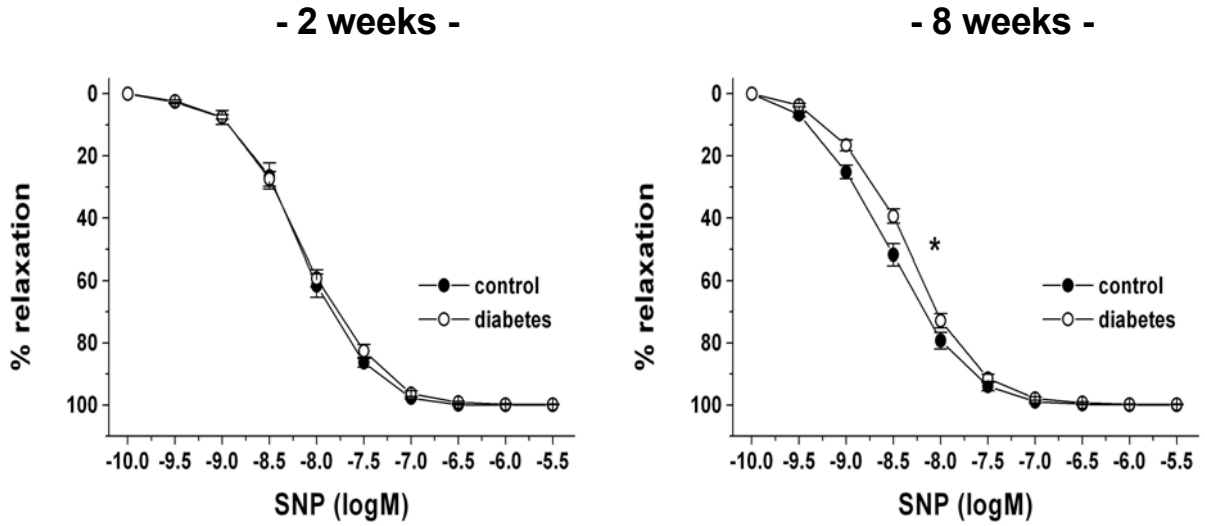

Fig. 3.5. Effect of the endothelium-independent vasodilator sodium nitroprusside (SNP) on the relaxtion of aortic rings of 2 and 8 week control and diabetic animals. Data are expressed as the mean ± SEM of 8-10 animals per group, EC_{50} * $p<0.05$ compared to controls.

3.2.2 Vasoreactivity in response to KCl and phenylephrine

In order to test the receptor-independent vasocontractile capability of aortic rings, we established the dose response curve to KCl. In aortic rings of control animals of the 2 week treatment group, KCl elicited half maximal contraction at 29.63 mM ($logEC_{50}$: 1.472±0.015) with an efficacy of 5.39±0.21 g. In the diabetic animals of this group, the half maximal response was significantly reduced (33.32 mM) ($logEC_{50}$: 1.523±0.014, $p<0.05$ vs control), as was the efficacy (4.26±0.18 g, $p<0.05$ vs control) (Fig. 3.6.). In the control animals of the 8 week treatment group, half maximal contraction was similar to that of the 2 week treatment group (29.49 mM ($logEC_{50}$: 1.470±0.035)) as was the efficacy: 5.08±0.16 g. However, the diabetic animals of this group showed a marked reduction in half maximal contraction compared to controls (36.07 mM ($logEC_{50}$: 1.56±0.023), $p<0.05$) while the efficacy was also significantly attenuated (3.66±0.2 g, $p<0.05$ vs controls). Furthermore, the efficacy of the diabetic animals of the 8 week treatment group was significantly reduced compared to that of

the diabetic animals of the 2 week treatment group (2 weeks: 4.26±0.18 g, 8 weeks: 3.66±0.2 g, $p<0.05$) (Fig. 3.6.).

When the endothelium was removed from the aortic rings, the control animals of the 2 week treatment group showed a half maximal contraction at 14.87 mM ($logEC_{50}$: 1.173±0.031) which was not significantly different from that of the diabetic animals of this group (17.32 mM ($logEC_{50}$: 1.238±0.0189)) (Fig. 3.7.) Furthermore, there was no difference in the efficacy of KCl between control (5.32±0.49 g) and diabetic (4.70±2.7 g) animals. However, in the diabetic animals of the 8 week treatment group, endothelium denudation caused a further decrease in vasoconstrictor response to KCl as compared to the already reduced vasoconstriction observed with intact endothelium (Fig. 3.7.) (half maximal response: control: 18.61 mM ($logEC_{50}$: 1.27±0.031), diabetes: 22.73 mM ($logEC_{50}$: 1.357±0.026), $p<0.05$; efficacy: control: 7.12±0.32 g, diabetes: 4.41±0.43 g, $p<0.05$).

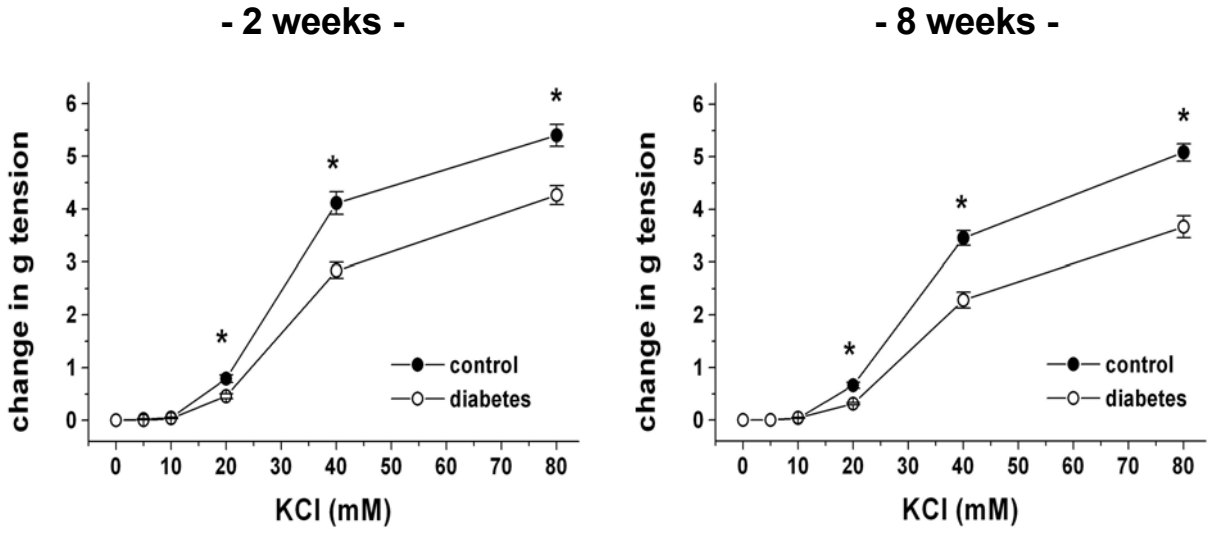

Fig. 3.6. Effect of KCl on the vasoconstriction of aortic rings of 2 and 8 week control and diabetic animals. Data are expressed as the mean ± SEM of 38 animals per group, * $p<0.05$ compared to controls.

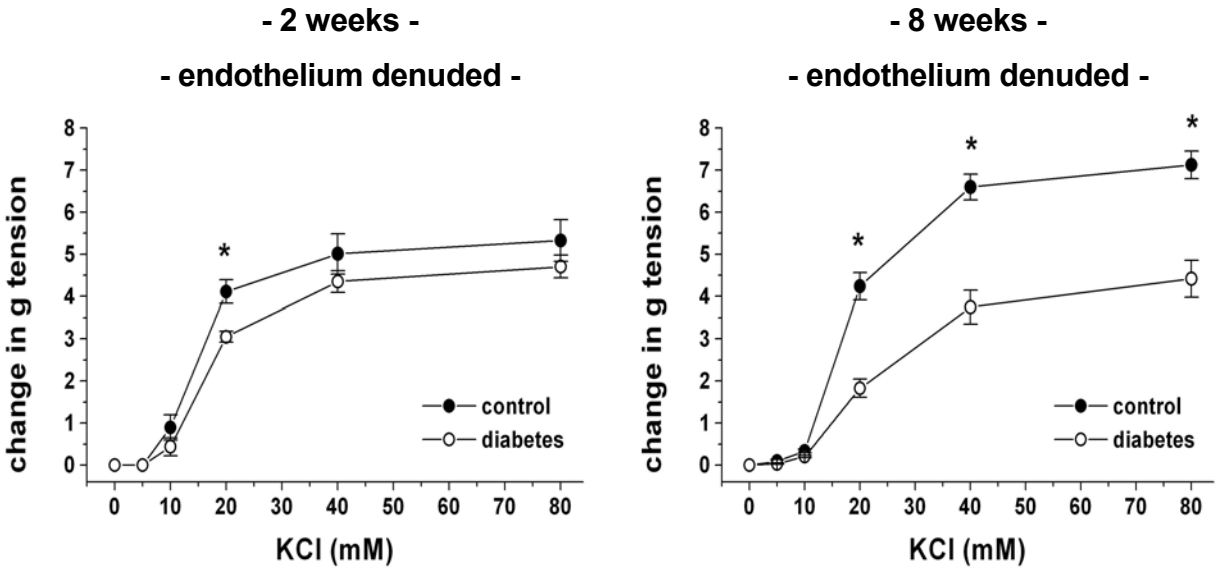

Fig. 3.7. Effect of KCl on the constriction of endothelium-denuded aortic rings of 2 and 8 week control and diabetic animals. Data are expressed as the mean ± SEM of 8 animals per group, * $p<0.05$ compared to controls.

In order to assess the α_1-adrenergic receptor stimulated vasoconstrictor response, we used Phe. In control aortic rings of the 2 week treatment group, Phe elicited half maximal vasoconstriction at (-logM) 6.98±0.04, with an efficacy of 4.29±0.27 g (Fig. 3.8.). These responses were not different from those of the diabetic animals of this group (EC_{50}: (-logM) 7.07±0.03) and efficacy: 4.19±0.16 g. In the control animals of the 8 week treatment group, we observed Phe-induced half maximal contraction at (-logM) 6.83±0.06 with an efficacy of 3.58±0.35 g. In the diabetic animals of this group, the half maximal contraction was shifted slightly but not significantly to the left (EC_{50}: (-logM) 7.03±0.04) compared to controls, which may point towards a tendency of increased hypersensitivity of the SMC to contracting stimuli. The efficacy of Phe in the diabetic animals of this group (3.66±0.1 g) was similar to that of controls (3.58±0.35 g) (Fig. 3.8.).

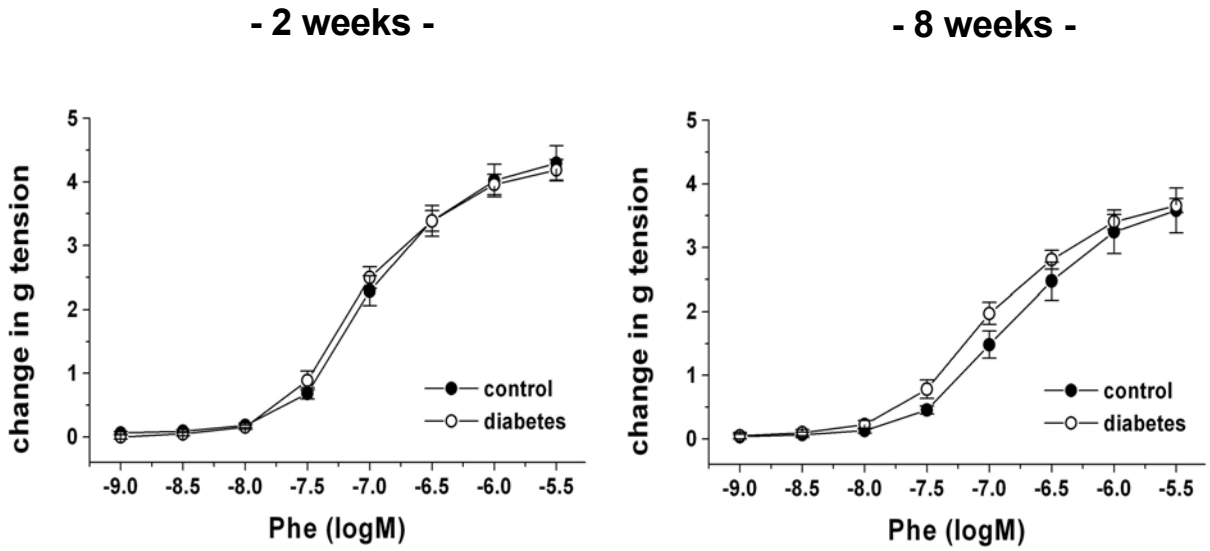

Fig. 3.8. Effect of phenylephrine (Phe) on the constriction of aortic rings of 2 and 8 week control and diabetic animals. Data are expressed as the mean ± SEM of 10 animals per group.

3.3 ACE activity in serum

Because of the observed positive effects of ACE inhibitors and angiotensin II receptor blockade on the etiology of micro- and macrovascular disease, the renin/angiotensin system is thought to play a role in cardiovascular complications associated with diabetes. Therefore, we measured the ACE activity in serum of control and diabetic animals. In both the 2 and 8 week treatment group, ACE activity was significantly increased in the diabetic animals as compared to controls (Fig. 3.9).

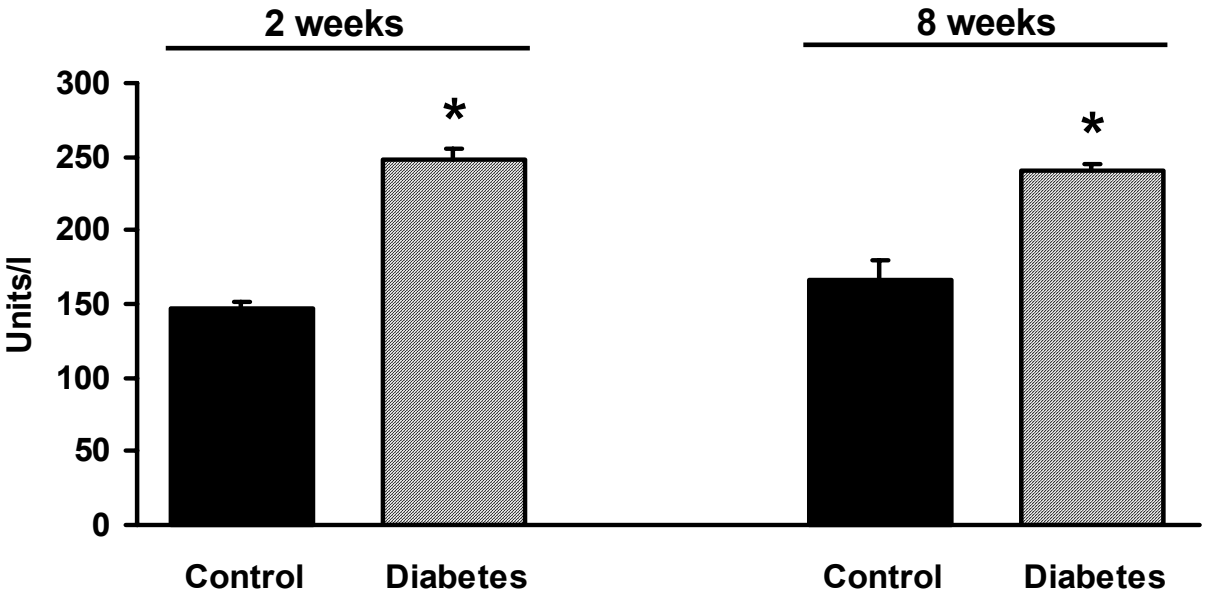

Fig. 3.9. ACE activity in serum of 2 and 8 week control and diabetic animals. Data are expressed as the mean ± SEM of 6 animals. * $p<0.05$ compared to control animals within same treatment group.

3.4 sGC activity in aorta

sGC activity was assessed on the basis of the formation of [^{32}P]cGMP in aortic homogenates. There was no difference in basal sGC activity between control or diabetic animals in either of the two treatment groups (Fig. 3.10.). However, the addition of 100 µM SNP (which stimulates only $^{\bullet}$NO-sensitive sGC and not pGC) resulted in a 10 to 14 fold increase above basal activity. In the 2 week diabetic group, SNP stimulation resulted in a significant, 1.6 fold increase in sGC activity as compared to the control group with SNP. In the 8 week treatment group, there was no significant difference in sGC activity between the control and diabetic group when stimulated with SNP (Fig. 3.10.).

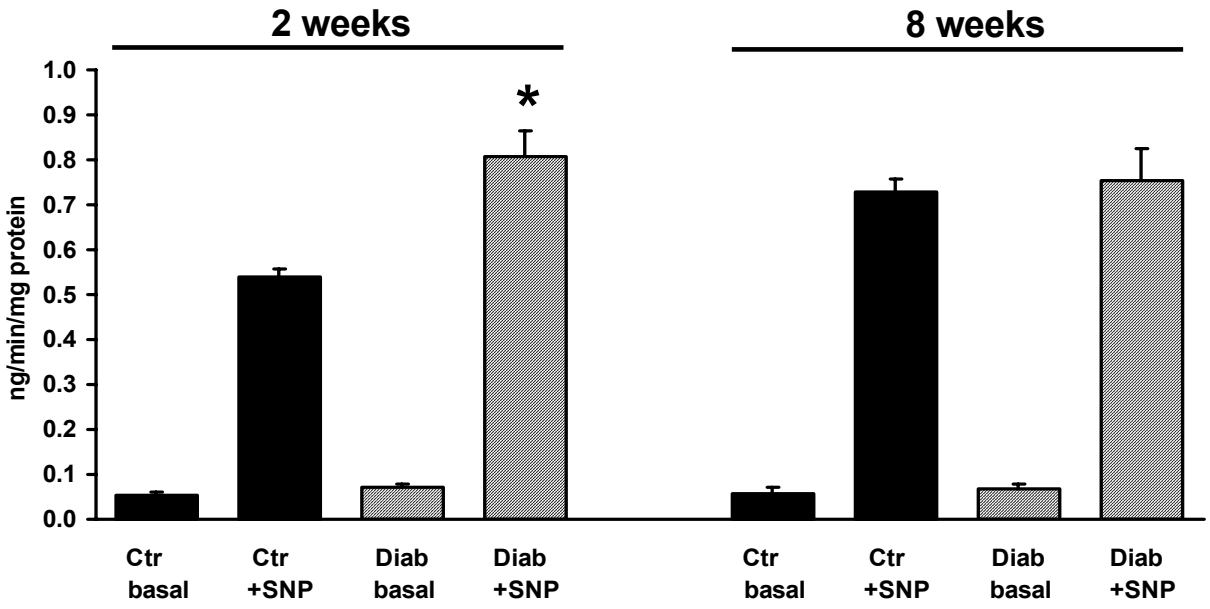

Fig. 3.10. sGC activity of aortic homogenates of 2 and 8 week control (Ctr) and diabetic (Diab) animals. Basal sGC activity was determined on the basis of the formation of [^{32}P]cGMP during 10 min at 37°C. To measure the $^{\bullet}$NO-sensitive sGC activity, homogenates were stimulated with sodium nitroprusside (SNP) (100 μM). Data are expressed as the mean ± SEM of 3 animals. *$p<0.05$ compared to control with SNP within the same treatment group.

3.5 Measurement of cGMP levels in aorta

In order to determine whether sGC enzyme activity determined in vitro translates into corresponding product formation in intact tissue, we measured the cGMP levels in aortic rings of 2 and 8 week control and diabetic animals. The basal cGMP levels of the diabetic animals increased significantly in both treatment groups compared to their controls (by 3 and 1.2 fold in the 2 and 8 week group, respectively) (Fig. 3.11.). In the 2 week treatment group, 100 nM SNP caused a significant 4-fold increase in cGMP levels above basal in control and a 3-fold increase in diabetic animals. Furthermore, in the 8 week control group, stimulation with SNP resulted in a doubling of cGMP levels. In the 8 week diabetic group, SNP caused no significant increase in cGMP levels above basal levels and also resulted in much lower cGMP formation compared to the SNP-induced cGMP formation of the 2 week diabetic group (Fig. 3.11.).

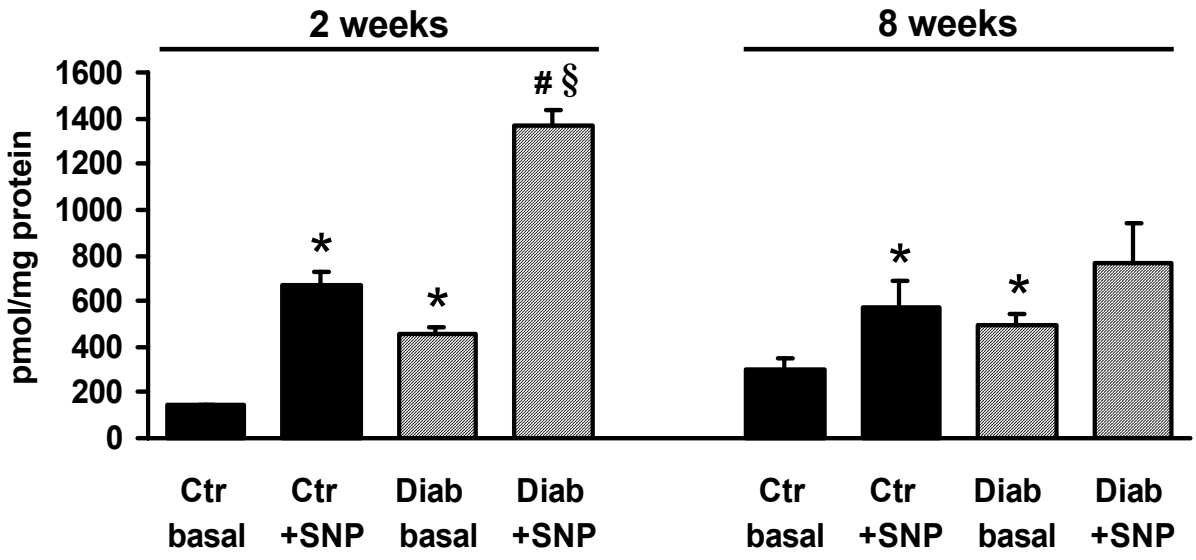

Fig. 3.11. cGMP levels of aorta of 2 and 8 week control (Ctr) and diabetic (Diab) animals. Basal and sodium nitroprusside- (SNP) (100 nM) stimulated cGMP levels of aortic rings were determined in control and diabetic animals. Data are expressed as the mean ± SEM of 5-10 animals. *p<0.05 compared to basal control levels within same treatment group, #<0.05 compared to basal diabetes levels within same treatment group, §<0.05 compared to control with SNP within same treatment group.

3.6 Measurement of cAMP levels in aorta

To determine the role of the arachidonic acid/PGI_2 pathway in our model of diabetes, we measured the levels of cAMP, an important second messenger which is activated by PGI_2. Overall, the cAMP levels in the 2 week treatment group were lower than those of the 8 week treatment group (Fig. 3.12.). In the 2 week treatment group, there was no difference in the basal cAMP levels, however 40 nM ACh caused a similar and significant increase in cAMP in the control and diabetic group. In the 8 week treatment group, basal cAMP levels in the diabetic group were increased by about 3 fold as compared to controls. Addition of ACh caused a significant increase in both the control and diabetic group, however in the diabetic group, ACh stimulation resulted in cAMP level that were twice as high as those of the control group (Fig. 3.12.).

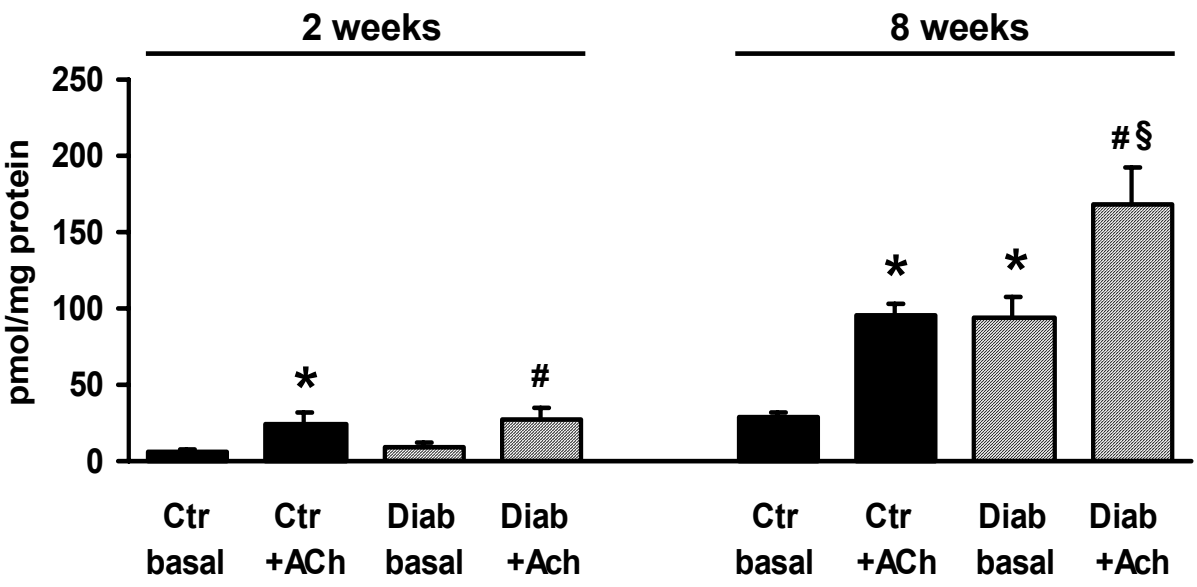

Fig. 3.12. cAMP levels in aorta of 2 and 8 week control (Ctr) and diabetic (Diab) animals. Basal and acetylcholine- (ACh) (40nM) stimulated cAMP levels of aortic rings were determined in control and diabetic animals. Data are expressed as the mean ± SEM of 5-10 animals. *p<0.05 compared to basal control levels within same treatment group, #<0.05 compared to basal diabetes levels within same treatment group, §<0.05 compared to control with ACh within same treatment group.

3.7 ROS levels in aortic rings detected by CL using lucigenin, coelenterazine and L-012

$O_2^{\bullet-}$ detection by chemiluminescence is a commonly employed method; however, much dispute exists as to the specificity of the compounds used. By using 3 different dyes, commonly used for the detection of ROS in vascular tissue, namely lucigenin, coelenterazine and L-012, we set out to compare ROS production in aortic rings of control and diabetic animals.

Using **lucigenin** (5µM) as the CL probe for extracellular ROS production, our results show that in the 2 week treatment group, basal ROS production was significantly increased in the diabetic group (by 50 %) as compared to controls (Fig. 3.13.). ACh, which induces $^{\bullet}$NO production, significantly decreased ROS levels in the control group by 25 %, however, it had no effect in the diabetic group. L-NNA had no effect in the control group while in the diabetic group, ROS

production was slightly but not significantly reduced. In the 8 week treatment group, ACh again caused a significant decrease in ROS production in the control group (by 15 %), however in the diabetic group, ACh resulted in a slight, yet significant increase in ROS production (Fig. 3.13.). The addition of L-NNA also resulted in a slight but significant increase in the control group (by 17 %) but had no effect in the diabetic group (Fig. 3.13.).

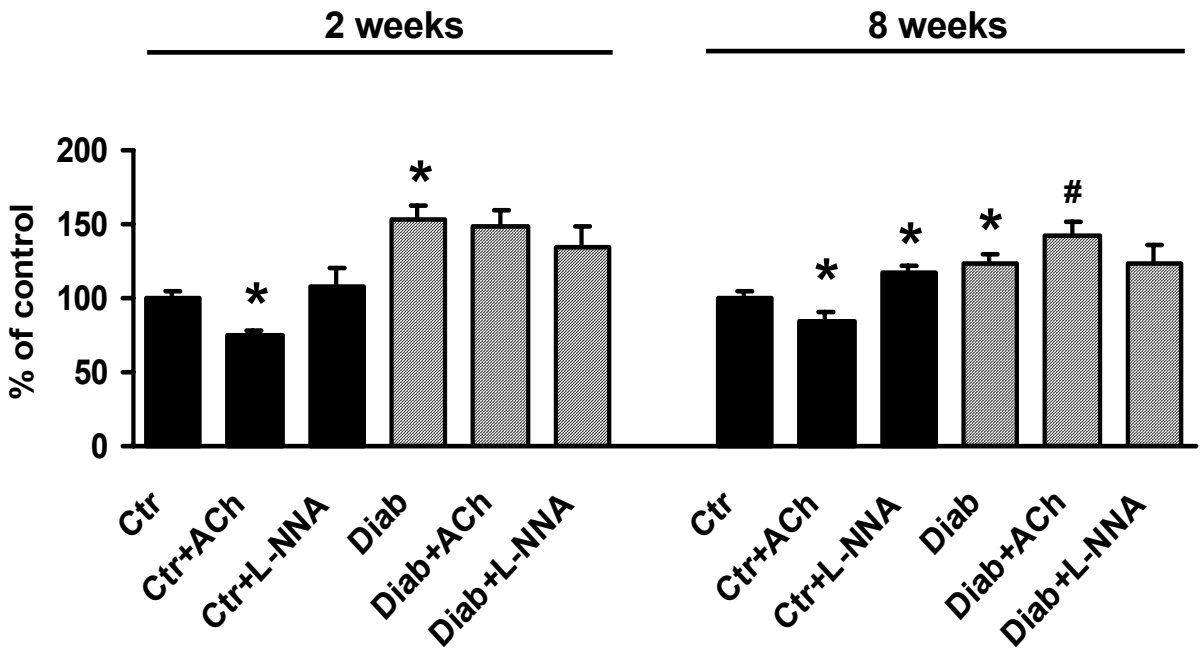

Fig. 3.13. ROS formation in aortic rings of 2 and 8 week control (Ctr) and diabetic (Diab) animals detected with the chemiluminescent dye lucigenin. Basal, L-NNA- (1 mM) and ACh- (1 μM) stimulated ROS production was determined in aortic rings using 5 μM lucigenin. Data are calculated as % of control within each treatment group and are expressed as the mean ± SEM of 7-14 animals. *$p<0.05$ compared to control within the same treatment group, #<0.05 compared to diabetes within the same treatment group.

Results obtained with the intracellular superoxide- and peroxynitrite-sensitive CL dye **coelenterazine** (5 μM) showed that in the 2 week treatment group, basal ROS production in the diabetic group decreased to nearly 50 % of that of control levels (Fig. 3.14). The addition of L-NNA caused a slight but not significant increase in ROS production in the control group; however, in the diabetic group, ROS production markedly increased (by over 50 %). In the 8 week treatment group, basal ROS production was increased by about 20 % in the diabetic

group. Similar to the 2 week treatment group, L-NNA caused a slight but not significant increase in ROS production in the control group. However, in the diabetic group, L-NNA had no effect (Fig. 3.14).

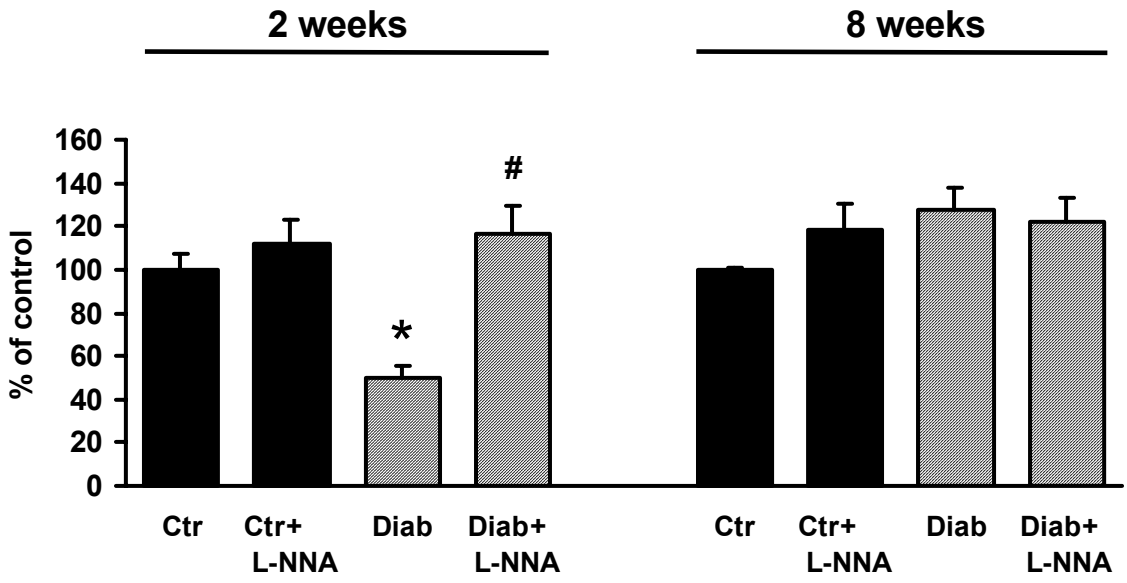

Fig. 3.14. ROS formation in aortic rings of 2 and 8 week control (Ctr) and diabetic (Diab) animals detected with the chemiluminescent dye coelenterazine. Basal and L-NNA- (1 mM) stimulated chemiluminescent signal intensity was detected in aortic rings using coelenterazine (5 μM). Data are calculated as % of control within each treatment group and are expressed as the mean ± SEM of 4 animals. *p<0.05 compared to control, #<0.05 compared to diabetes without L-NNA within the same treatment group.

Lastly, we used the luminol analogue **L-012** (100 μM), which detects both superoxide and peroxynitrite. In the 2 week treatment group, we found no significant change in basal L-012 signal (Fig. 3.15.). The addition of the NOS inhibitor L-NNA, which inhibits all $^{\bullet}$NO production, resulted in a doubling in the L-012 signal intensity in the control group. In the diabetic group, L-NNA caused a dramatic 4-fold increase as compared to basal levels. In the 8 week treatment group, the L-012 signal intensity in the diabetic group was double that of the control group, although this was not significant. In both control and diabetic animals, L-NNA caused an increase in L-012 signal intensity, but again no significance could be shown (Fig. 3.15).

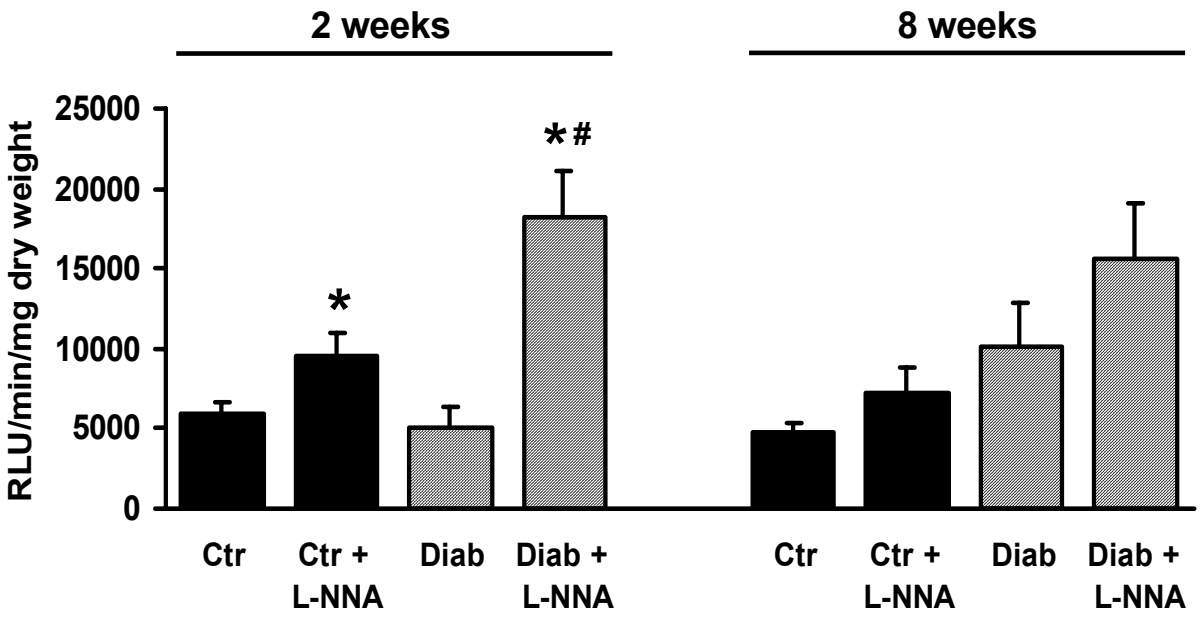

Fig. 3.15. ROS formation in aortic rings of 2 and 8 week control (Ctr) and diabetic (Diab) animals detected with the chemiluminescent dye L-012. Basal and L-NNA- (1 mM) stimulated chemiluminescent signal intensity was detected in aortic rings using L-012 (100 μM). Data are expressed as the mean ± SEM of 6-15 animals. RLU: relative light units. *p<0.05 compared to same group without L-NNA, #<0.05 compared to control with L-NNA within the same treatment group.

3.8 Oxidative fluorescent microtopography

The dye DHE, which has a blue fluorescence in solution, is freely permeable through the cell membrane in its reduced form. Once inside the cell, it becomes trapped when it is oxidized specifically by superoxide and diffuses into the nucleus were it intercalates with DNA and thereafter fluoresces red. This is a common method used to localize $O_2^{\bullet-}$ production in tissue.

In the 2 week control group, bright red fluorescence was detected in the endothelium, the media and the adventitia (Fig. 3.16. A). This finding indicates that $O_2^{\bullet-}$ is produced throughout all layers of the vessel wall. In the diabetic group, however, we observed a marked decrease in staining as compared to the control group, particularly in the endothelium and the adventitia (Fig. 3.16. B).

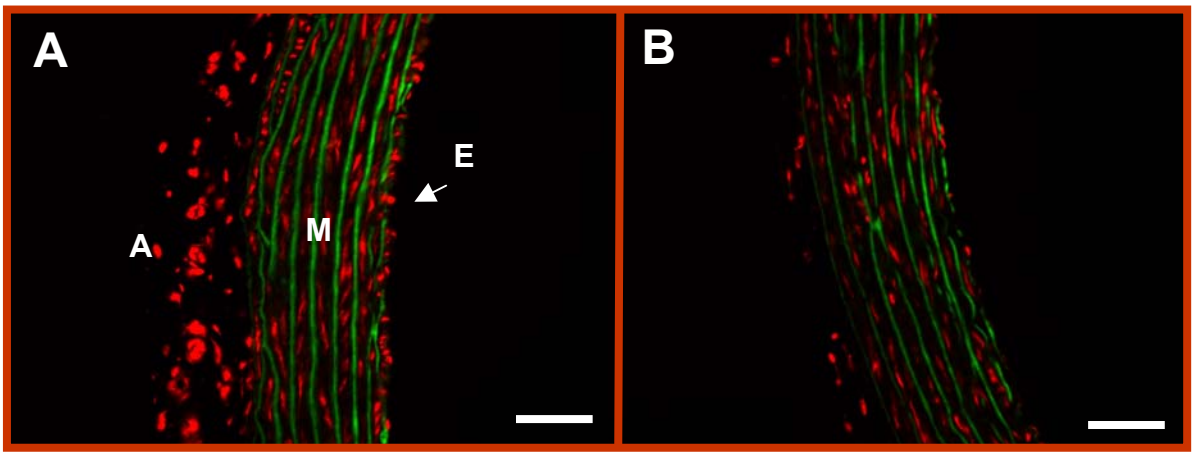

Fig. 3.16. Localization of superoxide production using DHE staining in vessels of 2 week control (A) and diabetic (B) animals. Cryosections of aorta were incubated with DHE (1 µM) which fluoresces red when oxidized by superoxide. The autofluorescence of the elastic laminae is green. A: adventitia, M: media, E: endothelium. The bar denotes 50 µm. Pictures are representative of 5 independent experiments.

In the controls of the 8 week treatment group, $O_2^{\bullet-}$ was also produced throughout the whole vessel wall (Fig. 3.17. A). However, in the diabetic group, there was a marked increase in staining as compared to the control group, particularly in the media and the adventitia (Fig. 3.17. B).

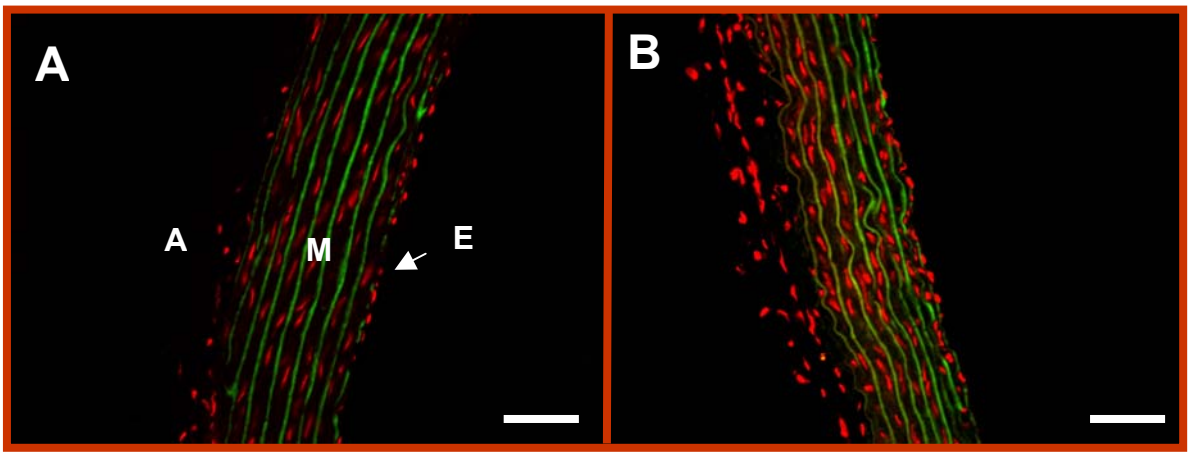

Fig. 3.17. Localization of superoxide production using DHE staining in vessels of 8 week control (A) and diabetic (B) animals. Cryosections of aorta were incubated with DHE (1 µM) which fluoresces red when oxidized by superoxide. The autofluorescence of the elastic laminae is stained green. A: adventitia, M: media, E: endothelium. The scale bar denotes 50 µm. Pictures are representative of 5 independent experiments.

3.9 Measurement of NADPH-dependent oxidase(s) activity of membrane fractions from heart and aorta

To see whether our rather qualitative fluorescent data on vascular $O_2^{\bullet-}$ production are associated with the $O_2^{\bullet-}$-generating NAD(P)H oxidase, we assessed the NAD(P)H-oxidase activity in membrane fractions of both heart and aortic tissue from control and diabetic rats by lucigenin (5 μM)-derived CL, either with or without the addition of 200 μM NADPH.
In heart membranes of the 2 week treatment group, there was no difference in basal (unstimulated) CL signal intensity between control and diabetic animals (Fig. 3.18.). The addition of NAPDH resulted in a 10 and 20 fold increase in CL signal intensity above basal levels in the control and diabetic group, respectively. Thus, the NADPH-stimulated signal intensity in the diabetic group was significantly higher (2 fold) compared to the control group. In the diabetic group, the addition of DPI (10 μM), a flavoprotein oxidase inhibitor, normalized the NADPH-induced CL signal to near background levels, while the NOS inhibitor L-NNA (1 mM) had no effect. Furthermore, the addition of NADH (200 μM) had no effect on the CL signal in the diabetic group compared to basal levels (Fig. 3.18.).

Similar results were obtained in the 8 week treatment group. Again we saw no difference in basal (unstimulated) CL signal intensity between control and diabetic animals (Fig. 3.18.). The addition of NAPDH resulted in a 12 and 24 fold increase in CL signal intensity above basal levels in the control and diabetic group, respectively. In the diabetic group, the addition of DPI (10 μM) normalized the NADPH-induced CL signal to near background levels, while L-NNA (1mM) and rotenone, an inhibitor of mitochondrial respiration, had no effect. Neither NADH (200 μM), nor hypoxanthine (1 mM), a substrate for xanthine oxidase, had any significant effect on the basal CL signal (Fig. 3.18.).

In aortic membranes of the 2 week treatment group, there was no difference in NADPH-(200 μM) stimulated CL signal intensity between the control and diabetic group; however, in the diabetic animals of the 8 week treatment group, the NADPH-stimulated CL signal was significantly increased by 1.6-fold as compared to controls (Fig. 3.19.).
These results indicate that NADPH-dependent oxidase is a pre-eminent superoxide source in both cardiac and aortic membranes.

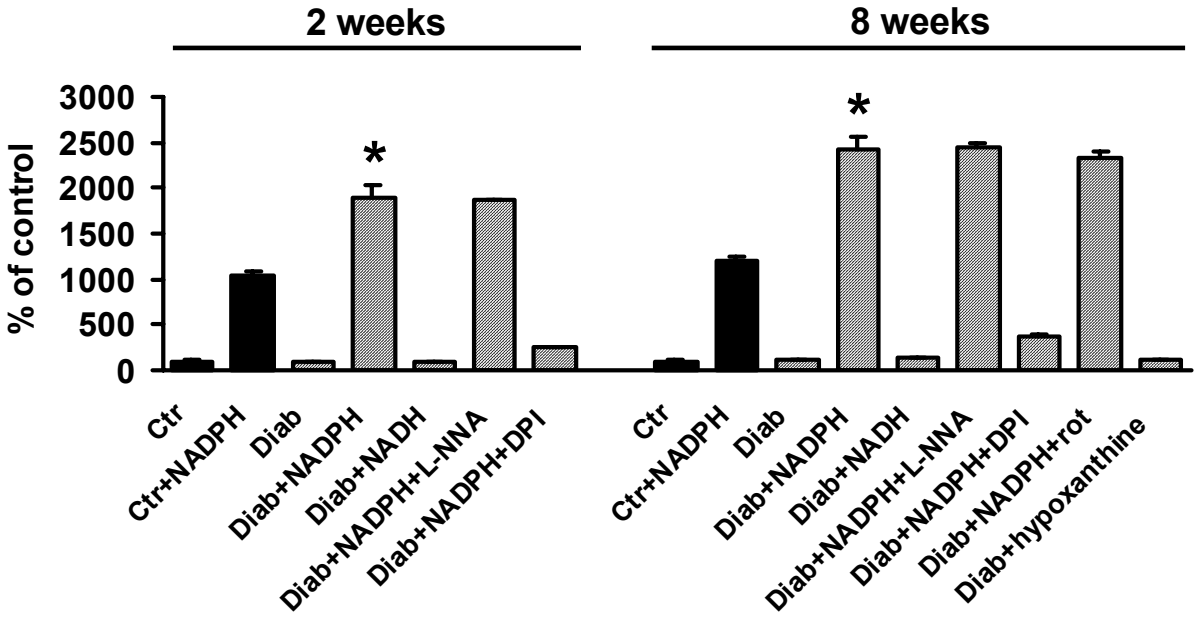

Fig. 3.18. NADPH-dependent oxidase activity of membrane fractions from heart of 2 and 8 week control (Ctr) and diabetic (Diab) animals. Membrane fractions were incubated with either NADPH (200 μM), NADH (200 μM), L-NNA (1 mM), DPI (10 μM), rotenone (10 μM) or hypoxanthine (1 mM) in the presence of 5 μM lucigenin. Data are expressed as the mean ± SEM of 2-7 animals, *p<0.05 compared to control within the same treatment group.

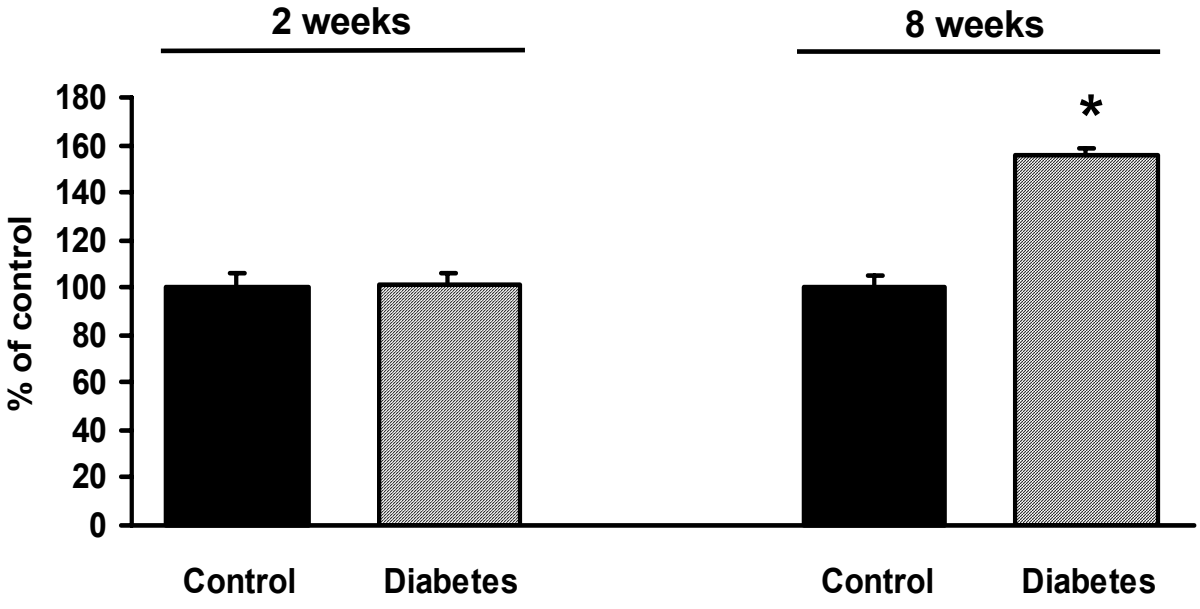

Fig. 3.19. NADPH-dependent oxidase activity of membrane fractions from aorta of 2 and 8 week control and diabetic animals. Membrane fractions were incubated with NADPH (200 μM) in the presence of 5 μM lucigenin. Data are expressed as the mean ± SEM of 4 animals, *p<0.01.

3.10 Immunohistochemical detection of eNOS

Aortic cryosections (see section 2.2.8) were used to determine the expression of eNOS in control and diabetic animals. In the 2 week treatment group, there was no apparent difference in eNOS expression between control and diabetic animals (Fig. 3.20. A and B). However, in the 8 week treatment group there was a marked increase in eNOS expression in the diabetic group (shown by the increase in red staining) as compared to controls (Fig. 3.20. C and D).

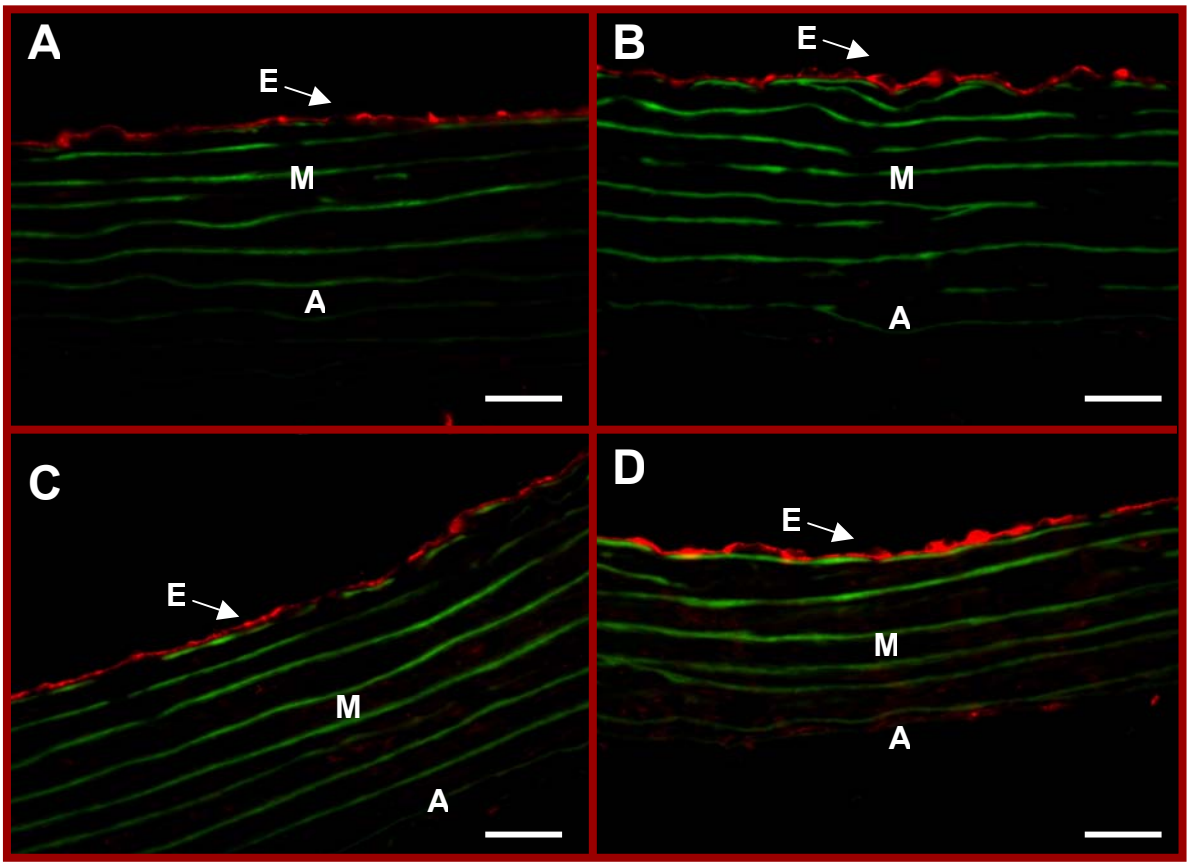

Fig. 3.20. Immunohistochemical detection of eNOS of 2 week (A and B) and 8 week (C and D) control (A and C) and diabetic (B and D) animals. Cryosections of aorta were stained with a monoclonal anti-eNOS antibody and detected with a fluorescently-labeled secondary antibody (red staining). The autofluorescence of the elastic laminae is green. A: adventitia, M: media, E: endothelium. The scale bar denotes 25 µm. Pictures are representative of 4 independent experiments.

3.11 Vascular •NO levels measured by EPR spin trapping

One of the most reliable methods of detecting •NO in biological systems is the EPR spin trapping technique. We used the highly hydrophobic trap $Fe^{II}(DETC)_2$ to determine the ACh- (1 μM) and calcium ionophore A23187 (10 μM) stimulated •NO formation in aortic rings of control and diabetic animals.

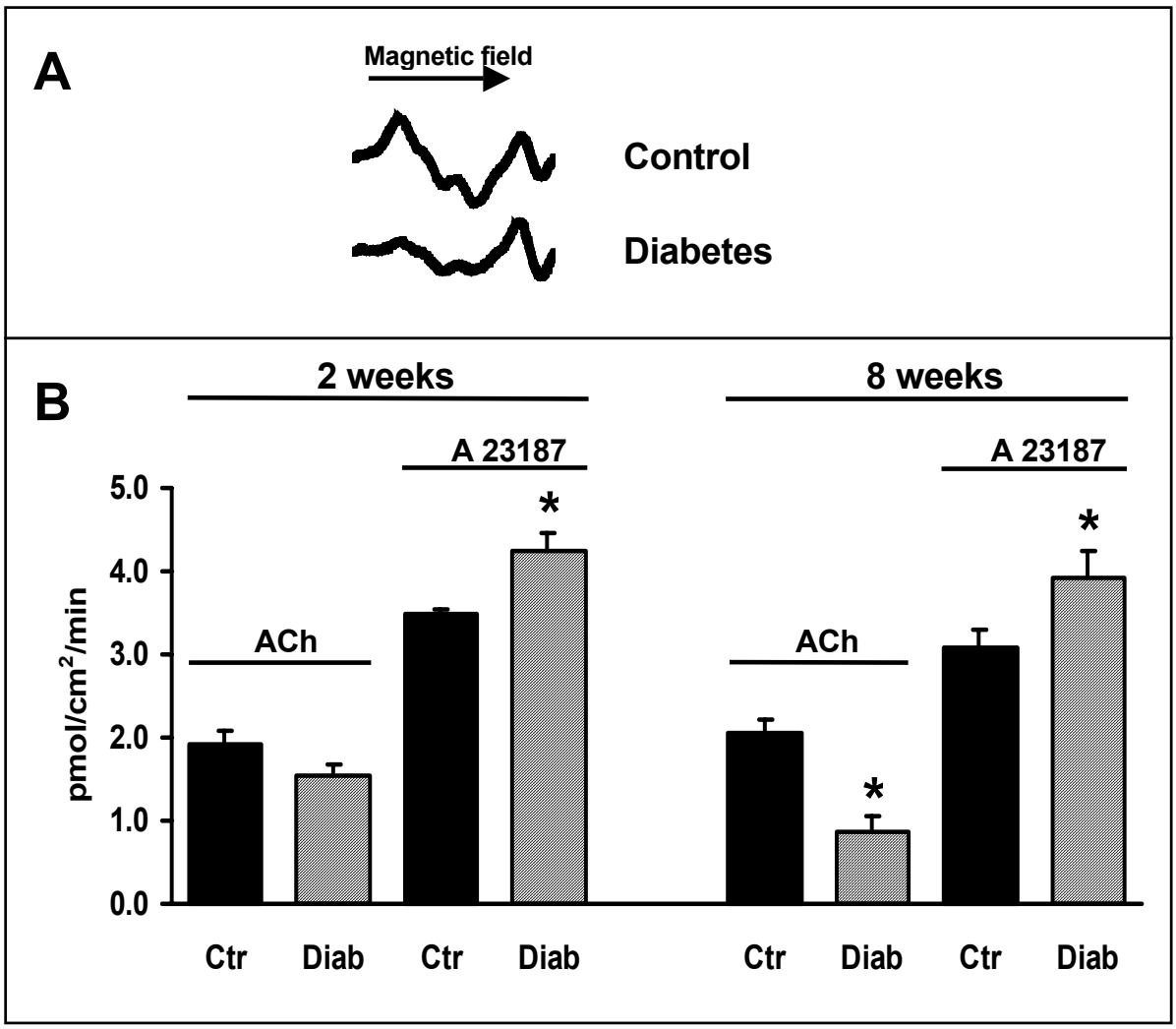

Fig. 3.21. Measurement of •NO by EPR of 2 and 8 week control (Ctr) and diabetic (Diab) animals. (A) Original •NO spectra of a representive control and diabetic rat. **(B)** Aortic rings were incubated with either acetylcholine (ACh, 1 μM) or the calcium ionophore A23187 (10 μM). Data are expressed as the mean ± SEM of 4-10 animals, * $p<0.05$ compared to control within the same treatment group. Unstimulated, basal levels of both control and diabetic animals could not reliably be determined, as they were found to be close to the detection limit of the assay.

In the 2 week treatment group, there was no significant difference in the ACh-stimulated •NO production in the diabetic group compared to the controls, while stimulation with A23187 induced a significantly higher increase in •NO production in the diabetic group than in the control rats (Fig. 3.21.). The 8 week diabetic state induced a marked decrease (by nearly 50 %) in •NO production elicited by ACh compared to controls, while the •NO production stimulated by A23187 was again significantly increased compared to •NO formation in control animals (Fig. 3.21.).

3.12 Serum levels of NO_2^- and NO_3^-

Indirect indices of •NO production are NO_2^- and NO_3^-. The fluorescent probe DAN can be used to detect NO_2^- and by the addition of nitrate reductase one can monitor both NO_2^- and NO_3^- levels. Our results show that in the 2 week treatment group, serum NO_2^- was significantly increased in the diabetic group as compared to controls with no change in NO_3^- levels (Fig. 3.22.). On the contrary, in the 8 week treatment group, there was no change in NO_2^- levels between diabetic and control groups; however, the NO_3^- levels were significantly increased in the diabetic group (Fig. 3.22).

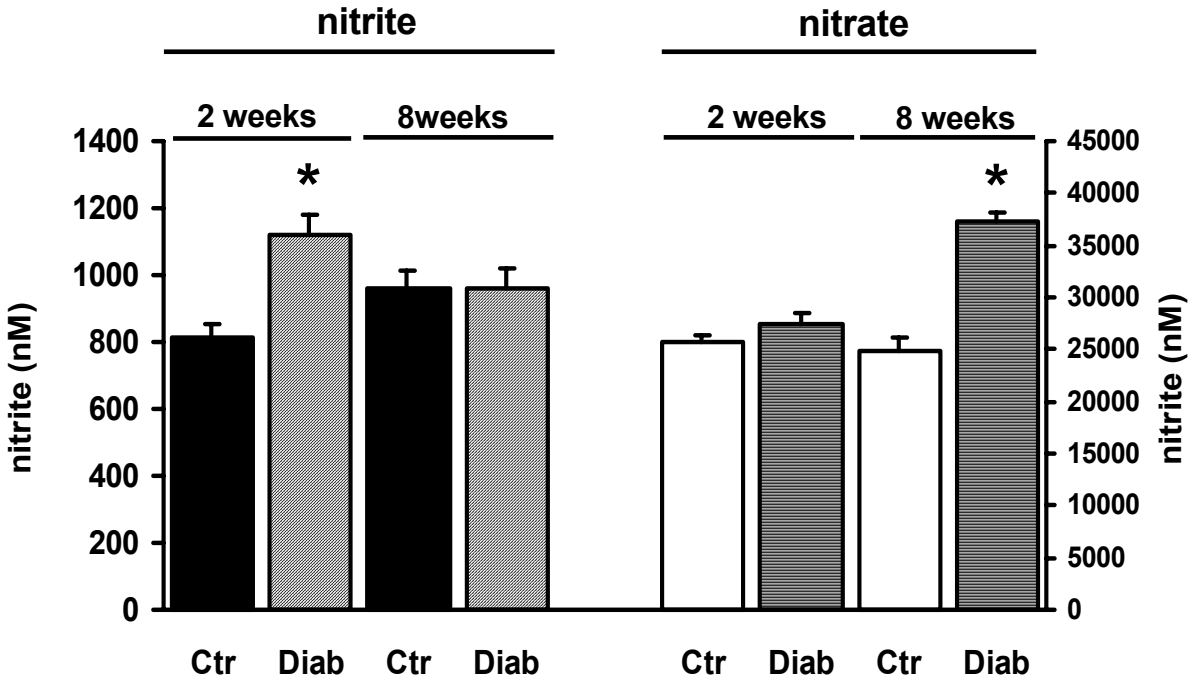

Fig. 3.22. Serum levels of nitrite and nitrate of 2 and 8 week control (Ctr) and diabetic (Diab) animals. The DAN assay was used to determine nitrite levels in serum samples. Nitrate was determined by the addition of nitrate reductase. Data are expressed as the mean ± SEM of 6-9 animals. * $p<0.05$ compared to control within the same treatment group.

3.13 Western blot analysis

3.13.1 Expression of the NAD(P)H oxidase subunits nox1, nox4 and p67^{phox}

To elucidate the role of the gp91^{phox} homologues nox1 and nox4 in the our observed changes in superoxide production, we looked at the expression of these two subunits in aortic homogenates of control and diabetic animals.

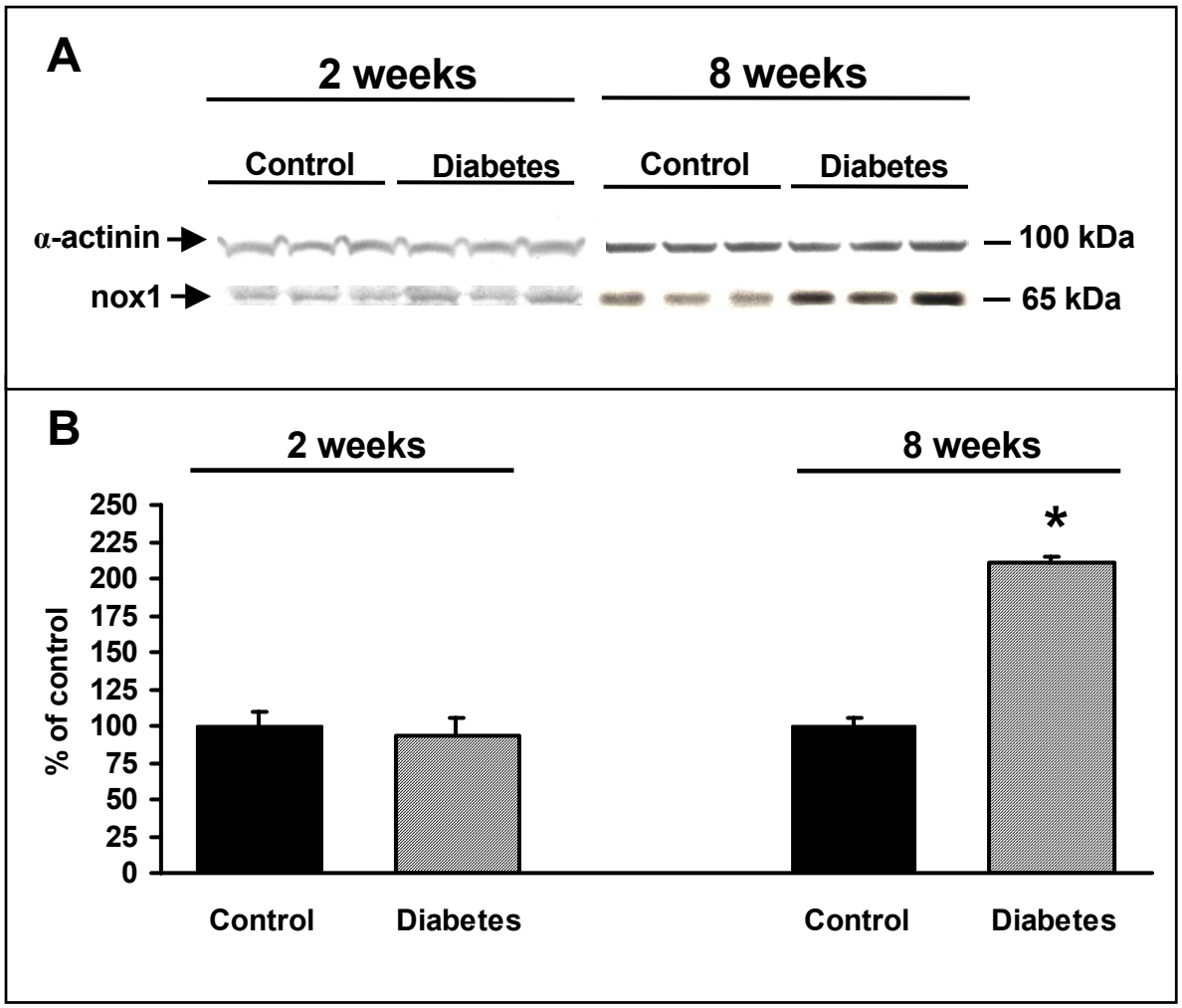

Fig. 3.23. Expression of nox1 in aorta of 2 and 8 week control and diabetic animals. **(A)** Original Western blots detecting nox1 protein in aortic homogenates of 3 representative control and diabetic animals. The expression of α-actinin was used to verify equal protein loading. **(B)** Densitometric analysis of Western blots. Data are expressed as the mean ± SEM of 12 animals per group.* $p<0.05$ compared control within same treatment group.

In the 2 week treatment group, there was no change in either nox1 (Fig. 3.23.) or nox4 (Fig. 3.24.) expression between control and diabetic animals. However, in the 8 week treatment group, nox1 expression increased by more than 2 fold in the diabetic group compared to the

control group (Fig. 3.23.), while the expression of nox4 was not significantly altered (Fig. 3.24.). In addition, in the diabetic animals of the 2 week treatment group, the expression of $p67^{phox}$, which translocates to the membrane to form the active oxidase complex, decreased to about 50% of that of controls while no change was observed in the 8 week treatment group (Fig. 3.25.).

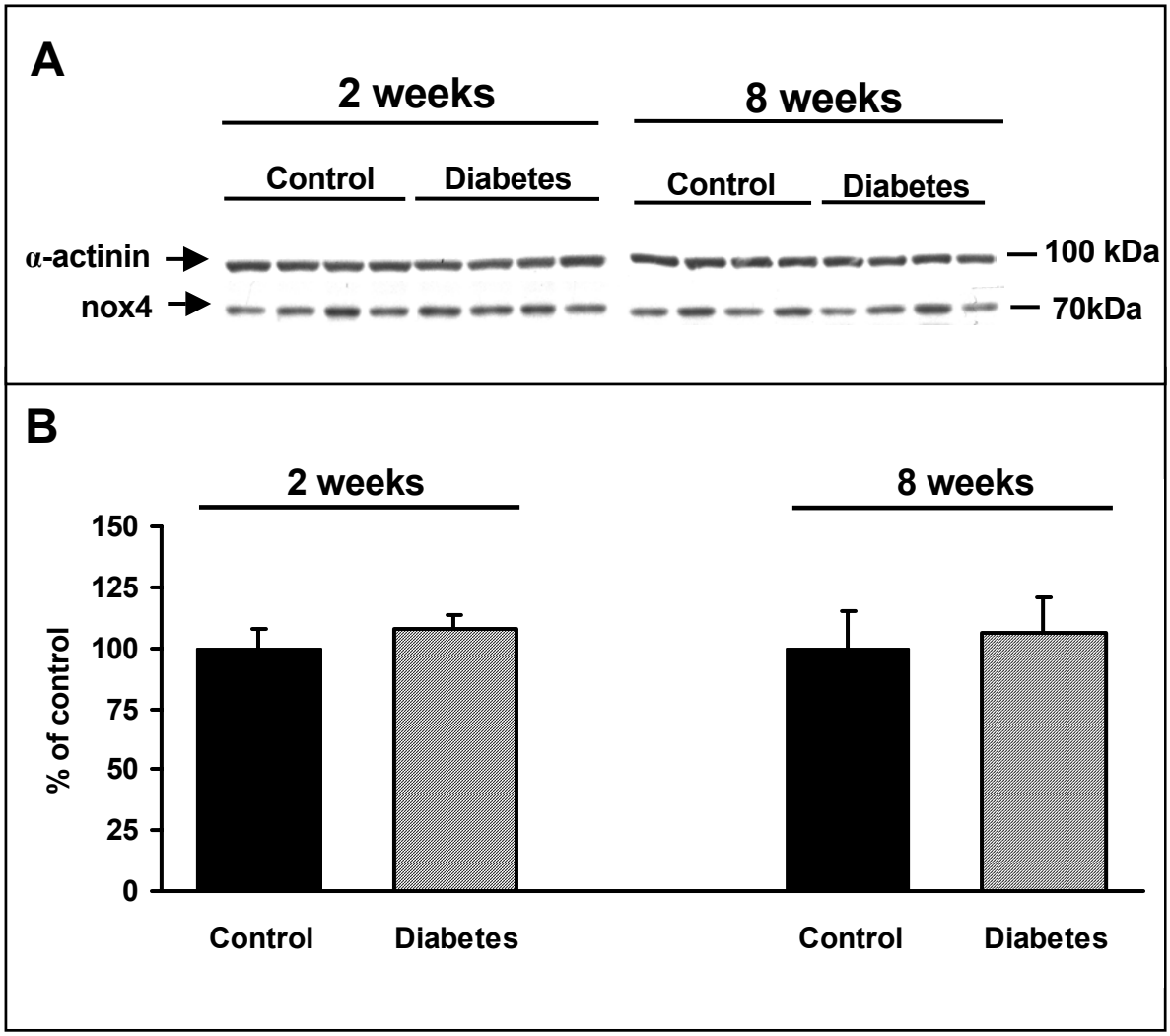

Fig. 3.24. Expression of nox4 in aorta of 2 and 8 week control and diabetic animals. **(A)** Original Western blots detecting nox4 protein in aortic homogenates of 4 representative control and diabetic animals. The expression of α-actinin was used to verify equal protein loading. **(B)** Densitometric analysis of Western blots. Data are expressed as the mean ± SEM of 6 animals per group.

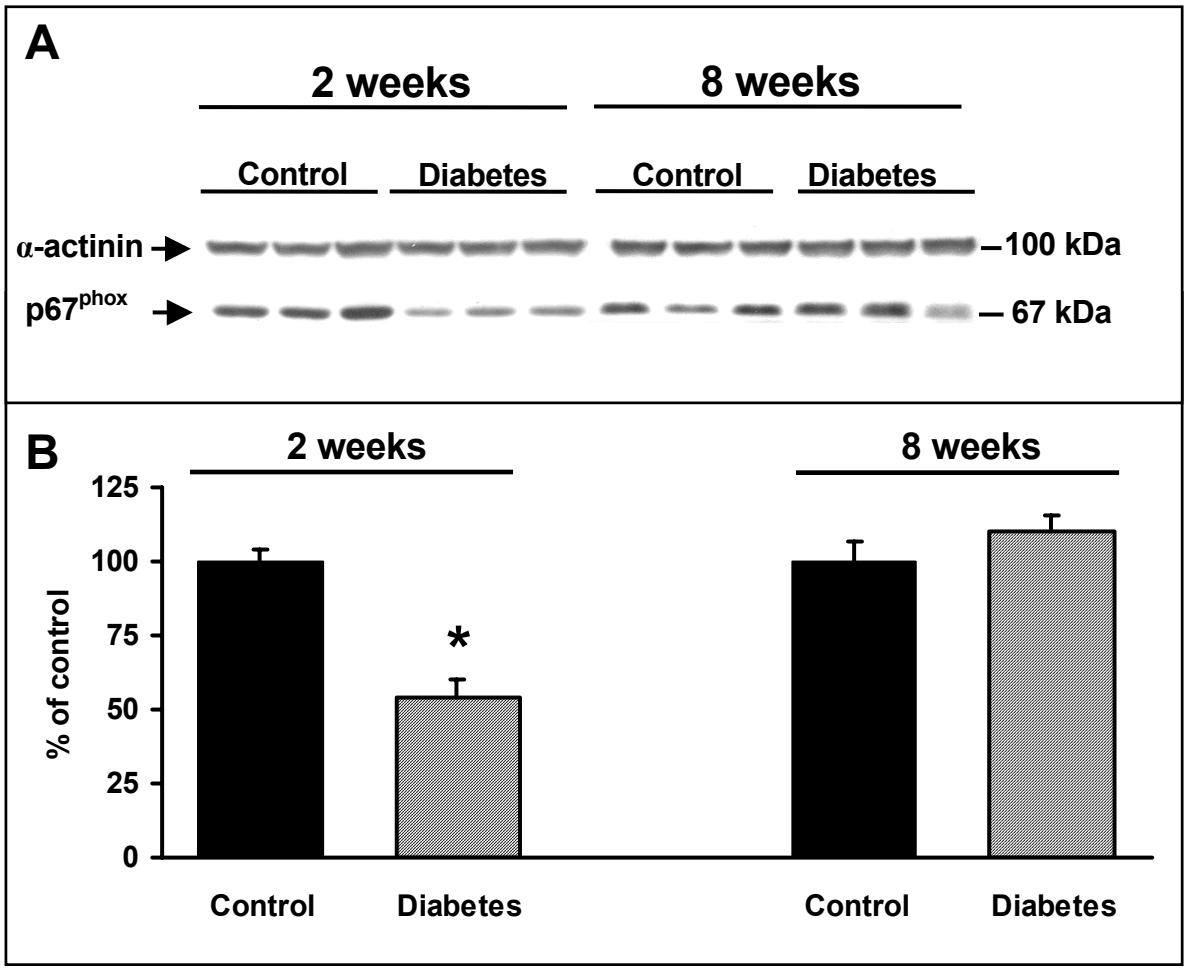

Fig. 3.25. Expression of p67^{phox} in aorta of 2 and 8 week control and diabetic animals. (A) Original Western blots detecting p67^{phox} protein in aortic homogenates of 3 representative control and diabetic animals. The expression of α-actinin was used to verify equal protein loading. **(B)** Densitometric analysis of Western blots. Data are expressed as the mean ± SEM of 3-6 animals. *$p<0.05$ compared to control within same treatment group.

3.13.2 Expression of eNOS

To elucidate the role of eNOS in the setting of diabetes, we used aortic homogenates to determine its protein expression. In the 8 week treatment group, we observed a significant increase (of nearly 50%) in eNOS expression in the diabetic group as compared to controls, while there was no difference in eNOS expression in the 2 week treatment group (Fig. 3.26.). These results support our observations obtained with immunohistochemical staining (see section 3.10.).

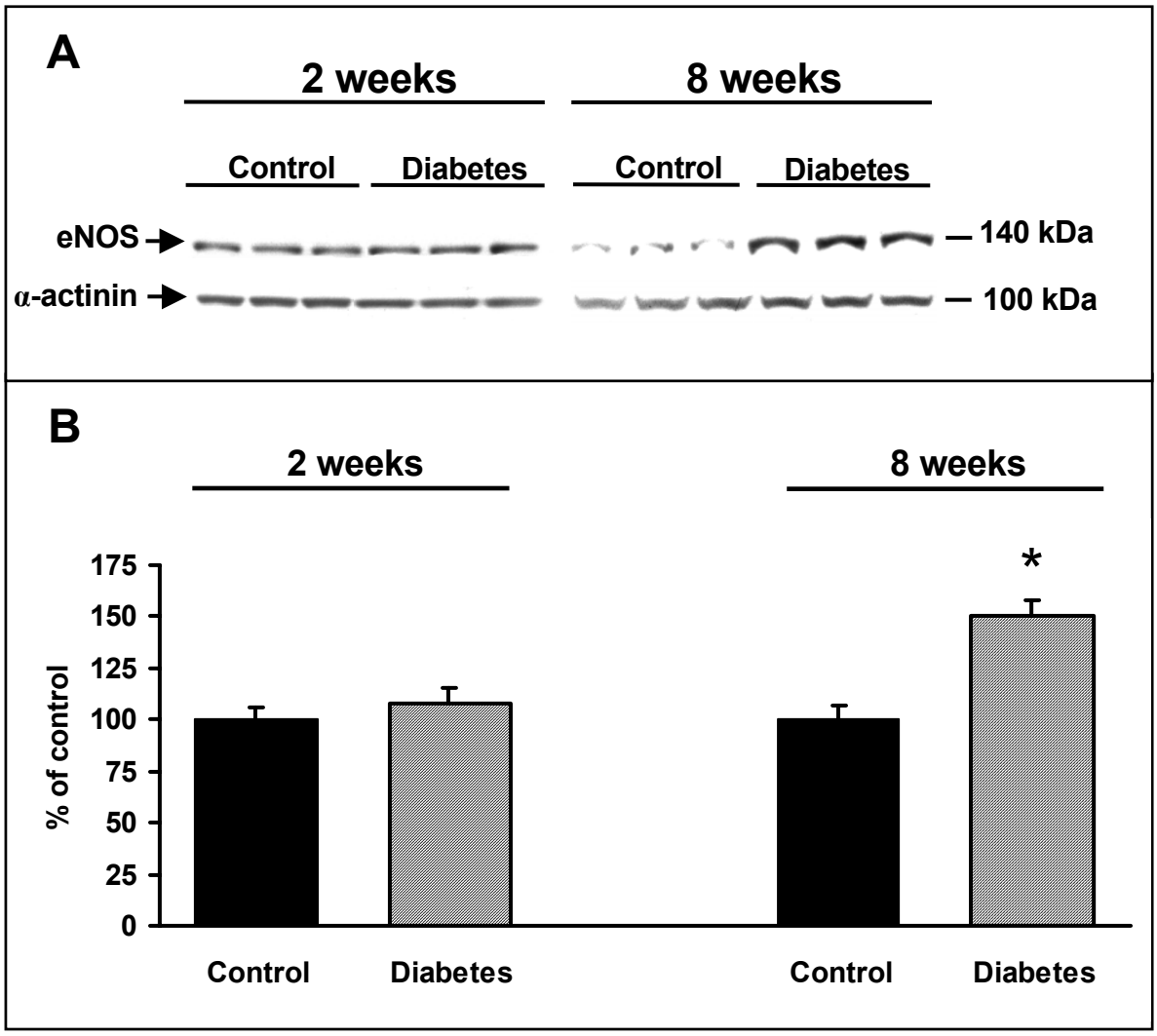

Fig. 3.26. Expression of eNOS in aorta of 2 and 8 week control and diabetic animals. **(A)** Original Western blots detecting eNOS protein in aortic homogenates of 3 representative control and diabetic animals. The expression of α-actinin was used to verify equal protein loading. **(B)** Densitometric analysis of Western blots. Data are expressed as the mean ± SEM of 12-18 animals. * $p<0.05$ compared to control within same treatment group.

3.13.3 Expression of SOD

Changes in ROS levels may be a result of either increased production or a decrease in anti-oxidative defense mechanisms. One such anti-oxidative enzyme found in the cytoplasm is the Cu/ZnSOD which is responsible for the dismutation of $O_2^{\bullet-}$. We therefore determined the expression of Cu/ZnSOD in aortic homogenates of control and diabetic animals. While we

observed no change in Cu/ZnSOD expression in the 2 week treatment group, the diabetic animals of the 8 week treatment group demonstrated a significant increase in Cu/ZnSOD expression (by about 60 %) as compared to controls (Fig.3.27.).

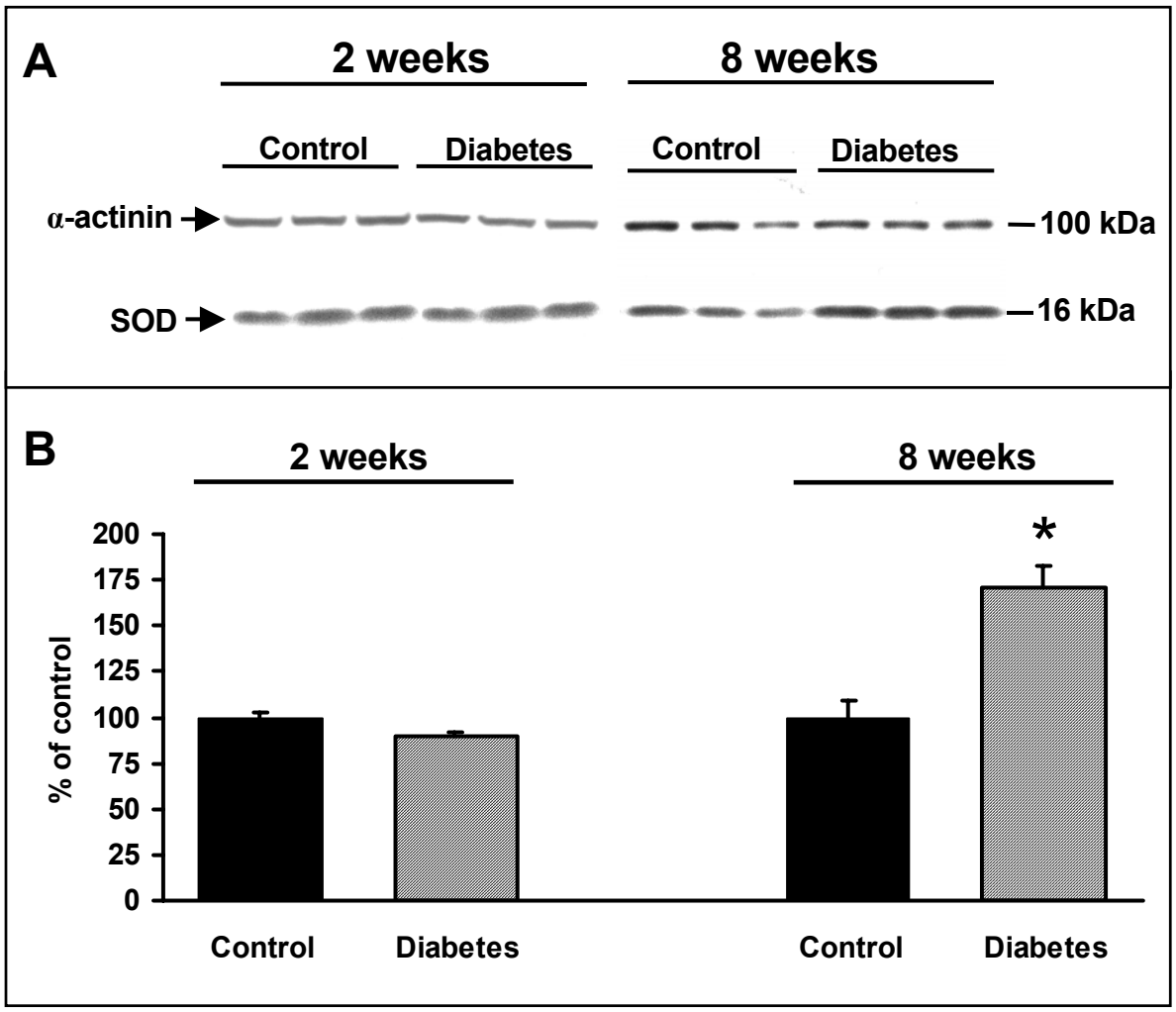

Fig. 3.27. Expression of Cu/Zn-SOD in aorta of 2 and 8 week control and diabetic animals. **(A)** Original Western blots detecting SOD protein in aortic homogenates of 3 representative control and diabetic animals. The expression of α-actinin was used to verify equal protein loading. **(B)** Densitometric analysis of Western blots. Data are expressed as the mean ± SEM of 5 animals per group. * $p<0.05$ compared to control within same treatment group.

3.13.4 Expression of sGC and cGK-I

Two NO-downstream effectors that are crucial in regulating vascular tone are sGC, which produces the second messenger cGMP, and cGK-I which is activated by cGMP. In aortic homogenates of the 2 week treatment group, we found a 20 % increase in sGCß$_1$ subunit expression in the diabetic group which was significantly higher than that of the control group (Fig. 3.28.). There was no change in sGC expression in the 8 week treatment group (Fig. 3.28.). Furthermore, no differences were found in cGK-I expression in either of the two treatment groups (Fig. 3.29.).

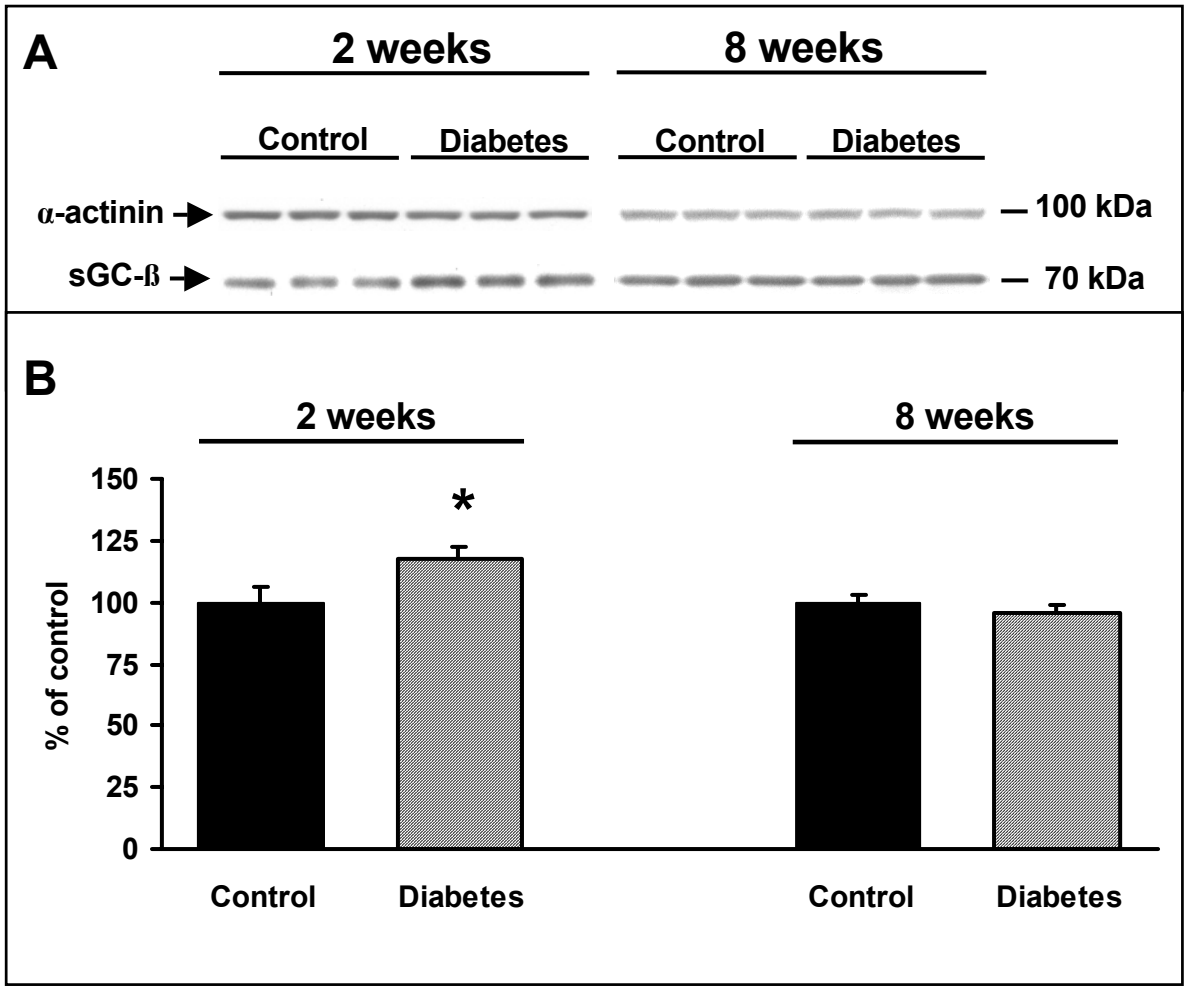

Fig. 3.28. Expression of sGC-ß in aorta of 2 and 8 week control and diabetic animals. **(A)** Original Western blots detecting sGC-ß protein in aortic homogenates of 3 representative control and diabetic animals. The expression of α-actinin was used to verify equal protein loading. **(B)** Densitometric analysis of Western blots. Data are expressed as the mean ± SEM of 9-12 animals per group. * $p<0.05$ compared to control within same treatment group.

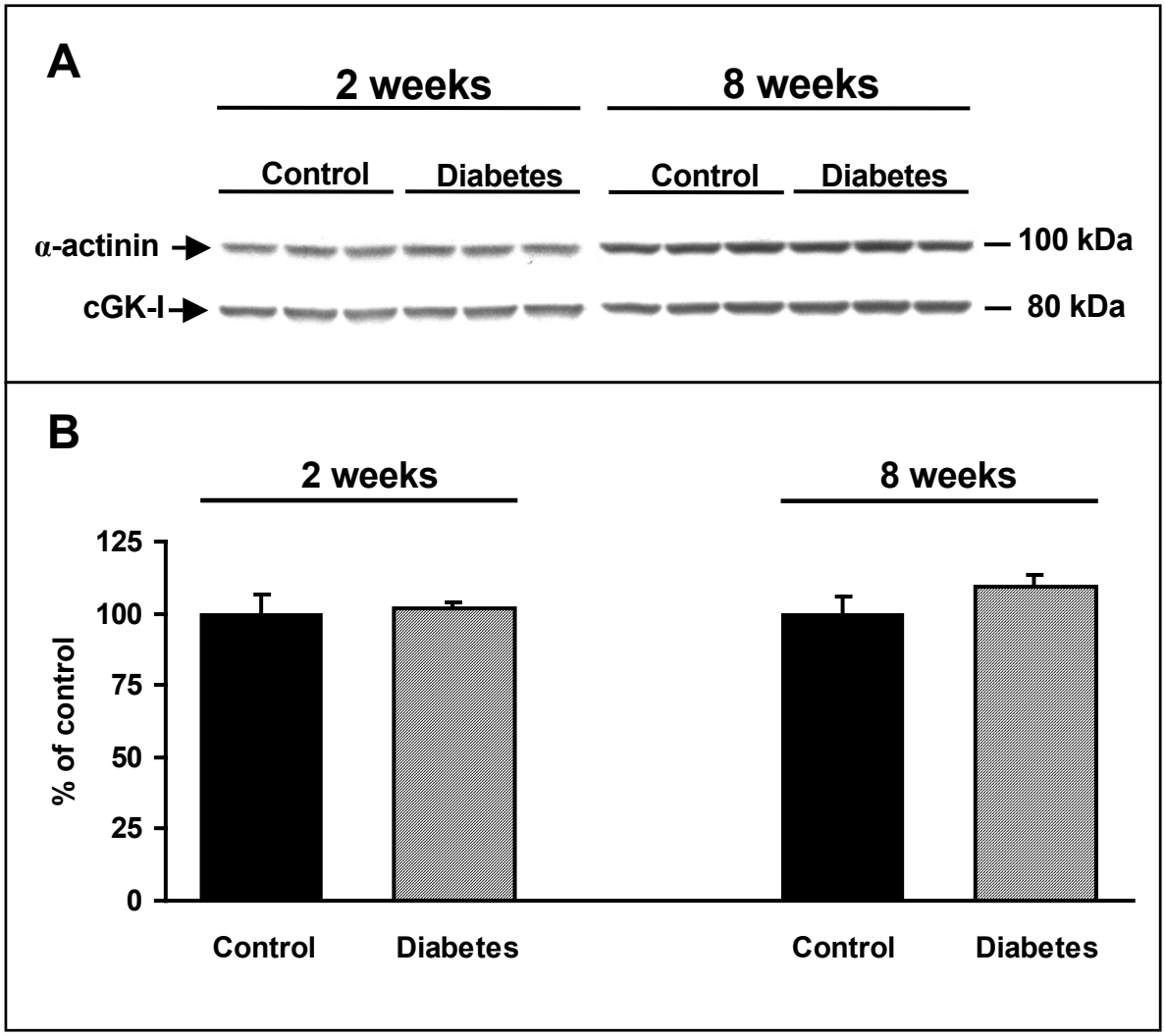

Fig. 3.29. Expression of cGK-I in aorta of 2 and 8 week control and diabetic animals. **(A)** Original Western blots detecting cGK-I protein in aortic homogenates of 3 representative control and diabetic animals. The expression of α-actinin was used to verify equal protein loading. **(B)** Densitometric analysis of Western blots. Data are expressed as the mean ± SEM of 4-6 animals per group.

3.13.5 Expression of P-VASPser239

In order to assess whether altered ROS formation in experimental diabetes translates into altered cGK activity, we looked at the expression of VASP phosporylation on ser239, a validated marker of cGK-I activity. We found no significant change in basal VASP phoshphorylation on ser239 expression in either of the two treatment groups (Fig. 3.30.). However, in the 2 week treatment group, ACh (1 μM) stimulation resulted in a 2-fold increase

in VASP phosphorylation on ser239 expression above basal levels in both control and diabetic animals. In the 8 week treatment group, ACh stimulation caused a marked (3-fold) increase in VASP phosphorylation on ser239 expression above basal levels in the control group; however, this effect of ACh was completely abolished in the diabetic group (Fig. 3.30.).

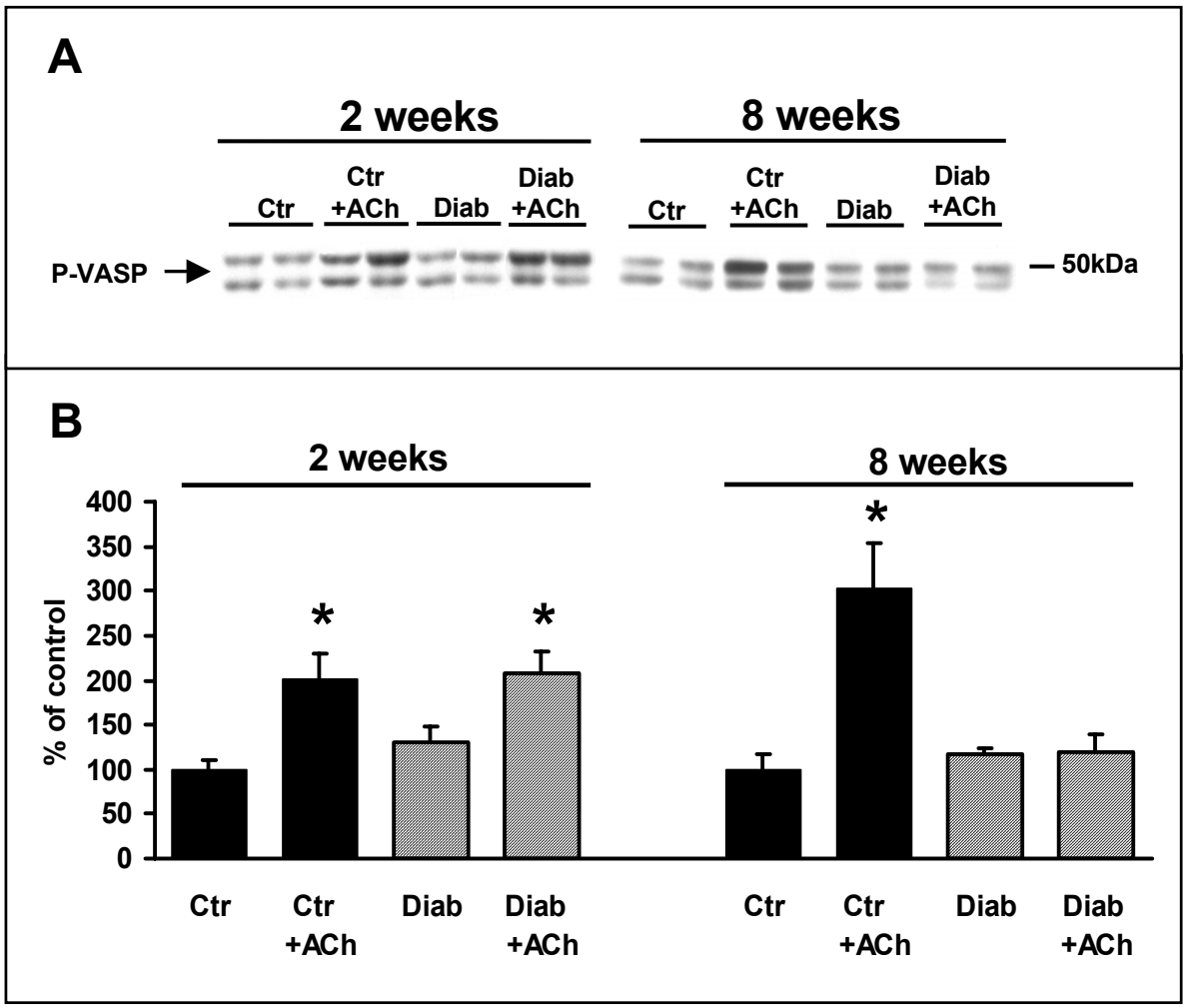

Fig. 3.30. Phosphorylation of VASP on ser239 in aorta of 2 and 8 week control (Ctr) and diabetic (Diab) animals. **(A)** Original Western blots detecting VASP phosphorylation on ser239 protein in ACh (1µM)-stimulated and unstimulated aortic homogenates of 2 representative control and diabetic animals. **(B)** Densitometric analysis of Western blots. Data are expressed as the mean ± SEM of 4-6 animals per group.

3.13.6 Expression of HO-1

In the 2 week treatment group, there was a striking decrease in the expression of HO-1 in the diabetic group as compared to the controls, while in the 8 week treatment group these levels returned to near control levels (Fig. 3.31.)

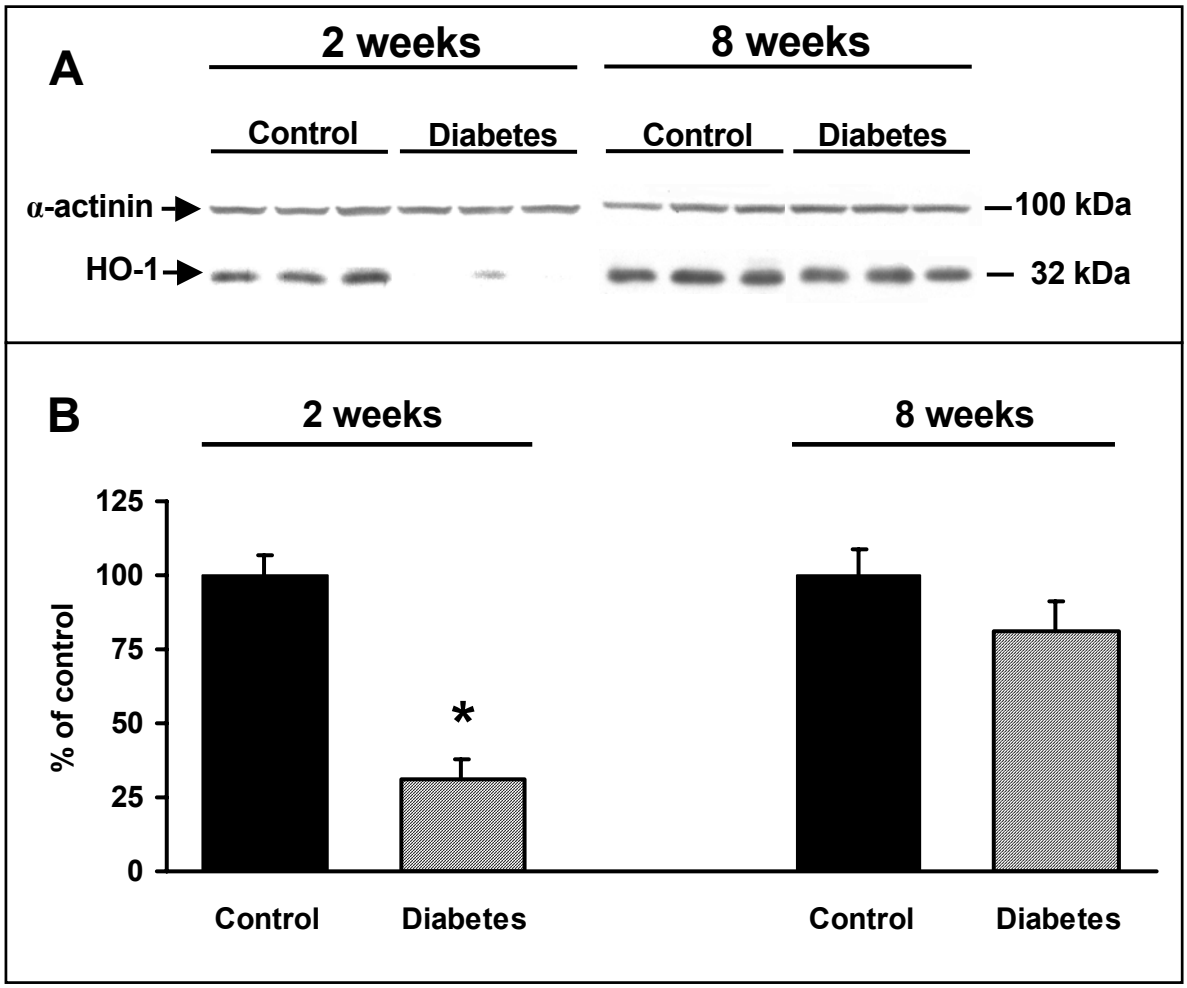

Fig. 3.31. Expression of HO-1 in aorta of 2 and 8 week control and diabetic animals. **(A)** Original Western blots detecting HO-1 protein in aortic homogenates of 3 representative control and diabetic animals. **(B)** Densitometric analysis of Western blots. Data are expressed as the mean ± SEM of 9-12 animals per group. * $p<0.05$ compared to control.

4 Discussion

It is well known, that the development of vascular complications in diabetes is associated with endothelial dysfunction, as indicated by reduced vasodilation in response to ACh. However, while pronounced macro- and microvascular endothelial dysfunction is a hallmark of late stage diabetes, the early stages of uncomplicated diabetes are characterized by increased blood flow and reduced peripheral resistance [67]. The underlying mechanisms of these divergent phenomena are still obscure. This study, for the first time, assessed the hypothesis, that early (2 week) and late (8 week) stage diabetes is associated with differences in ROS production with concomitant changes in the NO/cGMP signaling pathway. To facilitate the discussion of our data, a tabular summary of all results is given in Table 4.1.

Table 4.1. Tabular summary of results of this study: 0: no change, ↓/↑: decrease/increase, ↓↓/↑↑: highly significant decrease/increase, (↓)/(↑) trend towards decrease/increase, +e: endothelium intact, -e: endothelium denuded, ACh: acetylcholine, EPR: electron paramagnetic resonance, NTG: nitroglycerin, Phe: phenylephrine, SNP: sodium nitroprusside.

Vasoreactivity	**2 weeks**	**8 weeks**
ACh relaxation + e	↑	↓
- e	0	0
NTG relaxation + e	↑	↓
- e	0	↓ (high affinity)
SNP relaxation + e	0	(↓)
KCl contraction + e	↓	↓
- e	(↓)	↓↓
Phe contraction + e	0	(↓)
NO/cGMP pathway		
NO_2^- serum	↑	0
NO_3^- serum	0	↑
eNOS (Western blot)	0	↑↑
eNOS (immunohisto)	0	↑
$^{\bullet}NO$ (EPR) +ACh	0	↓↓
+A23187	↑	↑

HO-1		↓↓	0
sGC	basal	0	0
	+SNP	↑	0
cGMP	basal	↑	↑
	+SNP	↑	0
sGC-ß1		(↑)	0
cGK-I		0	0
P-VASPser239	basal	0	0
	+ACh	0	↓↓
ROS production			
lucigenin	basal	(↑)	(↑)
	+ACh	↑	↑
	+L-NNA	0	0
coelenterazine	basal	↓↓	(↑)
	+L-NNA	↑	0
L-012	basal	0	(↑)
	+L-NNA	↑↑	↑
DHE staining		↓	↑
NADPH oxidase activity (heart)		↑↑	↑↑
NADPH oxidase activity (aorta)		0	↑↑
nox1		0	↑↑
nox4		0	0
$p67^{phox}$		↓↓	0
Cu/ZnSOD		0	↑↑
Other			
cAMP	basal	0	↑
	+ACh	0	↑
ACE serum		↑	↑

4.1 Influence of early and late stage diabetes on vascular reactivity to relaxing stimuli

To test the endothelium-dependent vasoreactivity of aortic rings, we used the receptor-dependent agonist ACh. In agreement with the literature [65, 66], our results showed improved vasorelaxtion in response to ACh (10^{-7} to $10^{-5.5}$ M) in the diabetic animals of early stage diabetes (2 weeks), while late stage diabetes (8 weeks) was hallmarked by pronounced attenuation of ACh-induced vasodilation, signifying endothelial dysfunction (Fig.3.1.). Removing the endothelium from the aortic rings completely abolished the ACh-induced vasorelaxtion in both the 2 and the 8 week treatment groups (Fig. 3.2.), showing that an intact endothelium is needed for ACh to elicit its effect.

The impact of disease **duration** on endothelium-dependent vascular relaxation in this model of STZ-induced diabetes was underlined by a study by Willbrandt [73]. By using similar concentration of STZ as in our study, she showed a pronounced ACh-induced relaxation of aortic rings of diabetic animals at 2 weeks, no difference at 3 weeks, pronounced endothelial dysfunction at 6 weeks, which was attenuated at 12 weeks (Fig. 4.1.). However, these studies, in contrast to ours, where done in the absence of the cox inhibitor indomethacin, which may explain the more prominent differences in relaxation between control and diabetic animals of the 2 week treatment group compared to that observed in our study. At the same time, the study by Willbrandt showed a strong influence of the **dose** of STZ used (Fig. 4.1.). These findings underline the critical need to standardize procedures when studying endothelial dysfunction in this model of diabetes.

In further studies, we attempted to reveal the mechanism underlying the increased endothelium-dependent vasorelaxtion in early stage diabetes. Potential mechanisms may include increased ACh signaling efficiency, increased $^{\bullet}$NO formation and/or bioavailability or enhanced signaling efficiency of the NO/cGMP pathway. Diabetic animals of the 2 week treatment group also exhibited increased vasorelaxation to the endothelium-independent vasodilator NTG compared to controls (Fig. 3.3), pointing either towards increased bioactivation of NTG, or an increased sensitivity of the diabetic rat aorta to NO/cGMP-dependent vasodilators.

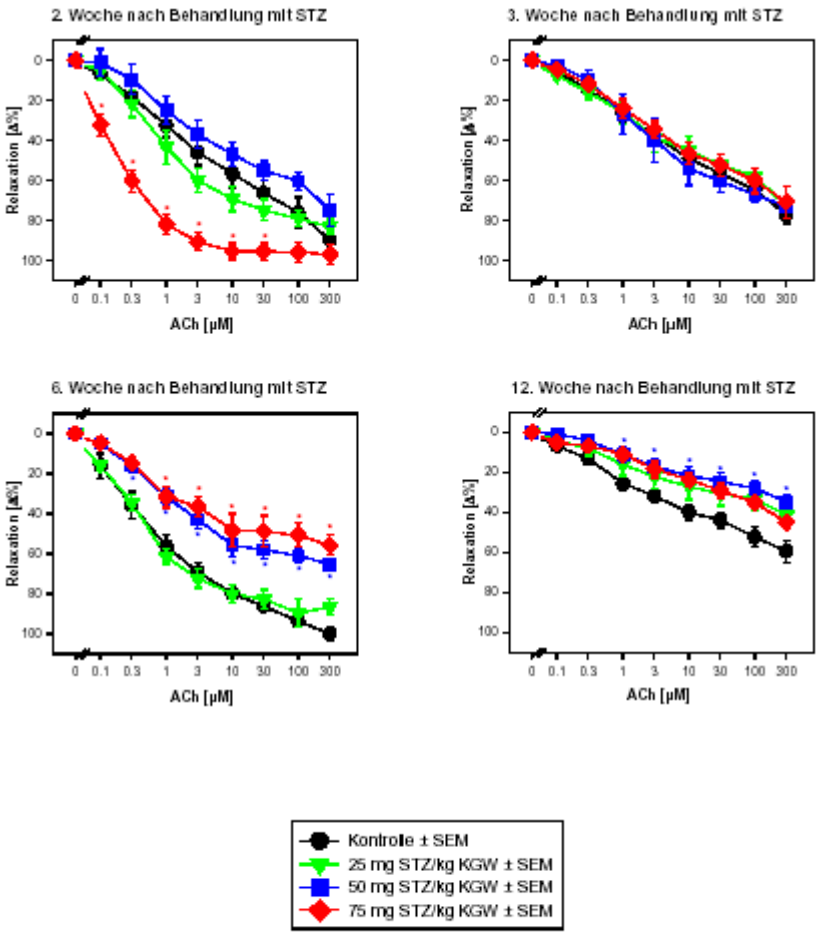

Fig. 4.1. Study showing the effect of STZ dose and disease duration on the development of endothelial dysfunction in STZ-induced diabetes. Wistar rats were injected into the tail vein with varying concentrations of STZ. The dose of 75 mg/kg (diamond symbol) is similar to the dose used in this study (70 mg/kg). Sham-injected control animals are denoted by the filled black circle. Blood glucose levels and body weights of the 2 week treatment group (graph top left corner) were similar to those recorded in our study (graph taken from the thesis by A. Willbrandt, http://elib.tiho-hannover.de/dissertations/willbrandta_2001.pdf).

When the aortic rings were denuded of the endothelium, the NTG response in the diabetic animals normalized (Fig. 3.4.), indicating that in these animals, the endothelium may sensitize the vessels to the vasodilatory action of NTG. A different mechanism may also account for this observation, including increased bioactivation of NTG by the mitochondrial aldehyde dehydrognease (mtALDH) in endothelial cells [74, 75]. Indeed, preliminary studies of our

group showed that mtALDH activity in diabetic rat aorta of the 2 week treatment group was slightly increased compared to controls (Daiber et al., unpublished results). Another explanation could be an increased bioavailability of NTG-derived $^{\bullet}NO$ and/or increased sensitivity of sGC to $^{\bullet}NO$-induced activation. Indeed, as discussed below, both mechansims seem to be functional. An improved bioavailability of $^{\bullet}NO$ is suggested by our observation that the NAD(P)H oxidase subunit $p67^{phox}$ was markedly **decreased** (Fig.3.25.), which could result in decreased $O_2^{\bullet-}$ formation in the endothelium (as observed with DHE staining (Fig. 3.16.)) and thus decreased scavenging of $^{\bullet}NO$. An increased sensitivity of sGC to $^{\bullet}NO$-elicited activation was indicated by our findings that in the aortic homogenates of the 2 week diabetic rats, SNP stimulated the sGC activity to a significantly higher degree than that of control homogenates (see below).

In contrast to our findings in early diabetes, the vasorelaxation to NTG in the 8 week treatment group was significantly reduced in the diabetic animals (Fig. 3.3.) and this effect was still observed when the rings were denuded of the endothelium (Fig. 3.4.) (although only at higher NTG concentrations). This points to either a decreased bioactivation of NTG in the smooth muscle mitochondria, and/or a decreased sensitivity of SMC to NTG-induced relaxation. It is well known and a common observation that NTG exhibits a biphasic concentration-response relationship, explained by two different pathways of NTG bioactivation [76]. According to recent findings by our group, the high affinity/potency pathway is mediated by mtALDH, and is therefore confined to endothelial and smooth muscle mitochondria [77]. The low affinity/potency pathway (NTG concentrations $>10^{-6}$ M), which generates EPR-detectable amounts of $^{\bullet}NO$, is mediated by an unknown bioactivation process of which possible candidates include CYP_{450} isoenzymes [78] and the xanthine oxidoreductase [79]. Closer inspection of our NTG dose-response curves (Fig. 3.4.) indeed shows a biphasic behaviour of endothelium-denuded vessels. Specifically, the efficacy of the high affinity pathway is significantly attenuated in diabetic aortas (Fig. 4.2., see dashed line), which may point to decreased bioactivation of NTG by reduced mtALDH activity.

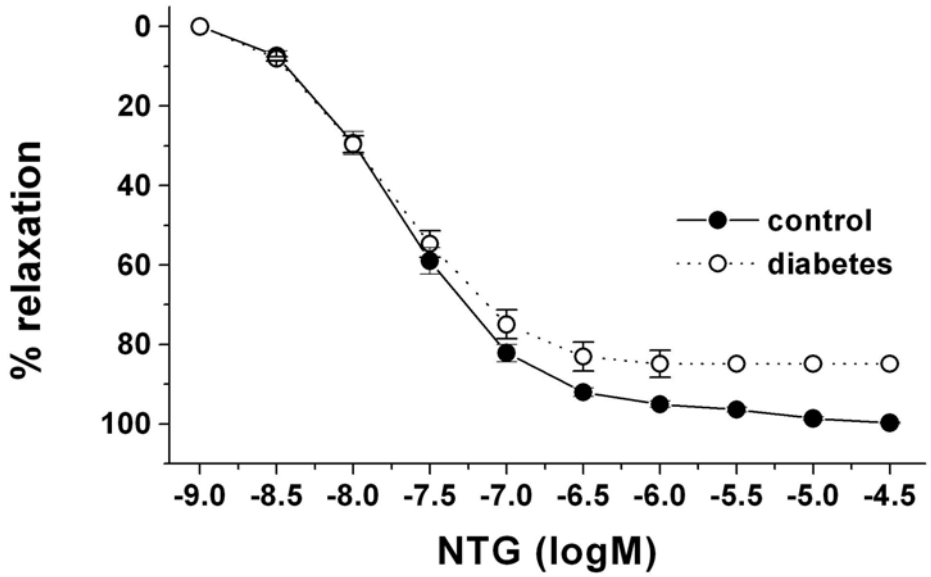

Fig. 4.2. Effect of the endothelium-independent vasodilator nitroglycerin (NTG) on the relaxtion of endothelium-denuded aortic rings of 8 week control and diabetic animals. The dashed line shows the extrapolated high affinity/potency NTG response curve that is dependent on mitochondrial aldehyde dehydrogenase activity, showing a decreased efficacy in the diabetic animals compared to controls (refer to Fig. 3.4.).

In order to test the $^{\bullet}$NO responsiveness of the aorta, we used the $^{\bullet}$NO donor SNP. We observed no differences in the vasodilatory response to SNP between control and diabetic animals of the 2 week treatment group (Fig. 3.5.). This observation was unexpected when comparing it to our findings of an **increased** vasodilator response to ACh and NTG (see above). A possible explanation for these apparently discrepant findings could be a reduced bioactivation of SNP [80]; however, this is not supported by our cGMP measurements (see section 4.4). Another reason may be that SNP relaxes aortic smooth muscle, in part, by a mechanism unrelated to cGMP formation, such as hyperpolarization of the SMC membrane by activation of large conductance calcium-dependent potassium (BK_{Ca}) channels [81] or by the inward rectifier channels [82]. Indeed, a decrease in the conductance of BK_{Ca} channels in the smooth muscle cells of STZ-induced diabetic mice was observed by Ye et al. [83].

In the 8 week diabetic group the EC_{50} for SNP-induced relaxation increased slightly but significantly compared to controls, pointing to a decreased sensitivity of the diabetic SMC to •NO-elicited vasorelaxation, possibly due to a defect in the •NO/cGMP signaling pathway (see section 4.4).

In summary, our results show that early diabetes is associated with increased endothelium-dependent vasorelaxation and an increased sensitivity of SMC to NTG-induced relaxation (which seems to be endothelial dependent), while in late stage diabetes these 2 pathways are impaired. The role of the NO/cGMP pathway in mediating these responses was further elucidated in this study.

4.2 Influence of early and late stage diabetes on contractile properties of rat aorta

Since vascular tone is the net result of contracting and relaxing mechanisms, and since diabetes has been reported to affect the contractile behaviour of blood vessels, we next analyzed the effect of early and late stage diabetes on the contractile reponses of isolated rat aortic rings.

Phe causes vasoconstriction by binding to the α_1-adrenergic receptor, which activates phospholipase C, increases formation of diacylglycerol (DAG) and inositol-3-phosphate (IP_3), thereby increasing intracellular calcium levels, leading to contraction. We found no significant difference in the Phe-induced contraction in the 2 week treatment group but a slight trend towards increased sensitivity to Phe in the diabetic animals of the 8 week treatment group. This data is in agreement with Chang et al. [84], who found no change in Phe-induced contraction of aortic rings in early stage (12 weeks) diabetes. This group did observe a hypersensitivity to Phe in the late stages of the disease, however they characterized their late stage diabetic animals at 52 weeks.

To investigate the influence of early and late stage diabetes on receptor-independent contraction, we tested the response of aortic rings to increasing concentrations of KCl. In both, the 2 and 8 week treatment group the contraction in response to KCl was attenuated in the diabetic animals as compared to controls (Fig. 3.6.). When the endothelium was removed, contraction occurred at much lower KCl concentrations. While there was a slight decrease in the response to KCl in the diabetic animals of the 2 week treatment group, the 8 week diabetic animals demonstrated markedly reduced KCl-induced contraction compared to controls (Fig. 3.7). The fact that we saw no differences in the contraction induced by Phe indicates that changes in KCl-dependent contraction occur at a stage that is independent of Phe-induced

α-receptor activation. It thus seems that late stage diabetes results in altered sensitivity of the tissue to KCl. Decreased contraction responses to KCl in diabetic aorta have been reported by others [85]; moreover, Pfaffman et al. [86] showed that this effect was completely reversible by insulin treatment. Possible explanations for this phenomenon include a decrease in the number of voltage-dependent calcium channels and alterations in the activation of these channels by membrane depolarisation. Indeed, a study by Wang et al. [87] showed a decrease in the L-type voltage dependent calcium channel currents in SMC of diabetic tail artery. Moreover, these currents, which are subject to inhibition by cAMP, demonstrated an increased sensitivity to cAMP in the diabetic animals. Interestingly, we found increased basal and ACh-stimulated levels of cAMP in the aorta of diabetic animals of the 8 week but not the 2 week treatment group (Fig.3.12.), which could explain the marked attenuation of the contraction response to KCl observed in these animals.

4.3 The role of $^{\bullet}NO$ in diabetic vascular dysfunction

$^{\bullet}NO$ is a crucial mediator in maintaining adequate vascular tone and we therefore looked at the expression of eNOS, the pre-eminent $^{\bullet}NO$ source in the vasculature, using both Western blot analysis and immunohistochemistry. In the 2 week treatment group, there was no difference in eNOS expression between control and diabetic animals as assessed with Western blotting; however, in the diabetic animals of the 8 week treatment group, eNOS expression was markedly increased (Fig. 3.26.). These data agree with results obtained by immunohistochemistry, showing no change in the 2 week treatment group but a marked increase in eNOS staining in the endothelium of the diabetic animals of the 8 week treatment group as compared to controls (Fig. 3.20.). This increase in eNOS expression seems contradictory to the observed endothelial dysfunction in these animals. Yet several other studies reported increased eNOS expression in the setting of oxidative stress and diabetes [88]. A possible explanation for this phenomenon could be a counter-regulatory mechanism, triggered by decreased biovailabitily of $^{\bullet}NO$. Decreased bioavailability of $^{\bullet}NO$, on the other hand, could be the result of increased degradation to inactive metabolites, increased scavenging by high prevailing levels of $O_2^{\bullet-}$ or increased adduct formation with the existing high levels of glucose in the plasma of diabetic animals [89]. Recently, it was shown that H_2O_2 potently stimulates eNOS expression [90] and it is conceivable that this plays a role in the upregulation of eNOS in the setting of oxidative stress and diabetes. This is supported by a study by Laude et al. [91] who observed an increase in eNOS expression in the aorta of mice with tissue-specific

overexpression of $p22^{phox}$ and nox1. These authors concluded, that H_2O_2 levels in the endothelium accounted for increased eNOS expression. H_2O_2 levels are likely to increase as a result of increased levels $O_2^{\bullet-}$ which undergoes dismutation by SOD. Interestingly, we found an increased expression of the Cu/ZnSOD in the diabetic animals of the 8 week treatment group (Fig. 3.27.), which could generate increased levels of H_2O_2. Higher expression of Cu/ZnSOD in this study and higher expression of the ecSOD in the study by Laude et al. are most likely adaptive responses to increased oxidative stress.

To see whether increased eNOS expression actually translates into increased formation of $^{\bullet}NO$, we measured $^{\bullet}NO$ in intact aortic rings by EPR using the $^{\bullet}NO$ spin trap $Fe^{II}(DETC)_2$. The detection of $^{\bullet}NO$ in vascular tissue can be difficult because of the extreme instability of this radical. However, by utilizing the high affinity of $^{\bullet}NO$ for certain Fe^{2+}-complexes, it can be caged to form a stable paramagnetic adduct whose characteristic spectrum can be detected by EPR. The spin trap $Fe^{II}(DETC)_2$ associates with the cell membrane due to its hydrophobic character, and is therefore especially useful in monitoring $^{\bullet}NO$ produced by eNOS, as this enzyme is associated with caveolae of cell membranes. In the 2 week treatment group, ACh elicited no significant difference in $^{\bullet}NO$ production between control and diabetic animals; however, in the 8 week treatment group, the ACh-induced $^{\bullet}NO$ production was significantly reduced in the diabetic group as compared to controls (Fig. 3.21.), pointing towards either a decreased bioavailability of receptor stimulated $^{\bullet}NO$, or a defect in the ACh/calcium signaling pathway, thereby leading to decreased stimulation of eNOS. A further explanation for this observation could be that the eNOS is uncoupled, producing $O_2^{\bullet-}$ instead of $^{\bullet}NO$, as has been reported for some pathological states, including diabetes [88]. When the calcium ionophore A23187 was used, $^{\bullet}NO$ production was increased to a similar extent in the diabetic rats of both treatment groups compared to controls. In the 8 week treatment group, the increase in $^{\bullet}NO$ may merely be ascribed to the observed increase in the expression of eNOS. The observation that calcium ionophore-induced maximal activation of eNOS was similar in early and late stage diabetes may best be explained by a reduced spin-trapping efficiency of $^{\bullet}NO$ in late diabetes because the spin trap can compete with the increased $O_2^{\bullet-}$ for $^{\bullet}NO$ [92]. The observed increase in calcium ionophore-induced maximal $^{\bullet}NO$ formation in the diabetic animals of the 2 week treatment group compared to controls may be explained by a similar mechanism, i.e. a higher $^{\bullet}NO$ spin trapping efficiency due to reduced $O_2^{\bullet-}$ formation (as observed with DHE staining). These results, however, argue against an uncoupled, non-functional NOS in the diabetic state.

It must be remembered that the NOS enzyme family consists of the three isoforms, namely eNOS, iNOS and nNOS. While most studies on vascular dysfunction have focused on the role of eNOS, little attention has been given to the other two isoforms, presumably because their importance in vascular dysfunction is much disputed. Yet several reports indicated that iNOS was increased in the vascular smooth muscle cells of STZ-induced diabetic rats [93] and a recent study by Gunnett et al. [94] showed that STZ-induced diabetes produced impairment of endothelial-dependent relaxation in arteries of wild type but not iNOS knock-out mice. The presence of nNOS in vascular tissue is controversial, but it was recently detected in the neointima and medial smooth muscle cells of mice where it suppresses atherosclerotic lesion formation [95]. However, because iNOS is calcium/calmodulin independent, effects seen after stimulation with ACh or the calcium ionophore A23187 are likely to involve only eNOS (or nNOS).

Another popular method of assessing $^{\bullet}NO$ bioavailability is the detection of the plasma level of NO_x (ie. the sum of NO_2^- and NO_3^-). In the presence of molecular oxygen, $^{\bullet}NO$ is rapidly oxidized to NO_2^- which forms the major breakdown product of $^{\bullet}NO$ in human plasma. NO_2^- may be taken up by red blood cells where it is oxidized in a hemoglobin-dependent manner to NO_3^-, which is subsequently released back into the plasma. In addition, excess $ONOO^-$ may decompose to yield NO_3^-. Both NO_2^- and NO_3^- have been used as biomarkers for $^{\bullet}NO$ bioavailability in human blood. Studies in both animal models [96] and human diabetes [97] report increases in plasma NO_x levels. However, it was recently reported that only plasma NO_2^- accurately reflects changes in eNOS activity, while changes in plasma NO_3^- or NO_x generally do not present useful markers as their levels are influenced by a variety of NOS-independent factors, including dietary NO_3^- intake, denitrifying liver enzymes and renal function [98]. We therefore used the DAN assay, capable of detecting NO_2^- in the nM range, and used nitrate reductase to differentiate between NO_3^- and NO_2^-. In the 2 week treatment group, we found a significant increase in NO_2^- in the serum of the diabetic animals with no change in NO_3^-, while in the 8 week treatment group, the diabetic animals showed no change in NO_2^- but a significant increase in NO_3^- (Fig. 3.22.). This points towards either an increase in $^{\bullet}NO$ formation, or an increased bioavailability of $^{\bullet}NO$ in the 2 week treatment group. Our data obtained for the 8 week treatment group is supported by Maejima et al. [99] who found no change in plasma NO_2^- but an increase in NO_3^- in patients with type 2 diabetes. Since NO_3^- plasma levels are mainly controlled by renal elimination, the increased NO_3^- levels in late diabetes seemingly indicate reduced elimination due to compromised kidney function, a common complication of

late diabetes [100]. Interestingly, Maejima et al. [99] also showed that the increase in NO_3^- was strongly associated with serum AGE levels, which have been shown to play an important role in causing hyperglycemia-induced oxidative stress and subsequent vascular dysfunction [27].

4.4 The role of the NO/sGC/cGK-I signaling pathway

To elucidate the role of NO-downstream signaling in our setting of diabetes, we looked at the sGC activity in homogenates of aortic rings. While we found no differences in basal activity in any of the groups, SNP-stimulated sGC activity was markedly increased in the diabetic animals of the 2 week treatment group compared to controls (Fig. 3.10.). This increase in activity may be due to increased protein expression or to increased sensitivity towards $^{\bullet}NO$. While we did see a significant increase in the expression of $sGC\beta_1$ in these animals, this is likely to be too slight to cause the observed marked increase in sGC product formation, namely cGMP in intact aortic tissue as assessed by EIA. However, it may explain the increase in basal cGMP levels in the diabetic animals of this group. On the other hand, the increased basal cGMP levels observed in the diabetic animals of the 8 week treatment group could be a potential counter-regulatory mechanism resulting in decreased PDE activity, as has been reported in the aorta of diabetic rats [101]. In the 8 week treatment group, there was no change in SNP-stimulated sGC activity, which correlated well with cGMP product formation, where again we found no difference between control and diabetic animals.Another possible explanation for the increased basal cGMP levels in both the 2 and 8 week treatment group could be the activation of pGC by ANP. Increased plasma ANP levels where found in STZ-rats treated for 2 and 4 weeks [102] as well as in patients with type 1 diabetes [103].

In the 8 week treatment group, there was no change in SNP-stimulated sGC activity, which correlated well with cGMP product formation, where again we found no difference between control and diabetic animals. These results are supported by a study by Witte et al. [104] who found no difference in $^{\bullet}NO$-stimulated sGC activity in the mammary artery of control and type 2 diabetic patients. Furthermore, Schaefer et al. [105] found **no increase** in sGC activity in the retina of rats 6 weeks after STZ injection, which they propose to be due to $O_2^{\bullet-}$ interfering with $^{\bullet}NO$-mediated sGC activation. Other studies, however, show a **reduction** in sGC activity in the aorta of the genetically modified type 2 diabetic Goto-Kakizaki rat [106] while still others showed an **increase** in the SNP-stimulated cGMP accumulation in cultured SMC from diabetic rats [107].

In recent years, the microsomal enzyme HO was shown to play an increasingly important role in conditions of oxidative stress. HO breaks down heme to generate biliverdin, free ferrous iron and CO. Biliverdin is than rapidly converted to bilirubin by biliverdin reductase and free iron is sequestered by ferritin. Three isoforms of HO exist: HO-1 is the inducible form, activated by heme and other oxidants, heavy metals, proinflammatory cytokines, hypoxia and shear stress. HO-2 and HO-3 are constitutively expressed and are similar in amino acid structure. HO-2 is expressed in many organs throughout the body, but particularly in brain and testes while the recently identified HO-3 is thought to be a less efficient heme catalyst.

The proposed protective role HO-1 is likely to be exerted by its ability to degrade pro-oxidant heme, by the production of biliverdin and bilirubin, both of which have antioxidant properties and by the generation of CO. CO is able to activate sGC with the formation of cGMP resulting in a vasodilatory response, as was shown for the coronary circulation [108]. However, CO may promote vasodilation independent of cGMP by stimulating calcium-activated potassium channels [109]. Furthermore, CO may inhibit the production of the potent vasoconstrictor endothelin [110]. In all, an increase in HO-1 is likely to go hand in hand with increased vasodilation. This could explain the marked decrease in HO-1 expression seen in the diabetic animals of the 2 week treatment group (Fig. 3.31.), whereby the decrease in HO-1 is counteracting the increased vasodilation seen in these animals. Moreover, the observed hypersensitivity of sGC to $^{\bullet}NO$ (and thus possibly to CO) could also result in the downregulation of CO production. Furthermore, HO was shown to inhibit $^{\bullet}NO$ formation, therefore a decrease in HO could result in increased $^{\bullet}NO$ production/bioavailability, as we postulate to occur in these animals [110].

However, an increase in HO would also mean an increase in the release of free iron which in turn would increase oxidative modification of proteins in Fenton chemistry based reactions. Therefore, HO is protective but within a narrow threshold of overexpression [111] since the iron released may obviate any cytoprotective effect. This could explain our results of the diabetic animals in the 8 week treatment group, where HO-1 expression normalized, but did not increase, as would be expected in the setting of oxidative stress.

We next examined cGK-I, the downstream target of cGMP. The expression of cGK-I did not differ between any of the treatment groups. Furthermore, when assessing the basal activity of this enzyme, by looking at the phosphorylation state of VASP on ser239, there was no significant difference in **basal** cGK-I activity between control and diabetic animals in the two treatment groups. However, when aortic rings in the 2 week treatment group were stimulated with ACh, we observed a significant but similar increase in phosphorylation of VASP on ser239 in both the control and diabetic animals. In the 8 week treatment group, ACh stimulation also resulted in a marked increase in VASP phosphorylation on ser239 expression in the control group; however, in the diabetic group, the effect of ACh was completely abolished. These results point towards a defective ACh/NO/cGK-I pathway in the 8 week treatment group and are in agreement with the observed endothelial dysfunction seen in the diabetic animals of this group. This data also agrees with our EPR experiments, where the ACh-induced $^{\bullet}NO$ production was markedly reduced in the diabetic animals of the 8 but not the 2 week treatment group.

In the 8 week treatment group there was no change in sGC activity or cGMP production; however, a defect in the ACh-induced cGK-I activity was observed that could explain the observed endothelial dysfunction.

4.5 Vascular ROS production

The growing number of studies showing the importance of oxidative stress in the development of vascular disease have increased the need to develop methods to detect ROS with high specificity and sensitivity in vascular tissue. One commonly employed method is the use of CL probes which, on exposure to $O_2^{\bullet-}$, release a photon that can be detected in a luminometer.

The most widely used CL compound is lucigenin which, due to its structure, is considered to primarily detect extracellular ROS. It has been used widely in cultured cells, tissue homogenates and intact vascular tissue, however, the credibility of using this compound for the detection of $O_2^{\bullet-}$ has been questioned because of a phenomenon called redox cycling. Hereby lucigenin undergoes cycles of univalent reduction followed by auto-oxidation to yield $O_2^{\bullet-}$. This results in an artificial overestimation of $O_2^{\bullet-}$, which becomes especially important in biological systems in which the $O_2^{\bullet-}$ levels are low. High concentrations (> 250 μM) of lucigenin favor redox cycling and although today it is generally excepted that low concentrations of lucigenin (ie. 5 μM) do not produce $O_2^{\bullet-}$, there are studies that do show redox cycling at lower

concentrations [112, 113]. In the control animals of the 2 week treatment group, ACh resulted in a slight decrease in CL signal (20 %) suggesting slightly increased $^{\bullet}NO$ scavenging of $O_2^{\bullet-}$. On the other hand, the CL signal was not significantly changed by addition of L-NNA, indicating that superoxide formation was not limiting $^{\bullet}NO$ bioavailability. The slight increase in CL in the diabetic group compared to controls is not consistent with our functional organ chamber experiments and other ROS (CL/immunofluorescent) data, where we observe an attenuation of $O_2^{\bullet-}$ production in these 2 week diabetic animals. One explanation could be an overestimation of $O_2^{\bullet-}$ due to the above mentioned phenomenon of redox cycling, which becomes especially important in systems of low $O_2^{\bullet-}$. Moreover, as lucigenin is likely to detect only extracellular $O_2^{\bullet-}$, it may be difficult to ascertain physiologically representative levels because our experimental ex-vivo setup does not take into account the effect of antioxidants in serum and extracellular fluid components, including low molecular weight oxidant scavengers and the extracellular SOD. In addition, the contribution of other intracellular scavenging systems and those in the mitochondria are not taken into account. In the diabetic animals of the 8 week group there was a slight but significant increase in the lucigenin signal compared to controls, and the addition of ACh resulted in a further slight increase, which may be due to increased ACh-induced protein kinase C activation, leading to increased NAD(P)H oxidase activity. L-NNA had no effect on the lucigenin signal, presumably due to the limitations of the lucigenin detection method.

Coelenterazine is a lipophilic luminophore that permeates membranes and detects intracellular ROS. It is directly oxidized by $O_2^{\bullet-}$, thus eliminating redox cycling artifacts; however, it is not entirely specific for $O_2^{\bullet-}$ and may also detect $ONOO^-$. In the diabetic animals of the 2 week group, we found a marked decrease in coelenterazine signal intensity compared to controls which increased by 2-fold after the addition of L-NNA. These results argue against the possibility of the signal being due to the detection of $ONOO^-$ as in this case one would expect a decrease rather than an increase in signal intensity (as a result of decreased scavenging of $O_2^{\bullet-}$ by $^{\bullet}NO$). In fact, the difference in coelenterazine signal intensity in the diabetic group with and without L-NNA points to an increased bioavailability of $^{\bullet}NO$ in the 2 week diabetic animals, due to reduced basal $O_2^{\bullet-}$. The data of the 8 week treatment group agrees with our data obtained with lucigenin, showing a slight increase in CL signal intensity in the diabetic animals as compared to controls while L-NNA had no effect, indicating that eNOS was not uncoupled.

L-012 is a novel luminol analogue that, according to its structure, may detect intra- and extracellular ROS. However, conventional SOD which does not penetrate membranes was shown to abolish the L-012-derived CL signal from mitochondria, which strongly points to a predominantly extracellular detection of ROS. L-012 was previously described to detect $O_2^{\bullet-}$ in inflammatory cells and by our group in vascular tissue [114] and does not undergo redox cycling. However, our group also showed that L-012 is not specific for $O_2^{\bullet-}$ but may also detect $ONOO^-$, whereby high concentrations of $^{\bullet}NO$ were shown to quench the $ONOO^-$ signal. In the 2 week treatment group, we observed no change in basal CL signal intensity between control and diabetic animals. At first glance this seems to contradict our data obtained with lucigenin (both lumiphores detect extracellular $O_2^{\bullet-}$), yet it may be possible that the high levels of $O_2^{\bullet-}$ (as observed with lucigenin) may react with $^{\bullet}NO$ to form $ONOO^-$. However, conditions where high levels of $^{\bullet}NO$ prevail (as we postulate to be the case in the 2 week treatment group) the $ONOO^-$ signal is quenched [115], which would account for the lack of difference in signal intensity between control and diabetic animals. However, when $^{\bullet}NO$ is removed from the system by the addition of L-NNA, no $ONOO^-$ is expected to be formed and the observed increase in signal may be ascribed entirely to $O_2^{\bullet-}$. This again is evidence for the fact that there must be a significant increase in $^{\bullet}NO$ bioavailability in these animals. In the 8 week treatment group, we found an increase in $O_2^{\bullet-}$ ($ONOO^-$) in the diabetic group compared to controls while L-NNA had no significant effect, suggesting limited $^{\bullet}NO$ bioavailability.

Finally, it must be remembered that the effects seen in the above experiments in the presence of the non-specific inhibitor L-NNA can not entirely be ascribed to the inhibition of eNOS alone, as iNOS and nNOS will also be inhibited, and it may be possible that these isozymes are differently expressed in early and late diabetes.

Another commonly employed method to detect $O_2^{\bullet-}$ in tissue sections is the DHE fluorescence. DHE is a cell-permeable compound that can undergo a two-electron oxidation to from the DNA-binding fluorophore ethidium bromide. Although this method is semi-quantitative, it can provide information about the topographical location of ROS in the vessel wall. DHE is reasonably specific for $O_2^{\bullet-}$ with little oxidation induced by H_2O_2, $ONOO^-$ or HOCl. One drawback of this method, however, is the capability of cytochrome c to oxidize DHE, which may play a role in situations where mitochondria form the major source of $O_2^{\bullet-}$, or where they release cytochrome c, for example in early apoptosis. Our results in the 2 week treatment group show a decrease in $O_2^{\bullet-}$-derived staining in the diabetic animals compared to controls. This

effect is particularly obvious in the endothelium and the adventitia, and indicates a marked reduction in superoxide formation in early diabetes, consistent with our hypothesis of increased $^{\bullet}NO$ bioavailability in this stage. In the 8 week treatment group, $O_2^{\bullet-}$ was markedly increased in the adventitia and the media but also in the endothelium, consitent with the notion that oxidative stress is increased in late diabetes and NO bioavailability is reduced. The staining observed in the adventitia should, however, be interpreted with caution, as this may merely reflect the extent to which the vessel was cleaned of surrounding tissue.

In summary, we used several different methods commonly employed to detect ROS (in particular $O_2^{\bullet-}$) in vascular tissue. However, the above mentioned drawbacks of each method have to be considered when interpreting any data. At the same time it demonstrates the absolute need to use at least 2 or 3 detection methods to be able to draw a reliable conclusion from the results.

From our data it can be concluded that in the vessels of the diabetic animals of 2 week treatment group there seems to be a decrease in $O_2^{\bullet-}$ levels (or oxidative stress) especially in the endothelium, which is associated with an increase in L-NNA sensitive $^{\bullet}NO$ bioavailability. In the vessels of the diabetic animals of the 8 week treatment group, however, there is an increase in $O_2^{\bullet-}$ levels (or oxidative stress) in the media and endothelium that seems to go hand in hand with a defect in the L-NNA sensitive $^{\bullet}NO$ bioavailability.

4.6 The role of the NAD(P)H oxidase in vascular tissue

The NAD(P)H oxidase is believed to be the major $O_2^{\bullet-}$ source in vascular tissue. To see what role this enzyme plays in our observed differences in ROS levels, we looked at the expression of the NADPH oxidase subunits nox1 and nox4 as well as $p67^{phox}$.

In the diabetic animals of the 2 week treatment group, we found no significant increase in nox1 or nox 4 expression as compared to controls; however, the expression of $p67^{pox}$ was markedly reduced in these animals (Figs. 3.23.-3.25.).

In the 8 week treatment group, there was a marked increase in nox1 expression in the diabetic group while the expression of both nox4 and $p67^{pox}$ remained unchanged compared to controls (Fig. 3.23.-3.25). While the catalytic subunit $gp91^{phox}$ plays an important role in neutrophils, endothelial cells and fibroblasts, it seems to be lacking in SMC of large arteries. However, in these cells two functional homologues of $gp91^{phox}$ have been identified, namely nox1 and nox4.

While nox1 and nox4 mRNA are also detectable in endothelial cells and fibroblasts, only nox1 is found in inflammatory cells [24]. Angiotensin II infusion [12] as well as carotid injury [116] drastically increase nox1 expression with no or minor change in nox4 expression. While nox1 mediates agonist induced-superoxide production and proliferation of smooth muscle cells [117], nox4 may be more involved in steady state production of low amounts of superoxide that are important in the control of metabolic and differentiation functions of the cell as well as in apoptosis. An important role for the NAD(P)H oxidase in diabetes was given by recent studies in vascular tissue from diabetic animals and patients showing increased NAD(P)H oxidase activity as well as increased expression of the NAD(P)H oxidase subunits $p22^{phox}$ and $gp91^{phox}$ as well as $p47^{phox}$ and $p67^{phox}$ at the mRNA and protein level, respectively [44, 88, 118]. However, these observations most likely do not reflect ROS produced in the media, since $gp91^{phox}$ is not the catalytic subunit in smooth muscle cells from large arteries. Interestingly, in vessels from atherosclerotic monkeys, increased levels of the NAD(P)H oxidase subunits $p22^{phox}$ and $p47^{phox}$ co-localized with macrophages [118]. This suggests that macrophage infiltration may represent another potential and distinct source of $O_2^{\bullet-}$ in diabetic vascular tissue.

While an increased expression of nox4 and $p22^{phox}$ was observed in the kidney of STZ-induced diabetic rats, no data are available on the expression of either nox1 or nox4 in the aorta of these animals. We here, for the first time, demonstrate the disease duration-dependent upregulation of the $gp91^{phox}$ homologue nox1 in the aorta of diabetic rats. This upregulation may explain the increase in superoxide production observed with DHE staining in the media of the 8 week treatment group. The decreased staining observed in the media of the 2 week diabetic group seems not to be due to a decrease in the expression of nox1 but may be the result of increased scavenging of $O_2^{\bullet-}$ (by $^{\bullet}NO$) and the marked decrease in $p67^{phox}$, whereby the lack of association of $p67^{phox}$ with nox1, nox4, $gp91^{phox}$ or $p22^{phox}$ could result in a dysfunctional oxidase. In the 8 week treatment group, the expression of $p67^{phox}$ increased by 2-fold compared to the 2 week diabetic rats, and nox1 was now highly expressed. This upregulation of NAD(P)H oxidase components in late diabetes provides an increased capacity for superoxide formation.

Differential regulation of nox1 and nox4, as observed in our model of diabetes, was also shown in an angiotensin II-induced model of hypertension [12] and in a model of restenosis after balloon injury [116]. As previously mentioned, nox1 is thought to mediate the agonist-induced superoxide production as its mRNA in SMC was markedly upregulated in response to

angiotensin II, platelet derived growth factor and serum, while nox4 was rather downregulated by these stimuli [117]. Of note, ACE activity was found to be increased in the aorta of STZ-treated rats [119], while ACE inhibitors as well as angiotensin II blockers improved complications associated with diabetes [120]. Furthermore, a recent study by Forbes et al. [121] showed a reduction in the accumulation of AGE by ACE inhibition in diabetic nephropathy. In our study, we too found an increase in ACE activity in the serum of diabetic animals.

AGE were shown to play a major role in diabetic endothelial dysfunction by leading to altered gene expression in a range of cells via their receptors (RAGE) [122]. Interestingly, a recent study showed that AGE activate a NAD(P)H oxidase in human endothelial cells, which was inhibitable by the flavin-dependent inhibitor DPI [123]. It is thus tempting to speculate that AGE may also be involved in the agonist-induced superoxide production associated with nox1 in diabetes. Recently, two novel proteins (NOXO1 and NOXA1) were identified in mouse colon which activate the $O_2^{\bullet-}$ generation by nox1 [124]. This activation was stimulus-independent; however, in the presence of $p47^{phox}$ or $p67^{phox}$, activation of nox1 became stimulus-dependent. Other studies support this data, showing that $O_2^{\bullet-}$ generation by SMC which contain nox1 is stimulus dependent and involves $p47^{phox}$ [125]. Thus, an interaction of nox1 with phagocyte NAD(P)H oxidase subunits may occur in some tissue and this would make nox1 a versatile enzyme that could change activation mechanisms depending on the subunits present in the cell type it which it is expressed.

Taken together, reasons for the existence of distinct nox proteins and their differential regulation remain poorly understood but data point to the fact that their function may be determined by their different localization within the cell. While $gp91^{phox}$ is associated with the plasma membrane, recent studies have associated nox4 with focal adhesion complexes and nox1 with caveolae [126]. The latter is an interesting observation because NOS is also associated with caveolae and this makes it feasible to speculate that the vascular dysfunction observed in our 8 week treatment group may be due to a localized increase in the scavenging of $^{\bullet}NO$ by nox1-procuded $O_2^{\bullet-}$.

A critical question is whether increased expression of the NAD(P)H oxidase subunit is translated into increased NAD(P)H oxidase activity. Recently, Kim et al. [54], using lucigenin-enhanced CL (high lucigenin concentration of 250 µM), found that the NADH-driven $O_2^{\bullet-}$ production was significantly increased in homogenates from vessels of OLETF rats, a type 2 diabetes model. However, when using NADH to drive the NAD(P)H oxidase and high lucigenin concentrations as the detector, a considerable degree of redox-cycling occurs, which raises doubts of whether increased NADH-mediated superoxide production reflects increases in

the activity of the NAD(P)H oxidase or whether this is artifactual [127]. For this reason, we used low lucigenin concentrations (5 μM) and NADPH as an electron donor. In the membrane fraction of heart tissue of both the 2 and 8 week treatment group, we found a significant increase in $O_2^{\bullet-}$ in response to NADPH while no change in response to NADH was observed, indicating that in heart tissue NAD(P)H oxidases preferentially use NADPH rather than NADH to produce $O_2^{\bullet-}$. DPI quenched the signal, pointing towards the involvement of a flavin-containing enzyme, while neither rotenone (inhibitor of mitochondrial superoxide production) nor L-NNA had any effect on the NADPH-induced $O_2^{\bullet-}$ formation, thus excluding the mitochondria and NOS as $O_2^{\bullet-}$ sources. Furthermore, addition of hypoxanthine resulted in no change in signal intensity, thereby excluding the involvement of xanthine oxidase. There was no difference in basal activity (in the absence of NADPH) between control and diabetic animals. This would be expected because of the lack of available NADPH in preparations of membrane fractions.

In membrane fractions of aorta, we found a 1.6 fold increase in the NADPH-stimulated oxidase activity only in the 8 week treatment group, while there was no difference in the 2 week treatment group. This data goes hand in hand with the expression of nox1 and it may point to a critical role of this NAD(P)H oxidase subunit in the vascular dysfunction observed in diabetes.

The difference in the NAD(P)H oxidase activity between heart and aortic tissue in the 2 week treatment group is unclear. The subunits $gp91^{phox}$, $p22^{phox}$, $p67^{pox}$ and $p47^{phox}$ were found to exist in rat cardiac myocytes where they are thought to play a role in α-adrenoceptor stimulation-induced hypertrophy [128, 129]. Furthermore, $p47^{phox}$ protein was increased in rat ventricular myocytes cultured in high glucose medium [130]. However, heart tissue is a versatile mixture of cells, and one therefore can not exclude the possibility that the effects are due to increased infiltration of the heart tissue by inflammatory cells.

5 Summary and Conclusion

Vascular disease is the main etiology for death and for a great percent of morbidity in patients with diabetes mellitus. Although pronounced macro- and microvascular endothelial dysfunction is a hallmark of late stage diabetes, the early stage of uncomplicated diabetes is characterized by increased blood flow and reduced peripheral resistance. The underlying mechanisms of these divergent phenomena are still obscure and the aim of this study was to elucidate the role of oxidative stress and its effect on the NO/cGMP pathway in early and late stage diabetes, using the well established model of type 1 diabetes, the STZ-induced diabetic rat.

The data of this study shows that early diabetes is associated with increased ACh-induced, endothelium-dependent vasorelaxation that goes hand in hand with an increased sensitivity of SMC to the endothelium-independent vasodilator NTG. Early diabetes had no effect on the receptor- (Phe) mediated contraction nor on the KCl-induced contraction in the absence of the endothelium and moreover, cAMP levels were not affected. Although we observed no change in NADPH oxidase activity, ROS levels, as assessed with CL and DHE staining as well as the expression of the NAD(P)H oxidase subunit $p67^{phox}$ and HO-1, a marker of oxidative stress, were decreased in early diabetes. Serum NO_2^- , a marker of $^{\bullet}NO$ bioavailability, was increased in the diabetic animals and this was associated with an increased sensitivity of sGC to $^{\bullet}NO$ with a concomitant increase in cGMP levels. Furthermore, our results show that in early diabetes the contribution of $^{\bullet}NO$ to vasorelaxation may not occur via the cGMP/cGK-I pathway (as assessed with VASP phosphorylation on ser239) and further studies are needed to elucidate the exact mechanism by which $^{\bullet}NO$ elicits its vasodilatory effect in these animals.

Late stage diabetes, on the other hand, exhibited a marked decrease in ACh-induced, endothelium-dependent vasorelaxation, which was associated with decreased sensitivity of SMC to the endothelium-independent vasodilator NTG. Although we found no change in receptor- (Phe) mediated contraction of aortic rings, the KCl-induced contraction in the absence of the endothelium was markedly attenuated in late stage diabetes. This may be explained by our observed increase in cAMP in these animals, which was shown to inhibit voltage-dependent calcium channels. ROS levels, as assessed with CL and DHE staining, were increased in the aorta of late stage diabetic animals as was the expression of Cu/ZnSOD, the enzyme responsible for $O_2^{\bullet-}$ dismutation. This is associated with an increase in the NAD(P)H oxidase subunit nox1 as well as an increases in the NADPH oxidase activity of aorta. Although eNOS expression was significantly increased in late stage diabetes, most likely due to a

compensatory mechanism, the ACh-induced •NO bioavailability was markedly reduced, concomitant with reduced ACh-induced cGK-I activity (as assessed by the phosphorylation state of VASP on ser239), leading to endothelial dysfunction.

We can thus conclude that in early diabetes the aorta seems to over-compensate for the oxidative stress that is associated with hyperglycemia by decreasing ROS levels, which in turn leads to a concomitant increase in •NO bioavailability and vasodilation. However, in late stage diabetes, these compensatory mechanisms fail, resulting in hyperglycemia-induced increases in ROS, decreased •NO bioavailability and eventually endothelial dysfunction.

This study reconciles the divergent data on endothelial dysfunction found in the literature and emphasizes the need to standardize all procedures when using this model of STZ-induced diabetes mellitus.

6 Abbreviations

ACE	angiotensin converting enzyme
ACh	acetylcholine
cAMP	adenosine 3',5'-cyclic monophosphate
cGMP	guanosine 3',5'-cyclic monophosphate
CL	chemiluminescence
DAN	2,3-diaminonaphthalene
DETC	diethyldithiocarbamate
DHE	dihydroethidium
dH_2O	distilled water
DPI	diphenyleneiodium
DTPA	diethylenetriaminepentaacetic acid
DTT	dithiothreitol
ECL	enhanced chemiluninescence
ecSOD	extracellular superoxide dismutase
EDTA	ethylenediaminetetraacetic acid
EGTA	ethylene glycol-bis(2-aminoethylether)-N,N,N',N'-tetraacetic acid
EIA	enzyme immunoassay
eNOS	endothelial nitric oxide
EPR	electroparamagnetic resonance
FAD	flavin adenine dinucleotide
GTP	guanosine 5'-triphosphate
IBMX	3-isobutyl-1-methylxanthine
L0-12	8-amino-5-chloro-7-phenylpyridol[3,4-*d*]pyridazine-1,4-(2H,3H)dione
L-NNA	N^G-nitro-L-arginine
NADH	ß-nicotinamide adenine dinuleotide, reduced form
NADPH	ß-nicotinamide adenine dinuleotide phosphate, reduced form
NO_2^-	nitrite
NO_3^-	nitrate
NOS	nitric oxide synthase
NTG	nitroglycerin
$O_2^{\bullet-}$	superoxide

OLETF	Otsuka Long Evans Tokushima Fatty
PAGE	polyacrylamide gel electrophoresis
PBS	phospate buffered saline
PDE	phosphodiesterase
pGC	particulate guanylate cyclase
Phe	phenylephrine
PMSF	phenylmethanesulfonyl fluoride
P-VASP	vasodilator stimulated phosphoprotein, phosphorylated on ser239
ROS	reactive oxygen species
SDS	sodium dodecyl sulfate
sGC	soluble guanylyl cyclase
SMC	smooth muscle cells
SNP	sodium nitroprusside
SOD	superoxide dismutase
STZ	streptozotocin
TEMED	N,N,N',N'-tetramethylethylenediamine
TMB	3,3',5'5'-tetramethylbenzidine
VASP	vasodilator stimulated phosphoprotein

7 References

1. Zimmet, P.; Alberti, K. G.; Shaw, J. Global and societal implications of the diabetes epidemic. *Nature.* **414**:782-787; 2001.
2. Myers, M. A.; Mackay, I. R.; Rowley, M. J.; Zimmet, P. Z. Dietary microbial toxins and type 1 diabetes-a new meaning for seed and soil. *Diabetologia.* **44**:1199-1200; 2001.
3. Furchgott, R. F.; Zawadzki, J. V. The obligatory role of endothelial cells in the relaxation of arterial smooth muscle by acetylcholine. *Nature.* **288**:373-376; 1980.
4. Palmer, R. M.; Ferrige, A. G.; Moncada, S. Nitric oxide release accounts for the biological activity of endothelium-derived relaxing factor. *Nature.* **327**:524-526; 1987.
5. Radomski, M. W.; Palmer, R. M.; Moncada, S. The anti-aggregating properties of vascular endothelium: interactions between prostacyclin and nitric oxide. *Br J Pharmacol.* **92**:639-646; 1987.
6. Garg, U. C.; Hassid, A. Nitric oxide-generating vasodilators and 8-bromo-cyclic guanosine monophosphate inhibit mitogenesis and proliferation of cultured rat vascular smooth muscle cells. *J Clin Invest.* **83**:1774-1777; 1989.
7. Kuhn, M. Structure, regulation, and function of mammalian membrane guanylyl cyclase receptors, with a focus on guanylyl cyclase-A. *Circ Res.* **93**:700-709; 2003.
8. Friebe, A.; Koesling, D. Regulation of nitric oxide-sensitive guanylyl cyclase. *Circ Res.* **93**:96-105; 2003.
9. Pfeifer, A.; Klatt, P.; Massberg, S.; Ny, L.; Sausbier, M.; Hirneiss, C.; Wang, G. X.; Korth, M.; Aszodi, A.; Andersson, K. E.; Krombach, F.; Mayerhofer, A.; Ruth, P.; Fassler, R.; Hofmann, F. Defective smooth muscle regulation in cGMP kinase I-deficient mice. *Embo J.* **17**:3045-3051; 1998.
10. Smolenski, A.; Bachmann, C.; Reinhard, K.; Honig-Liedl, P.; Jarchau, T.; Hoschuetzky, H.; Walter, U. Analysis and regulation of vasodilator-stimulated phosphoprotein serine 239 phosphorylation in vitro and in intact cells using a phosphospecific monoclonal antibody. *J Biol Chem.* **273**:20029-20035; 1998.
11. Oelze, M.; Mollnau, H.; Hoffmann, N.; Warnholtz, A.; Bodenschatz, M.; Smolenski, A.; Walter, U.; Skatchkov, M.; Meinertz, T.; Munzel, T. Vasodilator-stimulated phosphoprotein serine 239 phosphorylation as a sensitive monitor of defective nitric oxide/cGMP signaling and endothelial dysfunction. *Circ Res.* **87**:999-1005; 2000.

12. Mollnau, H.; Wendt, M.; Szocs, K.; Lassegue, B.; Schulz, E.; Oelze, M.; Li, H.; Bodenschatz, M.; August, M.; Kleschyov, A. L.; Tsilimingas, N.; Walter, U.; Forstermann, U.; Meinertz, T.; Griendling, K.; Munzel, T. Effects of angiotensin II infusion on the expression and function of NAD(P)H oxidase and components of nitric oxide/cGMP signaling. *Circ Res.* **90**:E58-65; 2002.

13. Schulz, E.; Tsilimingas, N.; Rinze, R.; Reiter, B.; Wendt, M.; Oelze, M.; Woelken-Weckmuller, S.; Walter, U.; Reichenspurner, H.; Meinertz, T.; Munzel, T. Functional and biochemical analysis of endothelial (dys)function and NO/cGMP signaling in human blood vessels with and without nitroglycerin pretreatment. *Circulation.* **105**:1170-1175; 2002.

14. Doroudi, R.; Gan, L. M.; Selin Sjogren, L.; Jern, S. Effects of shear stress on eicosanoid gene expression and metabolite production in vascular endothelium as studied in a novel biomechanical perfusion model. *Biochem Biophys Res Commun.* **269**:257-264; 2000.

15. Fisslthaler, B.; Popp, R.; Kiss, L.; Potente, M.; Harder, D. R.; Fleming, I.; Busse, R. Cytochrome P450 2C is an EDHF synthase in coronary arteries. *Nature.* **401**:493-497; 1999.

16. Schachinger, V.; Zeiher, A. M. Prognostic implications of endothelial dysfunction: does it mean anything? *Coron Artery Dis.* **12**:435-443; 2001.

17. Fleming, I.; Michaelis, U. R.; Bredenkotter, D.; Fisslthaler, B.; Dehghani, F.; Brandes, R. P.; Busse, R. Endothelium-derived hyperpolarizing factor synthase (Cytochrome P450 2C9) is a functionally significant source of reactive oxygen species in coronary arteries. *Circ Res.* **88**:44-51; 2001.

18. Lopes, L. R.; Dagher, M. C.; Gutierrez, A.; Young, B.; Bouin, A. P.; Fuchs, A.; Babior, B. M. Phosphorylated p40pox as a negative regulator of NADPH oxidase. *Biochemistry.* **43**:3723-3730; 2004.

19. Mohazzab, K. M.; Kaminski, P. M.; Wolin, M. S. NADH oxidoreductase is a major source of superoxide anion in bovine coronary artery endothelium. *Am J Physiol.* **266**:H2568-2572; 1994.

20. Griendling, K. K.; Minieri, C. A.; Ollerenshaw, J. D.; Alexander, R. W. Angiotensin II stimulates NADH and NADPH oxidase activity in cultured vascular smooth muscle cells. *Circ Res.* **74**:1141-1148; 1994.

21. Pagano, P. J.; Clark, J. K.; Cifuentes-Pagano, M. E.; Clark, S. M.; Callis, G. M.; Quinn, M. T. Localization of a constitutively active, phagocyte-like NADPH oxidase in rabbit

aortic adventitia: enhancement by angiotensin II. *Proc Natl Acad Sci U S A.* **94**:14483-14488; 1997.

22. Suh, Y. A.; Arnold, R. S.; Lassegue, B.; Shi, J.; Xu, X.; Sorescu, D.; Chung, A. B.; Griendling, K. K.; Lambeth, J. D. Cell transformation by the superoxide-generating oxidase Mox1. *Nature.* **401**:79-82; 1999.
23. Lambeth, J. D.; Cheng, G.; Arnold, R. S.; Edens, W. A. Novel homologs of gp91phox. *Trends Biochem Sci.* **25**:459-461; 2000.
24. Sorescu, D.; Weiss, D.; Lassegue, B.; Clempus, R. E.; Szocs, K.; Sorescu, G. P.; Valppu, L.; Quinn, M. T.; Lambeth, J. D.; Vega, J. D.; Taylor, W. R.; Griendling, K. K. Superoxide production and expression of nox family proteins in human atherosclerosis. *Circulation.* **105**:1429-1435; 2002.
25. Shiose, A.; Kuroda, J.; Tsuruya, K.; Hirai, M.; Hirakata, H.; Naito, S.; Hattori, M.; Sakaki, Y.; Sumimoto, H. A novel superoxide-producing NAD(P)H oxidase in kidney. *J Biol Chem.* **276**:1417-1423; 2001.
26. Mahadev, K.; Motoshima, H.; Wu, X.; Ruddy, J. M.; Arnold, R. S.; Cheng, G.; Lambeth, J. D.; Goldstein, B. J. The NAD(P)H oxidase homolog Nox4 modulates insulin-stimulated generation of H2O2 and plays an integral role in insulin signal transduction. *Mol Cell Biol.* **24**:1844-1854; 2004.
27. De Vriese, A. S.; Verbeuren, T. J.; Van de Voorde, J.; Lameire, N. H.; Vanhoutte, P. M. Endothelial dysfunction in diabetes. *Br J Pharmacol.* **130**:963-974; 2000.
28. Antoniades, C.; Tousoulis, D.; Tountas, C.; Tentolouris, C.; Toutouza, M.; Vasiliadou, C.; Tsioufis, C.; Toutouzas, P.; Stefanadis, C. Vascular endothelium and inflammatory process, in patients with combined Type 2 diabetes mellitus and coronary atherosclerosis: the effects of vitamin C. *Diabet Med.* **21**:552-558; 2004.
29. Beckman, J. A.; Goldfine, A. B.; Gordon, M. B.; Garrett, L. A.; Keaney, J. F., Jr.; Creager, M. A. Oral antioxidant therapy improves endothelial function in Type 1 but not Type 2 diabetes mellitus. *Am J Physiol Heart Circ Physiol.* **285**:H2392-2398; 2003.
30. Uhlmann, S.; Rezzoug, K.; Friedrichs, U.; Hoffmann, S.; Wiedemann, P. Advanced glycation end products quench nitric oxide in vitro. *Graefes Arch Clin Exp Ophthalmol.* **240**:860-866; 2002.
31. Komers, R.; Anderson, S. Paradoxes of nitric oxide in the diabetic kidney. *Am J Physiol Renal Physiol.* **284**:F1121-1137; 2003.

32. Xu, B.; Chibber, R.; Ruggiero, D.; Kohner, E.; Ritter, J.; Ferro, A.; Ruggerio, D. Impairment of vascular endothelial nitric oxide synthase activity by advanced glycation end products. *Faseb J.* **17**:1289-1291; 2003.

33. Crijns, F. R.; Struijker Boudier, H. A.; Wolffenbuttel, B. H. Arteriolar reactivity in conscious diabetic rats: influence of aminoguanidine treatment. *Diabetes.* **47**:918-923; 1998.

34. Vallejo, S.; Angulo, J.; Peiro, C.; Sanchez-Ferrer, A.; Cercas, E.; Llergo, J. L.; Nevado, J.; Sanchez-Ferrer, C. F.; Rodriguez-Manas, L. Prevention of endothelial dysfunction in streptozotocin-induced diabetic rats by gliclazide treatment. *J Diabetes Complications.* **14**:224-233; 2000.

35. Nishikawa, T.; Edelstein, D.; Brownlee, M. The missing link: a single unifying mechanism for diabetic complications. *Kidney Int Suppl.* **77**:S26-30; 2000.

36. Ishii, H.; Koya, D.; King, G. L. Protein kinase C activation and its role in the development of vascular complications in diabetes mellitus. *J Mol Med.* **76**:21-31; 1998.

37. Koya, D.; King, G. L. Protein kinase C activation and the development of diabetic complications. *Diabetes.* **47**:859-866; 1998.

38. Inoguchi, T.; Battan, R.; Handler, E.; Sportsman, J. R.; Heath, W.; King, G. L. Preferential elevation of protein kinase C isoform beta II and diacylglycerol levels in the aorta and heart of diabetic rats: differential reversibility to glycemic control by islet cell transplantation. *Proc Natl Acad Sci U S A.* **89**:11059-11063; 1992.

39. Tesfamariam, B.; Brown, M. L.; Cohen, R. A. Elevated glucose impairs endothelium-dependent relaxation by activating protein kinase C. *J Clin Invest.* **87**:1643-1648; 1991.

40. Beckman, J. A.; Goldfine, A. B.; Gordon, M. B.; Garrett, L. A.; Creager, M. A. Inhibition of protein kinase C beta prevents impaired endothelium-dependent vasodilation caused by hyperglycemia in humans. *Circ Res.* **90**:107-111; 2002.

41. Inoguchi, T.; Li, P.; Umeda, F.; Yu, H. Y.; Kakimoto, M.; Imamura, M.; Aoki, T.; Etoh, T.; Hashimoto, T.; Naruse, M.; Sano, H.; Utsumi, H.; Nawata, H. High glucose level and free fatty acid stimulate reactive oxygen species production through protein kinase C-dependent activation of NAD(P)H oxidase in cultured vascular cells. *Diabetes.* **49**:1939-1945; 2000.

42. Cosentino, F.; Eto, M.; De Paolis, P.; van der Loo, B.; Bachschmid, M.; Ullrich, V.; Kouroedov, A.; Delli Gatti, C.; Joch, H.; Volpe, M.; Luscher, T. F. High glucose causes upregulation of cyclooxygenase-2 and alters prostanoid profile in human endothelial

cells: role of protein kinase C and reactive oxygen species. *Circulation.* **107**:1017-1023; 2003.

43. Hirata, K.; Kuroda, R.; Sakoda, T.; Katayama, M.; Inoue, N.; Suematsu, M.; Kawashima, S.; Yokoyama, M. Inhibition of endothelial nitric oxide synthase activity by protein kinase C. *Hypertension.* **25**:180-185; 1995.
44. Guzik, T. J.; Mussa, S.; Gastaldi, D.; Sadowski, J.; Ratnatunga, C.; Pillai, R.; Channon, K. M. Mechanisms of increased vascular superoxide production in human diabetes mellitus: role of NAD(P)H oxidase and endothelial nitric oxide synthase. *Circulation.* **105**:1656-1662; 2002.
45. Lee, H. B.; Yu, M. R.; Song, J. S.; Ha, H. Reactive oxygen species amplify protein kinase C signaling in high glucose-induced fibronectin expression by human peritoneal mesothelial cells. *Kidney Int.* **65**:1170-1179; 2004.
46. Zou, M. H.; Shi, C.; Cohen, R. A. Oxidation of the zinc-thiolate complex and uncoupling of endothelial nitric oxide synthase by peroxynitrite. *J Clin Invest.* **109**:817-826; 2002.
47. Shinozaki, K.; Nishio, Y.; Okamura, T.; Yoshida, Y.; Maegawa, H.; Kojima, H.; Masada, M.; Toda, N.; Kikkawa, R.; Kashiwagi, A. Oral administration of tetrahydrobiopterin prevents endothelial dysfunction and vascular oxidative stress in the aortas of insulin-resistant rats. *Circ Res.* **87**:566-573; 2000.
48. Heitzer, T.; Krohn, K.; Albers, S.; Meinertz, T. Tetrahydrobiopterin improves endothelium-dependent vasodilation by increasing nitric oxide activity in patients with Type II diabetes mellitus. *Diabetologia.* **43**:1435-1438; 2000.
49. Desco, M. C.; Asensi, M.; Marquez, R.; Martinez-Valls, J.; Vento, M.; Pallardo, F. V.; Sastre, J.; Vina, J. Xanthine oxidase is involved in free radical production in type 1 diabetes: protection by allopurinol. *Diabetes.* **51**:1118-1124; 2002.
50. Butler, R.; Morris, A. D.; Belch, J. J.; Hill, A.; Struthers, A. D. Allopurinol normalizes endothelial dysfunction in type 2 diabetics with mild hypertension. *Hypertension.* **35**:746-751; 2000.
51. Matsumoto, S.; Koshiishi, I.; Inoguchi, T.; Nawata, H.; Utsumi, H. Confirmation of superoxide generation via xanthine oxidase in streptozotocin-induced diabetic mice. *Free Radic Res.* **37**:767-772; 2003.
52. Nishikawa, T.; Edelstein, D.; Du, X. L.; Yamagishi, S.; Matsumura, T.; Kaneda, Y.; Yorek, M. A.; Beebe, D.; Oates, P. J.; Hammes, H. P.; Giardino, I.; Brownlee, M.

Normalizing mitochondrial superoxide production blocks three pathways of hyperglycaemic damage. *Nature.* **404**:787-790; 2000.

53. Lee, H. S.; Son, S. M.; Kim, Y. K.; Hong, K. W.; Kim, C. D. NAD(P)H oxidase participates in the signaling events in high glucose-induced proliferation of vascular smooth muscle cells. *Life Sci.* **72**:2719-2730; 2003.
54. Kim, Y. K.; Lee, M. S.; Son, S. M.; Kim, I. J.; Lee, W. S.; Rhim, B. Y.; Hong, K. W.; Kim, C. D. Vascular NADH oxidase is involved in impaired endothelium-dependent vasodilation in OLETF rats, a model of type 2 diabetes. *Diabetes.* **51**:522-527; 2002.
55. Bhardwaj, R.; Moore, P. K. Increased vasodilator response to acetylcholine of renal blood vessels from diabetic rats. *J Pharm Pharmacol.* **40**:739-742; 1988.
56. Shen, B.; Ye, C. L.; Ye, K. H.; Liu, J. J. Mechanism underlying enhanced endothelium-dependent vasodilatation in thoracic aorta of early stage streptozotocin-induced diabetic mice. *Acta Pharmacol Sin.* **24**:422-428; 2003.
57. Alabadi, J. A.; Miranda, F. J.; Llorens, S.; Ruiz de Apodaca, R. F.; Centeno, J. M.; Alborch, E. Diabetes potentiates acetylcholine-induced relaxation in rabbit renal arteries. *Eur J Pharmacol.* **415**:225-232; 2001.
58. Brands, M. W.; Fitzgerald, S. M. Acute endothelium-mediated vasodilation is not impaired at the onset of diabetes. *Hypertension.* **32**:541-547; 1998.
59. Mulhern, M.; Docherty, J. R. Effects of experimental diabetes on the responsiveness of rat aorta. *Br J Pharmacol.* **97**:1007-1012; 1989.
60. Lash, J. M.; Bohlen, H. G. Structural and functional origins of suppressed acetylcholine vasodilation in diabetic rat intestinal arterioles. *Circ Res.* **69**:1259-1268; 1991.
61. Kiff, R. J.; Gardiner, S. M.; Compton, A. M.; Bennett, T. Selective impairment of hindquarters vasodilator responses to bradykinin in conscious Wistar rats with streptozotocin-induced diabetes mellitus. *Br J Pharmacol.* **103**:1357-1362; 1991.
62. Diederich, D.; Skopec, J.; Diederich, A.; Dai, F. X. Endothelial dysfunction in mesenteric resistance arteries of diabetic rats: role of free radicals. *Am J Physiol.* **266**:H1153-1161; 1994.
63. Orie, N. N.; Aloamaka, C. P.; Iyawe, V. I. Duration-dependent attenuation of acetylcholine-but not histamine-induced relaxation of the aorta in diabetes mellitus. *Gen Pharmacol.* **24**:329-332; 1993.
64. Taylor, P. D.; Wickenden, A. D.; Mirrlees, D. J.; Poston, L. Endothelial function in the isolated perfused mesentery and aortae of rats with streptozotocin-induced diabetes:

effect of treatment with the aldose reductase inhibitor, ponalrestat. *Br J Pharmacol.* **111**:42-48; 1994.

65. Kobayashi, T.; Matsumoto, T.; Ooishi, K.; Kamata, K. Differential expression of alpha2D-adrenoceptor and eNOS in aortas from early and later stages of diabetes in Goto-Kakizaki rats. *Am J Physiol Heart Circ Physiol.* **287**:H135-143; 2004.
66. Pieper, G. M. Enhanced, unaltered and impaired nitric oxide-mediated endothelium-dependent relaxation in experimental diabetes mellitus: importance of disease duration. *Diabetologia.* **42**:204-213; 1999.
67. Mogensen, C. E. Glomerular filtration rate and renal plasma flow in normal and diabetic man during elevation of blood sugar levels. *Scand J Clin Lab Invest.* **28**:177-182; 1971.
68. Kohner, E. M.; Hamilton, A. M.; Saunders, S. J.; Sutcliffe, B. A.; Bulpitt, C. J. The retinal blood flow in diabetes. *Diabetologia.* **11**:27-33; 1975.
69. Houben, A. J.; Schaper, N. C.; Slaaf, D. W.; Tangelder, G. J.; Nieuwenhuijzen Kruseman, A. C. Skin blood cell flux in insulin-dependent diabetic subjects in relation to retinopathy or incipient nephropathy. *Eur J Clin Invest.* **22**:67-72; 1992.
70. Wascher, T. C.; Graier, W. F.; Bahadori, B.; Toplak, H. Time course of endothelial dysfunction in diabetes mellitus. *Circulation.* **90**:1109-1110; 1994.
71. Junod, A.; Lambert, A. E.; Orci, L.; Pictet, R.; Gonet, A. E.; Renold, A. E. Studies of the diabetogenic action of streptozotocin. *Proc Soc Exp Biol Med.* **126**:201-205; 1967.
72. Bradford, M. M. A rapid and sensitive method for the quantitation of microgram quantities of protein utilizing the principle of protein-dye binding. *Anal Biochem.* **72**:248-254; 1976.
73. Willbrandt: http://elib.tiho-hannover.de/dissertations/willbrandta_2001.pdf).
74. Chen, Z.; Zhang, J.; Stamler, J. S. Identification of the enzymatic mechanism of nitroglycerin bioactivation. *Proc Natl Acad Sci U S A.* **99**:8306-8311; 2002.
75. Sydow, K.; Daiber, A.; Oelze, M.; Chen, Z.; August, M.; Wendt, M.; Ullrich, V.; Mulsch, A.; Schulz, E.; Keaney, J. F., Jr.; Stamler, J. S.; Munzel, T. Central role of mitochondrial aldehyde dehydrogenase and reactive oxygen species in nitroglycerin tolerance and cross-tolerance. *J Clin Invest.* **113**:482-489; 2004.
76. Ahlner, J.; Axelsson, K. L.; Ljusegren, M. E.; Grundstrom, N.; Andersson, R. G. Demonstration of a high affinity component of glyceryl trinitrate induced vasodilatation in the bovine mesenteric artery. *J Cyclic Nucleotide Protein Phosphor Res.* **11**:445-456; 1986.

77. Daiber, A.; Oelze, M.; Coldewey, M.; Bachschmid, M.; Wenzel, P.; Sydow, K.; Wendt, M.; Kleschyov, A. L.; Stalleicken, D.; Ullrich, V.; Mulsch, A.; Munzel, T. Oxidative Stress and Mitochondrial Aldehyde Dehydrogenase Activity: A Comparison of Pentaerythrityl Tetranitrate (PETN) with Other Organic Nitrates. *Mol Pharmacol.* 2004.

78. Schroder, H. Cytochrome P-450 mediates bioactivation of organic nitrates. *J Pharmacol Exp Ther.* **262**:298-302; 1992.

79. O'Byrne, S.; Shirodaria, C.; Millar, T.; Stevens, C.; Blake, D.; Benjamin, N. Inhibition of platelet aggregation with glyceryl trinitrate and xanthine oxidoreductase. *J Pharmacol Exp Ther.* **292**:326-330; 2000.

80. Rochelle, L. G.; Kruszyna, H.; Kruszyna, R.; Barchowsky, A.; Wilcox, D. E.; Smith, R. P. Bioactivation of nitroprusside by porcine endothelial cells. *Toxicol Appl Pharmacol.* **128**:123-128; 1994.

81. Mistry, D. K.; Garland, C. J. Nitric oxide (NO)-induced activation of large conductance Ca2+-dependent K+ channels (BK(Ca)) in smooth muscle cells isolated from the rat mesenteric artery. *Br J Pharmacol.* **124**:1131-1140; 1998.

82. Schubert, R.; Krien, U.; Wulfsen, I.; Schiemann, D.; Lehmann, G.; Ulfig, N.; Veh, R. W.; Schwarz, J. R.; Gago, H. Nitric oxide donor sodium nitroprusside dilates rat small arteries by activation of inward rectifier potassium channels. *Hypertension.* **43**:891-896; 2004.

83. Ye, C. L.; Shen, B.; Ren, X. D.; Luo, R. J.; Ding, S. Y.; Yan, F. M.; Jiang, J. H. An increase in opening of BK(Ca) channels in smooth muscle cells in streptozotocin-induced diabetic mice. *Acta Pharmacol Sin.* **25**:744-750; 2004.

84. Chang, K. S.; Stevens, W. C. Endothelium-dependent increase in vascular sensitivity to phenylephrine in long-term streptozotocin diabetic rat aorta. *Br J Pharmacol.* **107**:983-990; 1992.

85. Fulton, D. J.; Hodgson, W. C.; Sikorski, B. W.; King, R. G. Attenuated responses to endothelin-1, KCl and CaCl2, but not noradrenaline, of aortae from rats with streptozotocin-induced diabetes mellitus. *Br J Pharmacol.* **104**:928-932; 1991.

86. Pfaffman, M. A.; Ball, C. R.; Darby, A.; Hilman, R. Insulin reversal of diabetes-induced inhibition of vascular contractility in the rat. *Am J Physiol.* **242**:H490-495; 1982.

87. Wang, R.; Wu, Y.; Tang, G.; Wu, L.; Hanna, S. T. Altered L-type Ca(2+) channel currents in vascular smooth muscle cells from experimental diabetic rats. *Am J Physiol Heart Circ Physiol.* **278**:H714-722; 2000.

88. Hink, U.; Li, H.; Mollnau, H.; Oelze, M.; Matheis, E.; Hartmann, M.; Skatchkov, M.; Thaiss, F.; Stahl, R. A.; Warnholtz, A.; Meinertz, T.; Griendling, K.; Harrison, D. G.; Forstermann, U.; Munzel, T. Mechanisms underlying endothelial dysfunction in diabetes mellitus. *Circ Res.* **88**:E14-22; 2001.

89. Brodsky, S. V.; Morrishow, A. M.; Dharia, N.; Gross, S. S.; Goligorsky, M. S. Glucose scavenging of nitric oxide. *Am J Physiol Renal Physiol.* **280**:F480-486; 2001.

90. Drummond, G. R.; Cai, H.; Davis, M. E.; Ramasamy, S.; Harrison, D. G. Transcriptional and posttranscriptional regulation of endothelial nitric oxide synthase expression by hydrogen peroxide. *Circ Res.* **86**:347-354; 2000.

91. Laude, K.; Cai, H.; Fink, B.; Hoch, N.; Weber, D. S.; McCann, L.; Kojda, G.; Fukai, T.; Schmidt, H. H.; Dikalov, S.; Ramasamy, S.; Gamez, G.; Griendling, K. K.; Harrison, D. G. Hemodynamic and biochemical adaptations to vascular smooth muscle overexpression of p22phox in mice. *Am J Physiol Heart Circ Physiol.* 2004.

92. Venkataraman, S.; Martin, S. M.; Buettner, G. R. Electron paramagnetic resonance for quantitation of nitric oxide in aqueous solutions. *Methods Enzymol.* **359**:3-18; 2002.

93. Bardell, A. L.; MacLeod, K. M. Evidence for inducible nitric-oxide synthase expression and activity in vascular smooth muscle of streptozotocin-diabetic rats. *J Pharmacol Exp Ther.* **296**:252-259; 2001.

94. Gunnett, C. A.; Heistad, D. D.; Faraci, F. M. Gene-targeted mice reveal a critical role for inducible nitric oxide synthase in vascular dysfunction during diabetes. *Stroke.* **34**:2970-2974; 2003.

95. Tsutsui, M. Neuronal nitric oxide synthase as a novel anti-atherogenic factor. *J Atheroscler Thromb.* **11**:41-48; 2004.

96. Goor, Y.; Peer, G.; Iaina, A.; Blum, M.; Wollman, Y.; Chernihovsky, T.; Silverberg, D.; Cabili, S. Nitric oxide in ischaemic acute renal failure of streptozotocin diabetic rats. *Diabetologia.* **39**:1036-1040; 1996.

97. Ozden, S.; Tatlipinar, S.; Bicer, N.; Yaylali, V.; Yildirim, C.; Ozbay, D.; Guner, G. Basal serum nitric oxide levels in patients with type 2 diabetes mellitus and different stages of retinopathy. *Can J Ophthalmol.* **38**:393-396; 2003.

98. Lauer, T.; Kleinbongard, P.; Kelm, M. Indexes of NO bioavailability in human blood. *News Physiol Sci.* **17**:251-255; 2002.

99. Maejima, K.; Nakano, S.; Himeno, M.; Tsuda, S.; Makiishi, H.; Ito, T.; Nakagawa, A.; Kigoshi, T.; Ishibashi, T.; Nishio, M.; Uchida, K. Increased basal levels of plasma nitric

oxide in Type 2 diabetic subjects. Relationship to microvascular complications. *J Diabetes Complications.* **15**:135-143; 2001.

100. Mitch, W. E.; Shahinfar, S.; Dickson, T. Z.; de Zeeuw, D.; Zhang, Z. Detecting and managing patients with type 2 diabetic kidney disease: Proteinuria and cardiovascular disease. *Kidney Int Suppl.*S97-98; 2004.

101. Miller, M. A.; Morgan, R. J.; Thompson, C. S.; Mikhailidis, D. P.; Jeremy, J. Y. Hydrolysis of cyclic guanosine monophosphate and cyclic adenosine monophosphate by the penis and aorta of the diabetic rat. *Br J Urol.* **78**:252-256; 1996.

102. Wu, S. Q.; Kwan, C. Y.; Tang, F. Streptozotocin-induced diabetes has differential effects on atrial natriuretic peptide synthesis in the rat atrium and ventricle: a study by solution-hybridization-RNase protection assay. *Diabetologia.* **41**:660-665; 1998.

103. Bojestig, M.; Nystrom, F. H.; Arnqvist, H. J.; Ludvigsson, J.; Karlberg, B. E. The renin-angiotensin-aldosterone system is suppressed in adults with Type 1 diabetes. *J Renin Angiotensin Aldosterone Syst.* **1**:353-356; 2000.

104. Witte, K.; Hachenberger, J.; Castell, M. F.; Vahl, C. F.; Haller, C. Nitric oxide-sensitive soluble guanylyl cyclase activity is preserved in internal mammary artery of type 2 diabetic patients. *Diabetes.* **53**:2640-2644; 2004.

105. Schaefer, S.; Kajimura, M.; Tsuyama, S.; Uchida, K.; Sato, E.; Inoue, M.; Suematsu, M.; Watanabe, K. Aberrant utilization of nitric oxide and regulation of soluble guanylate cyclase in rat diabetic retinopathy. *Antioxid Redox Signal.* **5**:457-465; 2003.

106. Witte, K.; Reitenbach, I.; Stolpe, K.; Schilling, L.; Kirchengast, M.; Lemmer, B. Effects of the endothelin a receptor antagonist darusentan on blood pressure and vascular contractility in type 2 diabetic Goto-Kakizaki rats. *J Cardiovasc Pharmacol.* **41**:890-896; 2003.

107. Etienne, P.; Pares-Herbute, N.; Monnier, L. Enhanced antiproliferative effect of nitric oxide in cultured smooth muscle cells from diabetic rats. *J Cardiovasc Pharmacol.* **27**:140-146; 1996.

108. McGrath, J. J.; Smith, D. L. Response of rat coronary circulation to carbon monoxide and nitrogen hypoxia. *Proc Soc Exp Biol Med.* **177**:132-136; 1984.

109. Yet, S. F.; Pellacani, A.; Patterson, C.; Tan, L.; Folta, S. C.; Foster, L.; Lee, W. S.; Hsieh, C. M.; Perrella, M. A. Induction of heme oxygenase-1 expression in vascular smooth muscle cells. A link to endotoxic shock. *J Biol Chem.* **272**:4295-4301; 1997.

110. Morita, T.; Kourembanas, S. Endothelial cell expression of vasoconstrictors and growth factors is regulated by smooth muscle cell-derived carbon monoxide. *J Clin Invest.* **96**:2676-2682; 1995.

111. Dennery, P. A. Regulation and role of heme oxygenase in oxidative injury. *Curr Top Cell Regul.* **36**:181-199; 2000.

112. Barbacanne, M. A.; Souchard, J. P.; Darblade, B.; Iliou, J. P.; Nepveu, F.; Pipy, B.; Bayard, F.; Arnal, J. F. Detection of superoxide anion released extracellularly by endothelial cells using cytochrome c reduction, ESR, fluorescence and lucigenin-enhanced chemiluminescence techniques. *Free Radic Biol Med.* **29**:388-396; 2000.

113. Janiszewski, M.; Souza, H. P.; Liu, X.; Pedro, M. A.; Zweier, J. L.; Laurindo, F. R. Overestimation of NADH-driven vascular oxidase activity due to lucigenin artifacts. *Free Radic Biol Med.* **32**:446-453; 2002.

114. Daiber, A.; August, M.; Baldus, S.; Wendt, M.; Oelze, M.; Sydow, K.; Kleschyov, A. L.; Munzel, T. Measurement of NAD(P)H oxidase-derived superoxide with the luminol analogue L-012. *Free Radic Biol Med.* **36**:101-111; 2004.

115. Daiber, A.; Oelze, M.; August, M.; Wendt, M.; Sydow, K.; Wieboldt, H.; Kleschyov, A. L.; Munzel, T. Detection of superoxide and peroxynitrite in model systems and mitochondria by the luminol analogue L-012. *Free Radic Res.* **38**:259-269; 2004.

116. Szocs, K.; Lassegue, B.; Sorescu, D.; Hilenski, L. L.; Valppu, L.; Couse, T. L.; Wilcox, J. N.; Quinn, M. T.; Lambeth, J. D.; Griendling, K. K. Upregulation of Nox-based NAD(P)H oxidases in restenosis after carotid injury. *Arterioscler Thromb Vasc Biol.* **22**:21-27; 2002.

117. Lassegue, B.; Sorescu, D.; Szocs, K.; Yin, Q.; Akers, M.; Zhang, Y.; Grant, S. L.; Lambeth, J. D.; Griendling, K. K. Novel gp91(phox) homologues in vascular smooth muscle cells : nox1 mediates angiotensin II-induced superoxide formation and redox-sensitive signaling pathways. *Circ Res.* **88**:888-894; 2001.

118. Hathaway, C. A.; Heistad, D. D.; Piegors, D. J.; Miller, F. J., Jr. Regression of atherosclerosis in monkeys reduces vascular superoxide levels. *Circ Res.* **90**:277-283; 2002.

119. Crespo, M. J.; Dunbar, D. C. Enalapril improves vascular and cardiac function in streptozotocin-diabetic rats. *Cell Mol Biol (Noisy-le-grand).* **49**:1311-1318; 2003.

120. Nosadini, R.; Tonolo, G. The role of the renin angiotensin hormonal system in the metabolic syndrome and type 2 diabetes. *Nutr Metab Cardiovasc Dis.* **14**:88-93; 2004.

121. Forbes, J. M.; Cooper, M. E.; Thallas, V.; Burns, W. C.; Thomas, M. C.; Brammar, G. C.; Lee, F.; Grant, S. L.; Burrell, L. A.; Jerums, G.; Osicka, T. M. Reduction of the accumulation of advanced glycation end products by ACE inhibition in experimental diabetic nephropathy. *Diabetes.* **51**:3274-3282; 2002.

122. Yamamoto, Y.; Yamagishi, S.; Yonekura, H.; Doi, T.; Tsuji, H.; Kato, I.; Takasawa, S.; Okamoto, H.; Abedin, J.; Tanaka, N.; Sakurai, S.; Migita, H.; Unoki, H.; Wang, H.; Zenda, T.; Wu, P. S.; Segawa, Y.; Higashide, T.; Kawasaki, K.; Yamamoto, H. Roles of the AGE-RAGE system in vascular injury in diabetes. *Ann N Y Acad Sci.* **902**:163-170; discussion 170-162; 2000.

123. Wautier, M. P.; Chappey, O.; Corda, S.; Stern, D. M.; Schmidt, A. M.; Wautier, J. L. Activation of NADPH oxidase by AGE links oxidant stress to altered gene expression via RAGE. *Am J Physiol Endocrinol Metab.* **280**:E685-694; 2001.

124. Banfi, B.; Clark, R. A.; Steger, K.; Krause, K. H. Two novel proteins activate superoxide generation by the NADPH oxidase NOX1. *J Biol Chem.* **278**:3510-3513; 2003.

125. Lavigne, M. C.; Malech, H. L.; Holland, S. M.; Leto, T. L. Genetic demonstration of p47phox-dependent superoxide anion production in murine vascular smooth muscle cells. *Circulation.* **104**:79-84; 2001.

126. Hilenski, L. L.; Clempus, R. E.; Quinn, M. T.; Lambeth, J. D.; Griendling, K. K. Distinct subcellular localizations of Nox1 and Nox4 in vascular smooth muscle cells. *Arterioscler Thromb Vasc Biol.* **24**:677-683; 2004.

127. Janiszewski, M.; Souza, H. P.; Liu, X.; Pedro, M. A.; Zweier, J. L.; Laurindo, F. R. Overstimation of verestimation of NADH-driven vascular oxidase activity due to lucigenin artifacts. *Free Radic Biol Med.* **32**:446-453; 2002.

128. Xiao, L.; Pimentel, D. R.; Wang, J.; Singh, K.; Colucci, W. S.; Sawyer, D. B. Role of reactive oxygen species and NAD(P)H oxidase in alpha(1)-adrenoceptor signaling in adult rat cardiac myocytes. *Am J Physiol Cell Physiol.* **282**:C926-934; 2002.

129. Nakagami, H.; Jensen, K. S.; Liao, J. K. A novel pleiotropic effect of statins: prevention of cardiac hypertrophy by cholesterol-independent mechanisms. *Ann Med.* **35**:398-403; 2003.

130. Privratsky, J. R.; Wold, L. E.; Sowers, J. R.; Quinn, M. T.; Ren, J. AT1 blockade prevents glucose-induced cardiac dysfunction in ventricular myocytes: role of the AT1 receptor and NADPH oxidase. *Hypertension.* **42**:206-212; 2003.

8 Publications, Abstracts and Presentations

8.1 Publications

1. Sodium transport in hypertension: assessment of membrane-associated defects in South African black and white hypertensives. WORTHINGTON MG, **WENDT MC**, OPIE LH. J Hum Hypertens 1993, 7: 291-297.
2. Local delivery of platelets with encapsulated iloprost to balloon injured pig carotid arteries: effects on platelet deposition and neointima formation. BANNING A, BREWER L, **WENDT MC**, CHEADLE H, PENNY W, CRAWFORD N. Thromb Haemost 1997, 77 (1): 190-6.
3. Application of cryo-high resolution SEM technique for imaging platelet morphology. **WENDT MC**, ROBINSON KA, CHRONOS NAF, CARAN KL, APKARIAN RP. Microsc Microanal 1999, 5: 1116-1117.
4. Antioxidants and endothelial dysfunction in hyperlipidemia. WARNHOLTZ A, MOLLNAU H, OELZE M, **WENDT M**, MÜNZEL T. Curr Hypertens Rep 2001, 3(1): 53-60.
5. Functional and biochemical analysis of endothelial (dys)function and NO/cGMP signaling in human blood vessels with and without nitroglycerin pretreatment. SCHULZ E, TSILIMINGAS N, RINZE R, REITER B, **WENDT M**, OELZE M, WOELKEN-WECKMÜLLER S, WALTER U, REICHENSPURNER H, MEINERTZ T, MÜNZEL T. Circulation 2002, 105: 1170-1175.
6. Mechanisms underlying nitrate-induced endothelial dysfunction: insight from experimental and clinical studies. WARNHOLTZ A, TSILIMINGAS N, **WENDT M**, MÜNZEL T. Heart Fail Rev 2002, 7(4): 335-45.
7. Effects of angiotensin II infusion on the expression and function of NAD(P)H oxidase and components of nitric oxide/cGMP signaling. MOLLNAU H, **WENDT M**, SZOCS K, LASSEGUE B, SCHULZ E, OELZE M, LI H, BODENSCHATZ M, AUGUST M, KLESCHYOV A, TSILIMINGAS N, WALTER U, FORSTERMANN U, MEINERTZ T, GRIENDLING K, MÜNZEL T. Circ Res 2002, 90(4): 58-65.
8. When sleeping beauty turns ugly. Mitochondria in hypoxia. WARNHOLTZ A, **WENDT M**, MÜNZEL T. Arterioscler Thromb Vasc Biol 2002, 22:525-527.

9. A new pitfall in detecting biological end products of nitric oxide – nitration, nitros(y)lation and nitrite/nitrate artefacts during freezing. DAIBER A, BACHSCHMID M, KAVAKLI C, FREIN D, **WENDT M**, ULLRICH V, MUNZEL T. Nitric Oxide 2003, 9: 44-52.
10. Nebivolol prevents NOSIII uncoupling in experimental hyperlipidemia and inhibits NADPH oxidase activity in inflammatory cells. MOLLNAU H, SCHULZ E, DAIBER A, BALDUS S, OELZE M, AUGUST M, **WENDT M**, WALTER U, MEINERTZ T, AGRAWAHL R, MUNZEL T. Arterioscler ThrombVasc Biol 2003, 23: 615-621.
11. Mechanisims underlying endothelial dysfunction in diabetes mellitus. HINK U, TSILIMINGAS N, **WENDT M**, MUNZEL T. Curr Opin 2003, 2: 293-304.
12. Clinical aspects of reactive oxygen and nitrogen species. WARNHOLTZ A, **WENDT M**, AUGUST M, MUNZEL T. Biochem Soc Symp 2004, 71: 121-133.
13. Central role of mitochondrial aldehyde dehydrogenase and reactive oxygen species in nitroglycerin tolerance and cross-tolerance. SYDOW K, DAIBER A, OELZE M, CHEN Z, AUGUST M, **WENDT M**, ULLRICH V, MULSCH A, SCHULZ E, KEANEY JF JR, STAMLER JS, MUNZEL T. J Clin Invest 2004, 113: 482-489.
14. Measurement of NADPH oxidase-derived superoxide with luminol analogue L-012. DAIBER A, OELZE M, AUGUST M, **WENDT M**, SYDOW K, WIEBOLDT H, KLESCHYOV AL, MUNZEL T. Free Radic Biol Med 2004, 36: 101-111.
15. Detection of superoxide and peroxynitrite in model systems and mitochondria by the chemiluminescence dye L-012. DAIBER A, OELZE M, AUGUST M, **WENDT M**, SYDOW K, WIEBOLDT H, KLESCHYOV A, MUNZEL T. Free Radic Res 2004, 38: 259-269.
16. Oxidative stress and mitochondrial aldehyde dehydrogenase activity: A comparison of pentaerythrityl tetranitrate (PETN) with other organic nitrates. DAIBER A, OELZE M, COLDEWEY M, BACHSCHMID M, WENZEL P, SYDOW K, **WENDT M**, KLESCHYOV AL, STALLEIKEN D, ULLRICH V, MULSCH A, MUNZEL T. Mol Pharmacol. 2004, ahead of print.
17. Differential effects of diabetes on the expression of the $gp91^{phox}$ homologues nox1 and nox4. **WENDT M,** DAIBER A, KLESCHYOV AL, MULSCH A, SYDOW K, SCHULZ E, CHEN K, KEANEY JF, LASSEGUE B, WALTER U, GRIENDLING KK, MUNZEL T (in press).

8.2 Abstracts

1. Use of electroporated platelets as a novel drug delivery system in preventing complications of coronary angioplasty. WARD SR, GUZMAN L, SUTTON JM, FORUDI F, **WENDT MC**, BREWER L, TOPOL E, CRAWFORD N. J Am Coll Cardiol 1995, 25: 303A.
2. Use of electroporated platelets as a novel drug delivery system in preventing complications of percutaneous coronary interventions. GUZMAN LA, WARD SR, SUTTON JM, FORUDI F, **WENDT MC**, BREWER L, TOPOL EJ, CRAWFORD N. J Invasive Cardiol 1996, 8: 64.
3. Detection of Chlamydia pneumoniae in human nonrheumatic sclerotic heart valves by immunohistochemical analysis and polymerase chain reaction. KRAUSE K, MALESIUS R, **WENDT MC**, KECK A, LASS M, VIERBUCHEN M, KUCK KH. JACC 1999, 33 (2): 552A.
4. Nachweis von Chlamydia pneumoniae in sklerotischen Aortenklappen bei Patienten mit koronarer Herzkrankheit. KRAUSE K, MALESIUS R, **WENDT MC**, LASS M, KECK A. Z Kardiol 1999, 88(1): 732.
5. Peroxidase activity of the extracellular superoxide dismutase. HINK U, FUKAI T, **WENDT M**, PARTHASARATHY S, HARRISON D. Free Radic Biol Med 1999, 27(Suppl 1): S20.
6. Peroxidase activity of the extracellular superoxide dismutase. HINK U, FUKAI T, **WENDT M,** PARTHASARATHY S, HARRISON D. FASEB J 2000, 14 (4): A492.
7. The role of the copper chaperone CCS in extracellular superoxide dismutase function. **WENDT MC**, HINK U, CULOTTA V, HARRISON D, FUKAI T. Circulation 2000, 102(18):234.
8. NO or iron-NO? That is the question. KLESCHYOV A, **WENDT M**, MULLER B, STOCLET JC, MÜNZEL T. Nitric Oxide 2002, 6(4):412.
9. Hemeoxygenase-1-mediated protection: potential role of nonheme iron-nitric oxide complexes. KLESCHYOV A, **WENDT M**, MÜNZEL T. Circulation 2002, 105: e196.
10. Comparable effects of vasopeptidase inhibition vs ACE inhibition on endothelial dysfunction and vascular superoxide production and NOS III expression in experimental congestive heart failure. MOLLNAU H, HEITZER T, SCHULZ E, AUGUST M, KLESCHYOV A, HINK U, WARNHOLTZ A, OELZE M, **WENDT M**, BALDUS S, MÜNZEL T. Circulation 2002, 106(19):II:248.

11. Extending possibilities of NO spin trapping in blood vessels. KLESCHYOV A, SYDOW K, AUGUST M, **WENDT M**, MÜNZEL T. Free Radic Biol Med 2002, 33(Suppl 2): S378.
12. In vivo nitroglycerin treatment increases the content of NO-reactive chelatable iron. Potential implication for endothelial dysfunction. KLESCHYOV A, SYDOW K, SCHULZ E, **WENDT M**, MÜNZEL T. Free Radic Biol Med 2002, 33(Suppl 2): S378.
13. Nitroglycerin induced peroxynitrite formation inhibits vascular prostacyclin formation and the activity of the cGMP-dependent protein kinase I. OELZE M, **WENDT M**, ZOU M, MOLLNAU H, KOLB PH, HOFFMANN N, ULLRICH V, MÜNZEL T. Z Kardiol 2002, 91(Suppl1): I-88.
14. Effects of Metoprolol on oxidant stress parameters and NO bioavailability in angiotensin II induced hypertension. HINK U, SCHULZ E, MOLLNAU H, VON SANDERSLEBEN A, AUGUST M, OELZE M, **WENDT M**, MÜNZEL T. Z Kardiol 2002, 91(Suppl 1): I-107.
15. Evidence for oxidant inactivation of extracellular and cytosolic SOD in atherosclerosis: prevention by uric acid. HINK U, FUKAI T, **WENDT M**, SANTANAM N, PARTHASARATHY S, HARRISON D. Z Kardiol 2002, 91(Suppl 1): I-107.
16. Differential expression of the NAD(P)H oxidase subunits nox1 and nox4 in diabetes mellitus. **WENDT M**, LASSEGUE B, SCHULZ E, GRIENDLING K, MÜNZEL T. Circulation 2002, 106(19):II-51.
17. Differential expression of the NAD(P)H oxidase subunits nox1 and nox4 in diabetes mellitus. **WENDT M**, LASSEGUE B, AUGUST M, CLEMPUS R, SYDOW K, SCHULZ E, CHENG G, LAMBETH D, GRIENDLING K, MÜNZEL T. Z Kardiol 2003, 92(Suppl 1)V-1461.
18. Nebivolol, a third generation ß-blocker has anti-inflammatory properties. DAIBER A, MOLLNAU H, SYDOW K, **WENDT M**, AUGUST M, KLESCHYOV A, OELZE M, MÜNZEL T. Z Kardiol 2003, 92(Suppl 1)P-961.

8.3 Presentations

1. Sodium transport in hypertension: assessment of membrane-associated defects in South African black and white hypertensives. WORTHINGTON MG, **WENDT MC**, OPIE LH.
   Poster: Annual Congress of the Physiological Society of Southern Africa 1989, Pretoria, RSA.
2. Application of cryo-high resolution SEM technique for imaging platelet morphology. **MC WENDT**, KA ROBINSON, NAF CHRONOS, KL CARAN, RP APKARIAN.
   Poster: Microscopy and Microanalysis Meeting 1999, Portland, Oregon, USA.
3. The role of the copper chaperone CCS in extracellular superoxide dismutase function. **WENDT MC**, HINK U, CULOTTA V, HARRISON D, FUKAI T. Circulation 2000, 102(18):234.
   Oral: American Heart Association 2000, New Orleans, Lousianna, USA.
   Oral: 1st Postdoctoral Research Retreat - Alabama University/Emory University 1999, Atlanta, Georgia, USA.
4. Differential expression of the NAD(P)H oxidase subunits nox1 and nox4 in diabetes mellitus. **WENDT M**, LASSEGUE B, CLEMPUS R, SCHULZ E, GRIENDLING K, MÜNZEL T. Circulation 2002, 106(19):II-51.
   Oral: **American Heart Association 2002, Chicago, Illinois, USA.**
5. Expression of the NAD(P)H oxidase subunit nox4 in diabetes mellitus. **WENDT M**, LASSEGUE B, SCHULZ E, GRIENDLING K, MÜNZEL T.
   Poster: VIII. NO-Forum 2002, Frankfurt, Germany.
6. Differential expression of the NAD(P)H oxidase subunits nox1 and nox4 in diabetes mellitus. **WENDT M**, LASSEGUE B, AUGUST M, CLEMPUS R, SYDOW K, SCHULZ E, CHENG G, LAMBETH D, GRIENDLING K, MÜNZEL T.
   Oral: 69 Annual Meeting of German Society of Cardiology 2003, Mannheim, Germany.